

ANALYZING OF USAGE OF COMPLEX-SHAPED CU-W PARTS PRODUCED
BY METAL INJECTION MOLDING PROCESS FOR HEAT SINK FOR HIGH-
PERFORMANCE ELECTRONIC DEVICES

A THESIS SUBMITTED TO
THE GRADUATE SCHOOL OF NATURAL AND APPLIED SCIENCES
OF
MIDDLE EAST TECHNICAL UNIVERSITY

BY

ALPER ATAK

IN PARTIAL FULFILLMENT OF THE REQUIREMENTS
FOR
THE DEGREE OF MASTER OF SCIENCE
IN
METALLURGICAL AND MATERIALS ENGINEERING

SEPTEMBER 2019

Approval of the thesis:

**ANALYZING OF USAGE OF COMPLEX-SHAPED CU-W PARTS
PRODUCED BY METAL INJECTION MOLDING PROCESS FOR HEAT
SINK FOR HIGH-PERFORMANCE ELECTRONIC DEVICES**

submitted by **ALPER ATAK** in partial fulfillment of the requirements for the degree
of **Master of Science in Metallurgical and Materials Engineering Department,**
Middle East Technical University by,

Prof. Dr. Halil Kalıpçılar
Dean, Graduate School of **Natural and Applied Sciences**

Prof. Dr. Hakan Gür
Head of Department, **Met. and Mat. Eng.**

Prof. Dr. Ali Kalkanlı
Supervisor, **Met. and Mat. Eng., METU**

Examining Committee Members:

Prof. Dr. Bilgin Kaftanoğlu
Manufacturing Engineering, Atılım University

Prof. Dr. Ali Kalkanlı
Met. and Mat. Eng., METU

Prof. Dr. İshak Karakaya
Met. and Mat. Eng., METU

Prof. Dr. Bilgehan Ögel
Met. and Mat. Eng., METU

Assist. Prof. Dr. Bilge İmer
Met. and Mat. Eng., METU

Date: 06.09.2019

I hereby declare that all information in this document has been obtained and presented in accordance with academic rules and ethical conduct. I also declare that, as required by these rules and conduct, I have fully cited and referenced all material and results that are not original to this work.

Name, Surname: Alper Atak

Signature:

ABSTRACT

ANALYZING OF USAGE OF COMPLEX-SHAPED CU-W PARTS PRODUCED BY METAL INJECTION MOLDING PROCESS FOR HEAT SINK FOR HIGH-PERFORMANCE ELECTRONIC DEVICES

Atak, Alper
Master of Science, Metallurgical and Materials Engineering
Supervisor: Prof. Dr. Ali Kalkanlı

September 2019, 119 pages

During the past decades, the rapid evolution of electronic and information technology has resulted in a significant increase in the performance of the processors of the electronic devices. In order to dissipate the heat generated at the interface of these electronic devices, heat spreaders or heat sinks should be produced from suitable materials. Thermal conductivity and coefficient of thermal expansion (CTE) are two important thermal properties to consider for choosing the suitable materials for this process. Aluminum and copper have high thermal conductivity values, but their high CTE values result in warping of the plate, crack for ceramic component or solder fatigue because of the large difference of CTE to ceramics or silicon. Copper-Tungsten (CuW) composites, which combines high thermal coefficient value with matched CTE value are used to overcome these problems. Since copper and tungsten are not mutually soluble, CuW parts are produced by powder metallurgy techniques. Metal injection molding (MIM) is a powder metallurgy technique which enables complex parts to be formed as easily as simple geometries, thereby allowing increased design freedom. The aim of this thesis is to produce Complex-Shaped CuW parts with necessary thermal properties by using MIM process.

Keywords: Heat Sinks, Copper-Tungsten, Metal Injection Molding, Powder metallurgy

ÖZ

TOZ ENJEKSİYON KALIPLAMA YÖNTEMİ İLE ÜRETİLEN KARMAŞIK GEOMETRİLİ CU-W MALZEMELERİN YÜKSEK PERFORMANSLI ELEKTRONİK CİHAZLARDA SOĞUTUCU OLARAK KULLANABİLİRLİĞİNİN İNCELENMESİ

Atak, Alper
Yüksek Lisans, Metalurji ve Malzeme Mühendisliği
Tez Danışmanı: Prof. Dr. Ali Kalkanlı

Eylül 2019, 119 sayfa

Günümüzde özellikle bilişim sektöründeki elektronik cihazlarda kullanılan işlemcilerin performansları sürekli olarak artmakta ve artan işlemci performansına paralel olarak cihazlarda ortaya çıkan ısı miktarı da yükselmektedir. Bu yüksek ısı miktarının cihaz bileşenlerine zarar vermeden dış ortama aktarılması gerekmektedir. Bu amaçla cihazlarda çeşitli ısı atım elemanları kullanılmaktadır. Bu elemanların malzemelerinin seçiminde öne çıkan en önemli iki özellik ise ısı iletkenlik ve ısı genleşme katsayısıdır. Klasik yöntemlerle üretilen ve yüksek ısı iletkenliğine sahip alüminyum, bakır gibi malzemeler silikon çipler veya seramik alt malzemelerle kullanıldığında termal genleşme uyumsuzluğu ortaya çıkmakta ve parçalarda çatlamlar hatta kırılmalar gözlemlenmektedir. Bu amaçla yüksek ısı iletkenliğini uygun ısı genleşme katsayılarıyla birleştiren bakır-tungsten (CuW) gibi kompozit malzemeler üretilmiştir. CuW bileşenleri birbirleriyle alaşım oluşturamadıklarından daha çok toz metalürji teknikleri ile üretilmektedirler. Nihai parçada elde edilebilecek şekil çeşitliliği karmaşıklığı açısından toz metalürji yöntemlerinden enjeksiyon kalıplama yöntemi(MİM) öne çıkmaktadır. Tez çalışması ile amaçlanan MIM teknolojisini CuW malzeme ile birlikte kullanarak mevcut yöntemlerle üretilmeyen ve gerekli termal özelliklere sahip karmaşık geometri parçalar üretebilmektir.

Anahtar Kelimeler: Soğutucu, Bakır-tungsten, Toz Metal Enjeksiyon, Toz Metalürjisi

To my family

ACKNOWLEDGEMENTS

Firstly, I would like to thank my supervisor, Prof. Dr. Ali Kalkanlı for his continuous guidance, support, and instruction.

Secondly, I am very grateful to my managers Bilal Bilgin and Serdar Terzi for endless support and courage to support during my studies. Without the opportunities they provide this study would never finish. I would also like to express my appreciation to ASELSAN is for encouraging and supporting the employees also on their academic career.

Secondly, I would also specially thank to my colleagues Kerem G ng r and Dr.Yiğit Akkuş for their technical guidance and valuable discussions throughout the study.

Finally, I wish to thank my love, Sonay, for her lifelong support. Her constant encouragement helped me overcome the many difficulties throughout the study.

TABLE OF CONTENTS

ABSTRACT	v
ÖZ.....	vii
ACKNOWLEDGEMENTS	x
TABLE OF CONTENTS	xi
LIST OF TABLES	xvi
LIST OF FIGURES	xviii
CHAPTERS	
1. INTRODUCTION	1
1.1. Background and Motivation	1
2. LITERATURE REVIEW AND THEORY	7
2.1. Thermal Managements in Electronic Systems	7
2.2. CPU Cooling Systems	9
2.2.1. Passive Cooling.....	9
2.2.2. Air Cooling	9
2.2.3. Liquid Cooling.....	10
2.2.4. Immersion Cooling	10
2.2.5. Heat Pipe.....	10
2.3. Heat Sink	11
2.3.1. General information About Heat Sinks	11
2.3.2. Heat Sink Materials	12
2.3.3. Heat Sink Manufacturing Methods.....	13
2.3.3.1. Extruded Heat Sinks.....	13

2.3.3.2. Cold Forged Heat Sinks	13
2.3.3.3. Stamped Heat Sinks	14
2.3.3.4. Bonded Heat Sinks	14
2.3.3.5. Skived Heat Sinks.....	15
2.3.3.6. CNC Machined Heat Sinks.....	16
2.3.3.1. Injected Molded Heat Sinks.....	16
2.3.4. Heat Sink Attachment Methods	17
2.3.4.1. Thermal Tape.....	18
2.3.4.2. Thermal Epoxy	18
2.3.4.3. Z-Clip Attachment to the PCB	19
2.3.4.4. Push Pins.....	20
2.3.4.5. Threaded Standoffs	20
2.3.5. Heat Sink Design.....	21
2.3.5.1. Material Selection.....	24
2.3.5.2. Geometry	28
2.4. Heat Sink Studies in Literature	29
2.5. MIM Operations.....	34
2.5.1. Feedstock Preparation	37
2.5.2. Injection.....	38
2.5.3. Debinding	39
2.5.3.1. Primary Debinding.....	40
2.5.3.2. Secondary Debinding.....	40
2.5.4. Sintering	41
2.5.4.1. Liquid Phase Sintering.....	42

2.5.4.1. Sintering Atmosphere.....	43
3. EXPERIMENTAL STUDY	45
3.1. Feedstock Purchase	45
3.2. Part Design	45
3.2.1. Heat Sink 9x9.....	46
3.2.2. Heat Sink 4x4.....	47
3.2.3. Expansion Specimen.....	47
3.2.4. Conduction Specimen	48
3.2.5. Tensile Specimen	48
3.3. Mold Design	49
3.4. Mold Production.....	52
3.5. Injection.....	54
3.5.1. Injection with W80Cu20 Feedstock	54
3.5.2. Injection with W85Cu15 Feedstock	56
3.6. Debinding	57
3.6.1. Water Debinding with W80Cu20 Feedstock	57
3.6.2. Solvent Debinding with W85Cu15 Feedstock.....	59
3.7. Sintering	61
3.7.1. Sintering Parameters	62
4. RESULTS AND DISCUSSION	65
4.1. Injection Operations	65
4.1.1. Injection of Heat Sink 9x9	65
4.1.2. Injection of other parts	67
4.2. Debinding Operations.....	69

4.2.1. Water Debinding of W80Cu20 Feedstock	69
4.2.2. Solvent Debinding of W85Cu15 Feedstock.....	70
4.3. Sintering	71
4.3.1. Sintered W80Cu20 parts	71
4.3.2. Sintered W85Cu15 parts	72
4.4. Shrinkage Ratios	73
4.4.1. Shrinkage Ratio of W-20Cu parts	74
4.4.1.1. Heat Sink	74
4.4.1.2. Tensile Specimen.....	75
4.4.1.3. Conductivity Specimen.....	76
4.4.1.4. Expansion Specimen.....	77
4.4.2. Shrinkage Ratio of W-15Cu parts	78
4.4.2.1. Heat Sink	78
4.4.2.2. Tensile Specimen.....	79
4.4.2.3. Conductivity Specimen.....	80
4.4.2.4. Expansion Specimen.....	81
4.4.3. Discussion of the shrinkage ratios.....	82
4.5. Density Measurements	83
4.5.1. Density of W-20Cu parts.....	84
4.5.2. Density of W-15Cu parts.....	85
4.6. Microstructure Analysis.....	86
4.6.1. SEM Analysis.....	86
4.6.1.1. SEM Analysis of W-20 parts.....	87
4.6.1.2. SEM Analysis of W-15 parts.....	88

4.6.2. EDX Analysis	89
4.6.2.1. EDX Analysis of W-20Cu parts.....	89
4.6.2.2. EDX Analysis of W-15 parts	92
4.7. Thermal Properties	93
4.7.1. Thermal Conductivity	94
4.7.2. Coefficient of Thermal Expansion Measurements	95
4.8. Thermal Performance Assessment of the Heat Sink.....	96
4.8.1. Experimentation.....	97
4.8.2. Simulation.....	102
4.9. Tensile Strength Measurements	105
5. CONCLUSIONS	109
6. SUGGESTED FUTURE WORK	113
REFERENCES.....	115

LIST OF TABLES

TABLES

Table 1.1. Some of future high performance electronic devices in defense industry..	2
Table 2.1. Thermal properties of various materials at room temperature[19].....	25
Table 2.2. Properties of tungsten-copper and molybdenum-copper heat sink materials[13]	26
Table 2.3. The physical properties of W and Cu at room temperature [20]	26
Table 2.4. Thermal properties of the copper-tungsten composite [22].....	27
Table 2.5. Thermal properties of the copper-tungsten and copper-molybdenum.....	33
Table 2.6. Comparison of MIM with other manufacturing methods.....	35
Table 2.7. Main Binder systems used in MIM	38
Table 3.1. Feedstock Properties	45
Table 3.2. Injection Parameters for Feedstock 1	54
Table 3.3. Injection Parameters for W85Cu15 Feedstock.....	56
Table 3.4. Water Debinding Parameters	59
Table 3.5. Solvent Debinding Parameters	60
Table 3.6. Theoretical Shrinkage Ratios.....	61
Table 4.1. Weight of the samples before and after water debinding process	69
Table 4.2. Weight of the samples before and after water debinding Process	71
Table 4.3. Sintering Parameters used for sintering W80Cu20 parts.....	72
Table 4.4. Shrinkage Ratios of the Feedstocks.....	73
Table 4.5. Heat Sink Dimensions before and after sintering	74
Table 4.6. Tensile Specimen Dimensions before and after sintering	75
Table 4.7. Conduction Specimen Dimensions before and after sintering	76
Table 4.8. Expansion Specimen Dimensions before and after sintering	77
Table 4.9. Heat Sink Dimensions before and after sintering	78
Table 4.10. Tensile Specimen Dimensions before and after sintering	79

Table 4.11. Conduction Specimen Dimensions before and after sintering.....	80
Table 4.12. Expansion Specimen Dimensions before and after sintering.....	81
Table 4.13. Theoretical and measured average shrinkage values for W-20Cu Parts.	82
Table 4.14. Theoretical and measured average shrinkage values for W-15Cu Parts.	82
Table 4.15. Measured Density Values for W-20Cu.....	84
Table 4.16. Measured Density Values for W-15Cu.....	85
Table 4.17. Thermal properties of W80Cu20 [46]	94
Table 4.18. Coefficient of thermal expansion values of the samples.....	96
Table 4.19. Temperature ranges for different thermal conductivity values	105
Table 4.20. Mechanical properties of W80Cu20 [51]	106
Table 4.21. Measured Mechanical Values	107

LIST OF FIGURES

FIGURES

Figure 1.1. A typical heat sink.....	2
Figure 1.2. A processor and attached heat sink.	3
Figure 1.3. Thermal Pad between chip and heat sink.	4
Figure 2.1. Microprocessors Transistor Counts 1971-2011 & Moore’s Law [8].....	8
Figure 2.2. Power dissipation Projection [9]	8
Figure 2.3. Heat sinks used in the electronic industry	11
Figure 2.4. Active Heat Sink	12
Figure 2.5. Extruded Heat Sinks.....	13
Figure 2.6. Cold forged heat sinks.....	14
Figure 2.7. Stamped Heat Sinks	14
Figure 2.8. Bonded heat sinks.....	15
Figure 2.9. Skived heat sinks	15
Figure 2.10. CNC Machined heat sinks	16
Figure 2.11. Injected molded heat sinks	17
Figure 2.12. Thermal Tape	18
Figure 2.13. Thermal Epoxy.....	19
Figure 2.14. Z-Clip Attachment.....	19
Figure 2.15. Push Pins	20
Figure 2.16. Threaded Standoffs	20
Figure 2.17. Thermal Conduction.....	21
Figure 2.18. Circuit Analysis in Electrical and Thermal Equations	22
Figure 2.19. Thermal Convection.....	22
Figure 2.20. Total Thermal Resistance.....	23
Figure 2.21. Heat sink used in a system	25
Figure 2.22. Pin (a), straight (b) and flared(c) fin designs	28

Figure 2.23. Thermal Resistances of fin-type and thin-walled type of heatsinks	29
Figure 2.24 Images of the W-Cu balls [26].....	30
Figure 2.25 μ -MIM moulded heat sink parts	30
Figure 2.26 Test part used in the study	31
Figure 2.27 An example MIM Cu heat sink	31
Figure 2.28. LED heat sink for thermal management.....	32
Figure 2.29. PIM shaped copper heat sinks designed for cooling in electronics	32
Figure 2.30. Global Metal Injection Molding Market [50].....	34
Figure 2.31 Comparison of MIM to the other process [33]	36
Figure 2.32. Metal Injection Molding Steps	36
Figure 2.33. Feedstock Preparation Steps	37
Figure 2.34. Injection Molding Machine (Courtesy Arburg).....	38
Figure 2.35. Sketch of the solvent debinding process	41
Figure 2.36. Liquid Phase Sintering Mechanism [40]	42
Figure 3.1. Heat Sink 9x9	46
Figure 3.2. Heat Sink 4x4	47
Figure 3.3. Thermal Expansion Specimen	47
Figure 3.4. Conductivity Specimen.....	48
Figure 3.5. Tensile test specimen according to ISO 2740	48
Figure 3.6. Typical Mold Parts	49
Figure 3.7. Cooling channels in the mold	50
Figure 3.8. Designed Molds	51
Figure 3.9. Technical Drawing of Molds a) for Heat Sink 9x9 b) for Heat Sink 4x4, Conduction and Expansion Samples c) for Tensile Samples	51
Figure 3.10. Production in milling machine	52
Figure 3.11. Mold for Heatsink 9x9.....	52
Figure 3.12. Mold for Heatsink 4x4 and Thermal Specimens	53
Figure 3.13. Mold for Test and Tensile Specimen.....	53
Figure 3.14. Arburg 221-175-350 Injection Molding Machine	54
Figure 3.15. Mold assembled to the Injection Molding Machine	55

Figure 3.16. Parts Produced from W80Cu20 Feedstock	56
Figure 3.17. Parts Produced from W85Cu15 feedstock	57
Figure 3.18. Water Debinding Operations.....	58
Figure 3.19. Weight Loss During Solvent Debinding of a)Heat Sink 4x4 b)Tensile sample c)Expansion Sample d)Conduction Sample	58
Figure 3.20. Solvent Debinding Operations	59
Figure 3.21. Weight Loss During Solvent Debinding of a)Heat Sink 4x4 b)Tensile sample c)Expansion Sample d)Conduction Sample	60
Figure 3.22. Sintering Furnace, CM 1512 H2 GS FL	61
Figure 3.23. Parts in Sintering Furnace	62
Figure 3.24. Sintering Curve	63
Figure 4.1. Injected heat sink 9x9 with defects.	65
Figure 4.2. Heat Sink 9x9 design a) original, b) short Pin version.	66
Figure 4.3. Injected short finned version of heat sink 9x9 with defects.	67
Figure 4.4. Excess material around the molded part	67
Figure 4.5. Injected samples from W80Cu20 feedstock	68
Figure 4.6. Injected samples from W85CU15 feedstock.....	68
Figure 4.7. W80Cu20 samples before and after debinding a)Heat Sink b)Conduction Specimen c)Expansion Specimen d)Tensile Specimen	69
Figure 4.8. SEM microstructure of injected samples before and after debinding	70
Figure 4.9. W85Cu15 samples before and after debinding a)Heat Sink b)Conduction Specimen c)Expansion Specimen d)Tensile Specimen	71
Figure 4.10. Three groups of W-Cu20 parts sintered	72
Figure 4.11. The easily broken sintered w-15Cu parts.	73
Figure 4.12. Heat Sink Part before and after sintering	74
Figure 4.13. Heat Sink Dimensions Notations	74
Figure 4.14. Tensile Specimen before and after sintering	75
Figure 4.15. Tensile Specimen Notations.....	75
Figure 4.16. Conduction specimen before and after sintering.....	76
Figure 4.17. Heat Sink Dimensions Notations	76

Figure 4.18. Expansion Specimen before and after sintering	77
Figure 4.19. Expansion Specimen Dimensions Notations	77
Figure 4.20. Heat Sink Part before and after sintering.....	78
Figure 4.21. Heat Sink Dimensions Notations.....	78
Figure 4.22. Tensile Specimen before and after sintering	79
Figure 4.23. Tensile Specimen Notations	79
Figure 4.24. Conduction specimen before and after sintering	80
Figure 4.25. Heat Sink Dimensions Notations.....	80
Figure 4.26. Expansion Specimen before and after sintering	81
Figure 4.27. Expansion Specimen Dimensions Notations	81
Figure 4.28. Weighing of samples a)in air, b)in water.....	84
Figure 4.29. Copper-Tungsten Microstructure.....	86
Figure 4.30. Electron-Sem Images of samples a) sintered at 1350 °C for 3 hours, (b) sintered at 1350 °C for 1 hour, c) sintered at 1200 °C	87
Figure 4.31. Porosities found in samples a) sintered at 1350 °C for 1 hour, b)sintered at 1200 °C	88
Figure 4.32. 5000x SEM image of a) W-20Cu samples b) W-15Cu samples	88
Figure 4.33. EDX Images of samples a)W-20Cu(1)(b) W-20Cu(2)c) W-20Cu(3) ...	90
Figure 4.34. Line analysis of samples group #1(WCu1) a) Microstructure image b) Copper and tungsten distribution along the specified line c)Elemental composition in point A d) Elemental composition in point B	91
Figure 4.35. Line analysis of samples group #2(WCu2) a) Microstructure image b) Copper and tungsten distribution along the specified line c)Elemental composition in point A d) Elemental composition in point B	91
Figure 4.36. Line analysis of samples group #2(WCu2) a) Microstructure image b) Copper and tungsten distribution along the specified line c)Elemental composition in point A d) Elemental composition in point B	92
Figure 4.37. EDX Images of W-15Cu sample	93
Figure 4.38. The samples for measurements a) thermal conductivity and b) thermal coefficient of expansion	93

Figure 4.39. Thermal conductivities of Copper-Tungsten Composites.....	95
Figure 4.40. Experimental setup.....	97
Figure 4.41. Components utilized during the experiment	98
Figure 4.42. Heater attached to the heat sink.....	99
Figure 4.43. Close up view of the heat sink and insulating material together with thermocouples.....	99
Figure 4.44. Heat Transfer Experimental Set-up.....	101
Figure 4.45. <i>Computational Set-up</i>	102
Figure 4.46. (a) Top view of the computational domain. (b) Front view of the computational domain	103
Figure 4.47. Temperature Distribution over the heat sink.....	104
Figure 4.48. Temperature Measurements	104
Figure 4.49. Tensile Strength Specimen.....	105
Figure 4.50. Experimental Tensile Test Setup and fractured samples	106

CHAPTER 1

INTRODUCTION

1.1. Background and Motivation

As electronic industries continuously progress, the performance expectations from the devices also increase. To meet these expectations high-performance processors have been implemented in the devices.

All these high-performance processors generate a considerable amount of heat during operation. For example, Table 1.1 shows some of high-performance electronic devices which are in design process in defense industry and expected to be produced in the following years. In all of these devices, great amount of heat will be created during their operations and this heat should be removed from the system to prevent failures due to the temperature increase in the device.

For the thermal management in electronic systems, generally a thermal conductive metal called “heat sink” shown in Figure 1.1 is used to remove the heat from the system. A proper heat sink should have good thermal properties and maximum surface area to transfer the highest possible amount of heat. However, since design requirements usually put limits on the size of the electronic devices, very limited spaces are left for placing heat sinks parts. Therefore, designing a proper heat sink for successful thermal management is one of the great challenges faced by design engineers in defense industry as well as in the rest of the world.

Table 1.1. Some of future high performance electronic devices in defense industry

Description	Visualization	<i>Expected Generated Heat During Operation</i>
V/UHF Naval-Fixed Station Radio		750-1000 W
IFF Mode 5/S Long Range Interrogator		330 W
ULAK Commercial and Public Safety 4.5G Macrocell Base Station		470 W
Ku-Band Receiver		500 W
Flyaway Satellite Communication		480 W

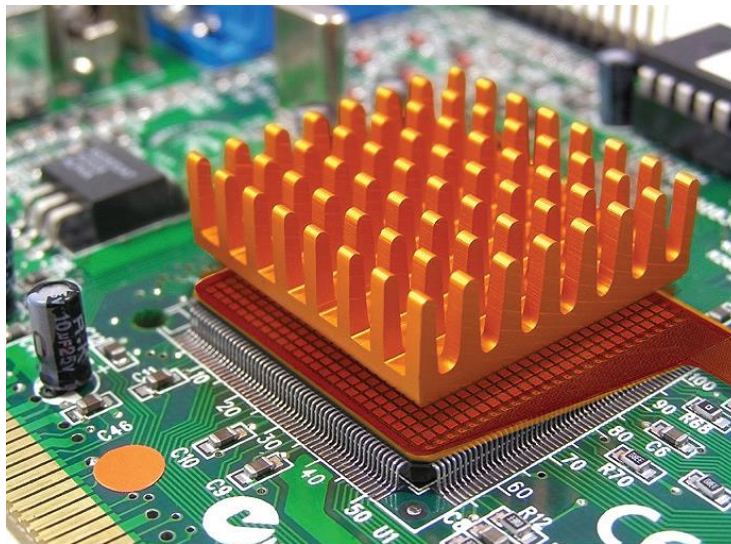


Figure 1.1. A typical heat sink

In order to successfully dissipate the heat generated at the interface of these electronic devices, the first requirement is to choose a suitable material for heat sinks. The thermal conductivity value is the most important criteria for material selection of a heat sink. Thermal conductivity value should be as high as possible, since materials with high thermal conductivity can remove the heat with a small temperature differential. Considering only the thermal conductivity value, it is sufficient to use materials such as copper and aluminum, which have relatively higher thermal conductivity values. Figure 1.2 shows a typical aluminum heat sink used in one of electronic devices used in defense industry.

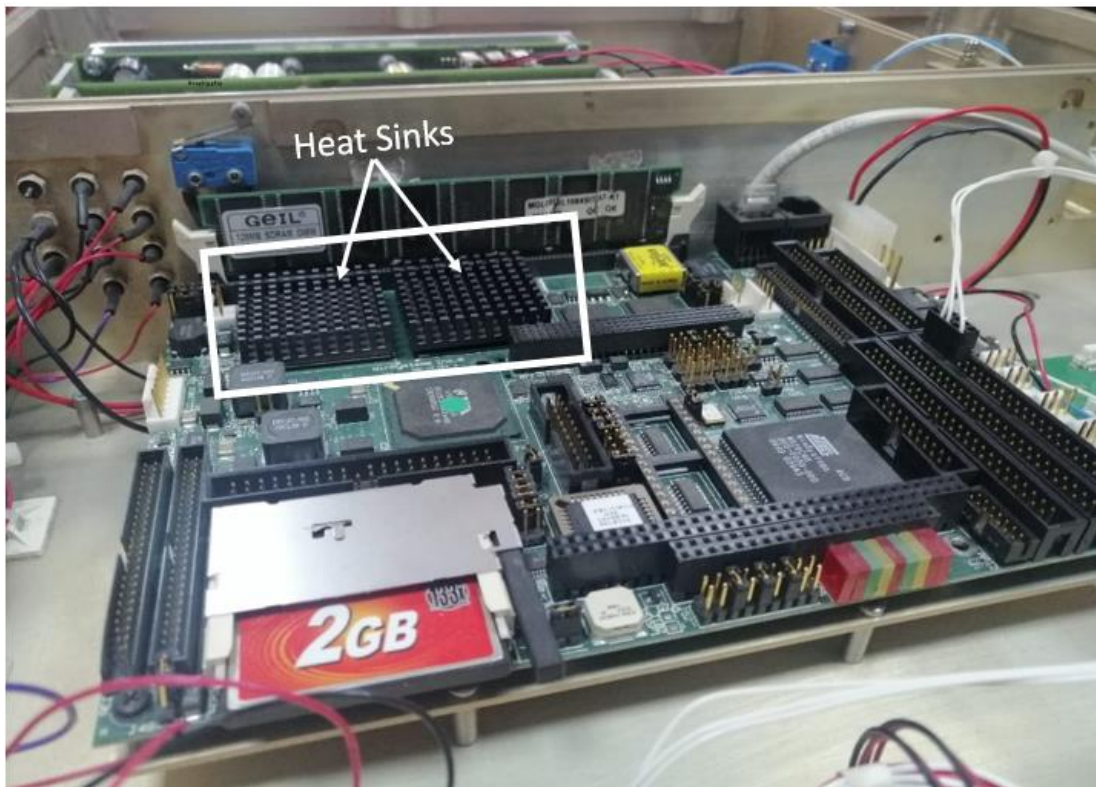


Figure 1.2. A processor and attached heat sink.

There is a second thermal requirement limiting the designers in the heat sink design which is the coefficient of thermal expansion (CTE) of the material used. The CTE value determines how much the material will expand with temperature. As shown in Figure 1.1, heat sinks are used by attaching them to the high performance integrated

electronic chips. Thus, the CTE value of the heat sink material should be compatible with the CTE values of the chip materials such as Al_2O_3 , BeO and AlN [1], so that both parts expand at the same rate when there is a temperature change. Otherwise, if there is a mismatch in the CTE values, both parts expand at a different rate, resulting in thermal stresses on the joint interface, resulting in cracks and fractures on the chip [2].

Aluminum and copper have high thermal conductivities, but they also have high CTE values, almost four or five times greater than the CTE of a typical chip, where the heat sink is attached [3]. This large thermal expansion mismatch gives rise to the thermal stress during the operation of chips, leading to an increase in the probability of thermal fatigue, and possible resultant device failure. Failure risk further increases as the amount of heat removed and consequently operating thermal limits increase. The traditional approach for avoiding this problem is using thermal pads between heat sink and chipset as shown in Figure 1.3.

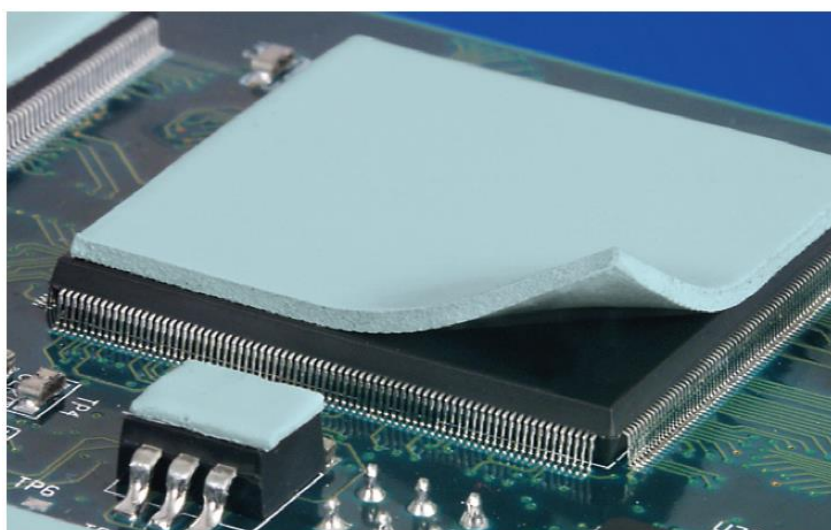


Figure 1.3. Thermal Pad between chip and heat sink.

A thermal pad is a heat conductive pad or plastic material of a certain thickness that is used to establish heat contact between the heat sink and chipset. Since most of the pads are elastic, they can absorb the stress related to thermal expansion differences

between components. It is also used in places where there is a significant gap between the heat sink and the microchip or there is no other way to establish contact between the two.

One of the most important drawbacks of using thermal pads is their thermal conductivity value, which changes between 1-5 (W/m·K). These values are considerably lower than those of heat sinks which are between 200-350 (W/m·K). This creates an additional thermal resistance, which decreases the performance of the heat sinks leading to a considerable increase in the chip temperature.

CHAPTER 2

LITERATURE REVIEW AND THEORY

2.1. Thermal Managements in Electronic Systems

The most important issue in thermal management of an electronic system is to remove the generated heat during operation away from the system to prevent failure. One of the most important factors affecting the heat generation rate of an electronic device is the number of transistors on the processor because as the device operates each transistor dissipates heat [7]. In early devices, transistor count was considerably small. Therefore, the total amount of generated heat was creating no risk for the system operation. During the evolution of microprocessor technology, the number of transistors on a single microprocessor increased exponentially. Moore's Law indicates that the transistor counts in a processor double every two years. The observation was named after Gordon Moore, who was the CEO of Intel, published a paper in 1965 stating that every two years', computers overall processing power will double. Figure 2.1 shows the actual transistor counts in microprocessors in years between 1971-2011, which verifies the Moore's Law. An increasing number of transistor results in greater heat dissipation rates. Moreover, the microprocessor size gets smaller, which creates a considerable amount of heat dissipation density.

Moreover, consumer demand is driving products and innovations toward further miniaturization and more enhanced energy consumption. Simultaneously, users want more capabilities in these smaller and more powerful platforms. Therefore, thermal management in the electronic system is becoming more and more important and critical for the electronics industry [10]. It has proven that the expected operating life of the device double as junction temperature reduces by 10 °C. Moreover, device efficiency will improve as the junction temperature decreases [6]. If simple thermal solutions cannot remove enough heat to preserve the efficiency of components, the system developer must look to more advanced measures, which are explained in section 2.2.

2.2. CPU Cooling Systems

One of the most important issues in thermal management of the electronic systems is to remove the generated heat during operation away from the system to keep the components in their safe operating temperatures. The main methods used for cooling the electronic devices are given in the following chapter:

2.2.1. Passive Cooling

Passive cooling involves an attached block of machined or extruded metal which is called heat sink. Detail information about the heat sinks is given in chapter 2.3.

2.2.2. Air Cooling

When passive cooling is insufficient to remove heat from the systems fans may be used for air cooling. In this type of cooling, fans force air to move which results in blowing away of hot air to outward of the system and forced convection is established. Heat removal capability this type of cooling is higher than passive heat sinks due to the possibility of the forced convection with a fan connected to it. This fan may be attached to the CPU and multiple fans may be contained in a system. Since there are mechanical parts attached to them air cooling is costlier compared to the passive cooling.

2.2.3. Liquid Cooling

Liquid cooling is an extremely efficient way to remove excess heat using a heat transfer fluid. Distilled water is usually used as the coolant in this type of cooling system. Since specific heat capacity and thermal conductivity of water is higher than air, this type of cooling methods provides better cooling efficiency compared to air cooling. In liquid cooling a pump pumps the liquid through the pipes throughout the case of the CPU. The liquid absorbs heat as it passes through the CPU and leaves the system. Compared to air cooling, more heat extraction is possible with this method. Also, ambient temperature has less influence on the liquid cooling and noise-level is lower compared to the active air cooling [54]. The disadvantages of this method include design complexity and potential leakage of the coolant. Leaking coolant and the additives present in the fluid may harm any electronic components which it comes into contact and repair services may be very difficult and costly.

2.2.4. Immersion Cooling

Another cooling method that has been recently applied is immersion cooling. In this type of cooling, CPU components are submerged in a liquid. The liquid should be thermally conductive however it should not conduct electric. The generated heat from the components is transferred to this liquid which they are immersed. This method is more effective compared to air cooling since heat-absorbing capacity of fluids are greater compared to air. The absorbed heat is dissipated from the surface of the liquid to the air. This method is mainly used to cool large electronic device components such as transformers and data centers [54].

2.2.5. Heat Pipe

Heat Pipe is also used for cooling CPU systems. It is basically a hollow tube containing a fluid used for heat transfer. At one end of the pipe, the heat is absorbed by the fluid, then fluid evaporates. The vapor moves to the other end of the pipe where

it condenses and gives up its latent heat. The condensed liquid moves back to the hot end of the tube and cycle repeats. Since effective thermal conductivity values of heat pipes are much higher compared to the solid materials, this method provides better heat transfer ratios compared to passive heat sinks. However, it is not a cost-effective solution and mostly applicable when there are limited spaces available in the design and low noise levels are necessary.

2.3. Heat Sink

2.3.1. General information About Heat Sinks

A heat sink is a thermal conductive metal instrument that is used for transferring the heat produced by mechanical or electrical systems. The heat is usually removed away from the system and transferred to the air, so that the temperature of the device can be controlled at optimum levels [6]. Figure 2.3 shows some of the heat sinks used in the electronic industry.



Figure 2.3. Heat sinks used in the electronic industry

There are two major types of heat sinks which are active and passive namely. Passive heat sinks have no mechanical parts whereas active heat sinks have a fan attached to it as seen in Figure 2.4. Since there are no mechanical parts attached to them, passive heat sinks are more reliable and cheaper. However, the heat removal capability of

active heat sinks is higher than passive heat sinks due to the possibility of the forced convection with a fan connected to it [11].



Figure 2.4. Active Heat Sink

2.3.2. Heat Sink Materials

Aluminum alloys are the most common heat sink materials since their thermal conductivity values are relatively higher and manufacturing Aluminum is easier compared to other elements. Low mechanical strength and low melting temperature make operations like extrusion, stamping or casting simpler. The thermal conductivity values depend on the series of aluminum used, generally grade of 6060 and 6063 [13].

Copper is often used for applications requiring thermal conductivities higher than Aluminum because it has conductivity about twice that. Copper, however, is three times as dense and about four to six times costlier than aluminum depending on the industry. Aluminum may be extruded, but it is not possible for copper. Copper heat sinks may be machined or skived. Another manufacturing technique is soldering the fins into the base of the heat sink [14].

Diamond is another heat sink material, which conducts heat five times better than copper and however since it is too expensive practically it has no usage in the heat sink industry.

Composite materials such as copper-tungsten, copper-molybdenum, etc. can also be used as heat sink materials. As their heat expansion coefficients can be matched to

ceramics and semiconductors, such materials are often used as substrates for heat sinks [14].

2.3.3. Heat Sink Manufacturing Methods

There are different manufacturing methods available for producing heat sinks which are described in the following chapter. [6,15,16]

2.3.3.1. Extruded Heat Sinks

Extrusion is the most common manufacturing method used in the production of the heat sinks. In this method, heat sinks are produced by extrusion under high pressure. This method produces heat sinks with plate fins, particularly by aluminum. Secondary operations are sometimes essential so dependingly general cost may increase. Examples of extruded heat sinks are given in Figure 2.5



Figure 2.5. Extruded Heat Sinks

2.3.3.2. Cold Forged Heat Sinks

Cold forging is an extremely accurate method. With this method, round pin and elliptical pin heat sinks can be produced. The forged heat sinks have excellent microstructure due to high pressure and low temperatures during operation. In forged heat sink the fin arrays are created by pushing raw material by a punch into a molding die. Common forging issues are the strangling of material in the die molding cavity,

which may lead to irregular fin heights. With cold forging, it is possible to produce uniform parts with superior surface finish and high mechanical properties. However, the method applies only the materials which can be forged i.e. aluminum and magnesium.

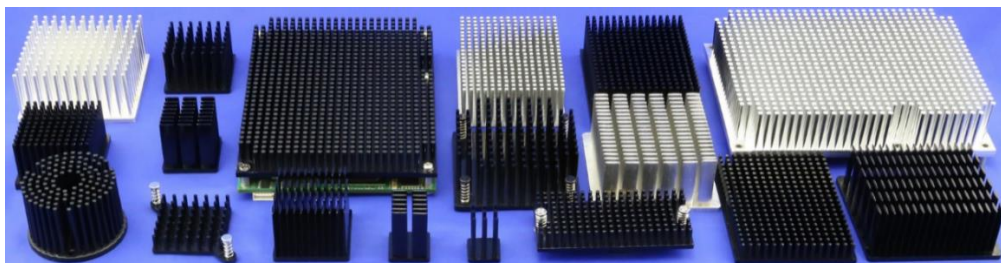


Figure 2.6. Cold forged heat sinks

2.3.3.3. Stamped Heat Sinks

In this process at first metal fins are stamped and then they are soldered onto the foundation. Typical shapes for stamped heat sinks are U shapes. These are usually used for applications in which the heat dissipation rates are small. The advantage of this method is that the manufacturing cost is small due to production automation.

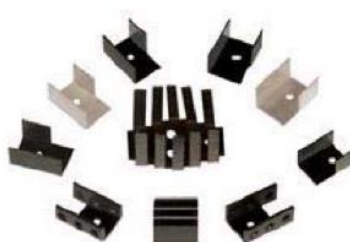


Figure 2.7. Stamped Heat Sinks

2.3.3.4. Bonded Heat Sinks

If the size of the heat sink is large bonding heat sink production method may be applicable. One advantage of this manufacturing method is that the base and fin materials may be different. Also, instead of just one fin material, a mixture of aluminum and copper fins can be used. This enables the enhancing heat efficiency by

adding minimum amount of weight. In general, the heat sinks manufactured by this method offer moderate performance, however, the manufacturing costs are high.



Figure 2.8. Bonded heat sinks

2.3.3.5. Skived Heat Sinks

Skived heat sinks are alternative to heat sinks which are extruded where extrusions cannot achieve the necessary fin densities. With this technology fins with 0.5 cm dense can be achieved. They are manufactured by using a series of sharp knives that curl a tiny metal layer that is bent vertically to shape as they move through the metal. These type of heat sinks are manufactured from a long bar material then they are trimmed to necessary length by the final application. A disadvantage of this process is that a lot of variation and burrs are produced if secondary machining is required.

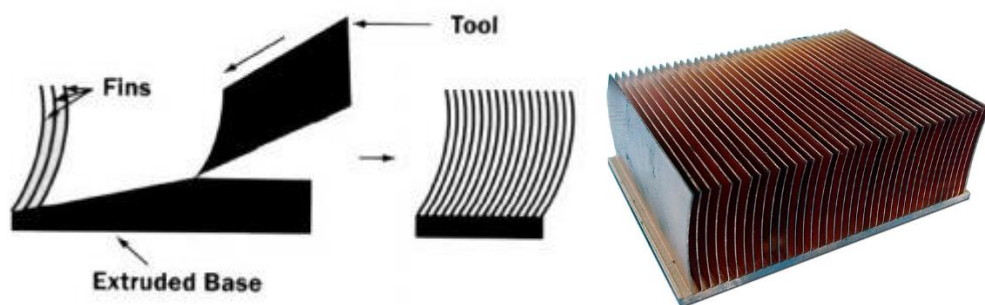


Figure 2.9. Skived heat sinks

2.3.3.6. CNC Machined Heat Sinks

CNC machined heat sinks offer better thermal conductivities and with this process complex geometries are achievable. However, CNC machining comes at a high cost and the longer production times make this method less ideal for large quantities.



Figure 2.10. CNC Machined heat sinks

2.3.3.1. Injected Molded Heat Sinks

The manufacturing method mentioned so far are the more familiar production techniques to the engineers. However, metal injection molding(MIM) process acquiring significance in the last few years and the advantages of the process becoming more evident. With MIM process it is possible to add complex characteristics to the heat sink design which increases thermal performance with much more economical process, especially for large quantities. Injection molding makes it possible to form complicated components as easily as simple geometries, thus enabling greater flexibility in design. With MIM it is also possible to produce several composite materials such as tungsten-copper and molybdenum copper [17].

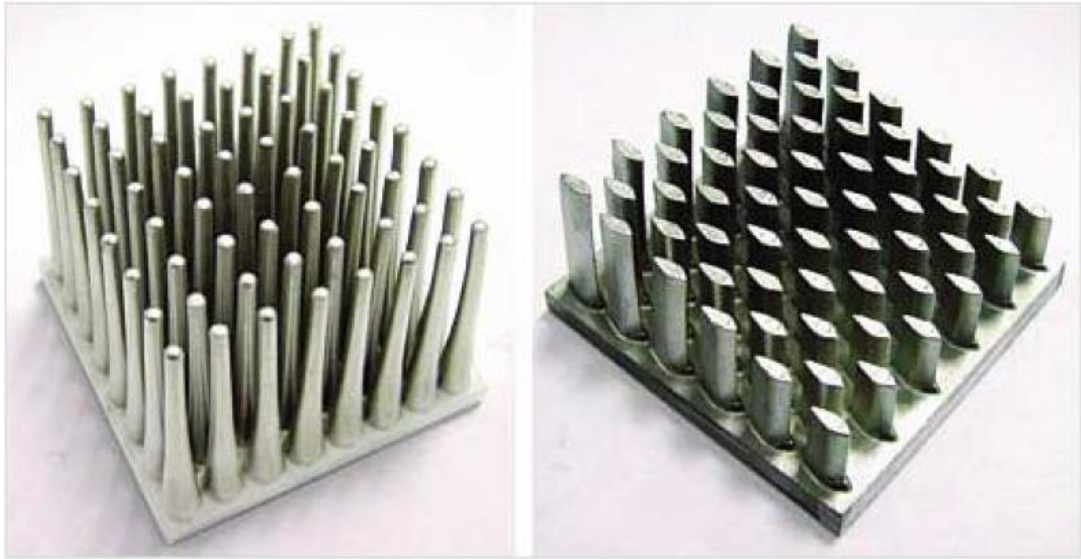


Figure 2.11. Injected molded heat sinks

2.3.4. Heat Sink Attachment Methods

There are different attachment methods used for securing the heatsinks to the electronic devices. Choosing the right method is important to obtain maximum efficiency from the heat sinks. While choosing the method heat sink type, size and application requirements should be carefully considered. A good heat sink attachment method should have the following properties:

- The attachment method should take up as little space as possible on the device and should not cause extra weight.
- The stress created due to attachment method should be minimized
- The method should provide protection and prevent separations under the event of a shock loading, such as an impact or drop.
- If necessary, the attachment method must ensure that the heat sink to be removable for service and maintenance.
- Considering the information's given the most appropriate type of attachment method given below should be selected.

2.3.4.1. Thermal Tape

This attachment method shown in Figure 2.12 is one of the most widely used application methods. The heat sinks are attached to the devices with thermal pads with double-sided adhesive. The method is easy to apply and the most cost effective solution. However, this method has some disadvantages. Since the conductivity of the thermal pads used primarily is low, it creates an additional point of resistance and adversely affects the conductivity. It is also not a very safe bonding method, especially for large and heavy coolers in size. Problems may arise especially in vibration tests. In addition, it is important that the surfaces of the chip and cooler should be very clean before the process to ensure effective adhesion.

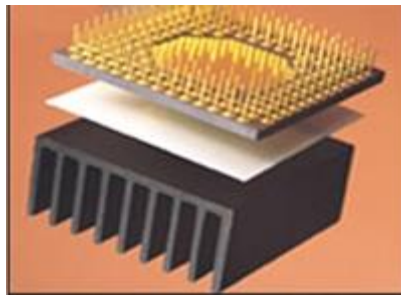


Figure 2.12. Thermal Tape

2.3.4.2. Thermal Epoxy

Attachment with epoxy is costlier than thermal tape, but offers a higher mechanical bond between heat sink and element, as well as increased thermal conductivity. Most epoxies have two-part liquid formulations that need to be carefully mixed before the application. The introduced epoxy is then cured for approximately 48 hours. In this attachment method, the bond between the heat sink and chip is permanent and re-work is almost impossible

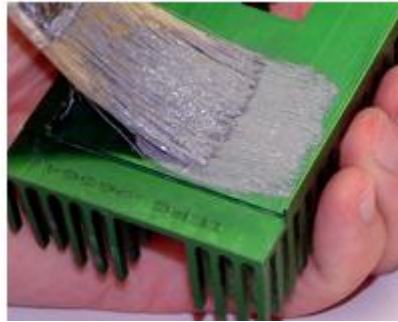


Figure 2.13. Thermal Epoxy

2.3.4.3. Z-Clip Attachment to the PCB

The z-clip attachment is a wire with a shape of Z as shown in Figure 2.14. For this type of attachment, holes and anchors are necessary on the printed circuit. One side of the clip hooks on to an anchor, then by deflecting and by passing through the heat sink fins, other side of the clip hooks on the opposite anchor. The spring load is developed on the component due to the deflection of the clip which retains a very good contact and provides mechanical attachment. This type of bonding method is more expensive than tapes and epoxies. Moreover, if Z-clip attachment is not designed properly, heat sink may warp due to high load and instead of surface contact point contact may be established between heat sink and chip, which decreases the total thermal efficiency.

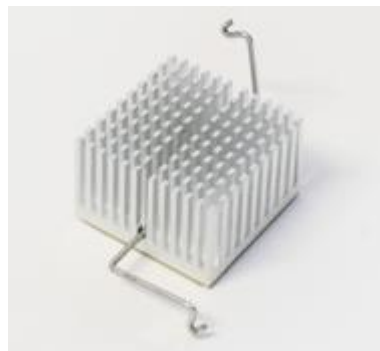


Figure 2.14. Z-Clip Attachment

2.3.4.4. Push Pins

For larger heat sinks, push pins with compression springs are an effective mounting. In this attachment method pushpins are used for attachment as shown in Figure 2.15. Assembly is held together by the compression spring. The spring also retains a strong and secure contact between heat sink and the chip. It should be noted that if too much force is applied during insertion there may be cracking or component failure, therefore care is needed during attachment.

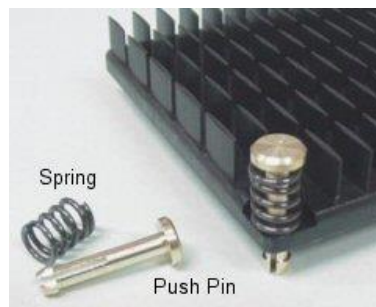


Figure 2.15. Push Pins

2.3.4.5. Threaded Standoffs

If the heat sink is very large the recommended method is threaded standoff which is a hollow metal tube with internal threads as shown in Figure 2.16. Heat sink is secured to the PCB with a screw. Two to four standoffs are used depending on the size of the heat sink which increases the cost. Moreover, holes in the PCB are necessary for this kind of attachment.



Figure 2.16. Threaded Standoffs

2.3.5. Heat Sink Design

When selecting and designing a heatsink the most important two parameters are the geometry of the heat sink and heat sink material. To understand the effects of these parameters, very basic heat transfer information is given below.

A heat sink dissipates heat by transferring energy from a high-performance device to a fluid which is usually air. The heat is transferred from heated chip to air first by conduction and then convection. By conduction, heat energy is transferred across a medium as given in Figure 2.17. The thermal conduction formula according to Fourier is given below:

$$Q = \frac{k \cdot A_c}{L} \cdot (T_1 - T_2) \quad (2-1)$$

Where

- Q : Heat (watts)
- k : Thermal conductivity (watt /m.°C)
- A_c : Contact area (m²)
- T : Temperature (°C)
- L : Material thickness (m)

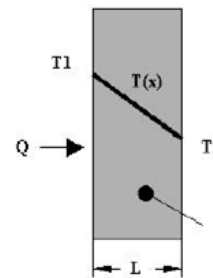


Figure 2.17. Thermal Conduction

Before the further debate, defining common terms and defining the concept of a thermal circuit is useful. As in electrical circuit analysis, it is possible to rewrite conduction equation (2-1) as:

$$Q = \frac{(T_1 - T_2)}{R_c} \quad (2-2)$$

Where

$$R_c = \frac{t}{k \cdot A_c} \quad (2-3)$$

R_c called thermal conduction resistance. Circuit analysis usage in electrical and thermal equations are shown in Figure 2.18

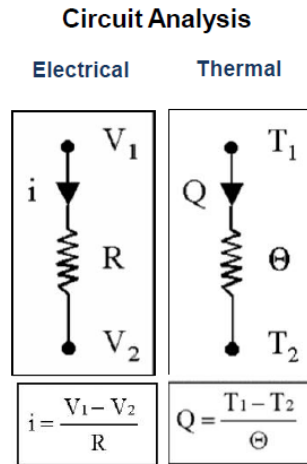


Figure 2.18. Circuit Analysis in Electrical and Thermal Equations

In the case of convection, the heat energy transferred between a moving fluid and a surface as shown in Figure 2.19. In heat sink design, the heat is transferred to air from the heat sink surface. The convection formula is given in (2-4).

$$Q = h_c A_c \cdot (T_s - T_a) \tag{2-4}$$

Where

- Q : Heat(watts)
- h_c : Heat transfer coefficient (watt /m.°C)
- A_c : Surface area (m²)
- T_s : Surface temperature(°C)
- T_a : Ambient temperature(°C)

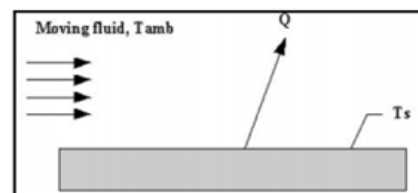


Figure 2.19. Thermal Convection

Equation (2-4) can be rewritten as:

$$Q = \frac{(T_s - T_a)}{R_h} \tag{2-5}$$

Where

$$R_h = \frac{1}{h_c \cdot A_c} \quad (2-6)$$

R_h called thermal convection resistance. Total thermal resistance of the heat sink is given as sum of the conduction and convection thermal resistances as shown in Figure 2.20

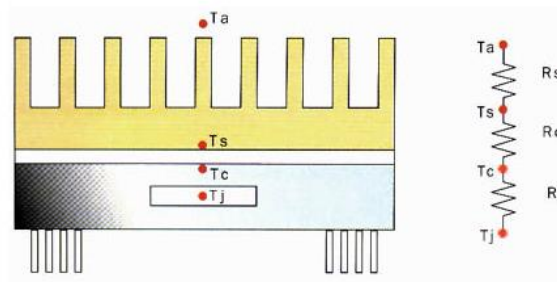


Figure 2.20. Total Thermal Resistance

The simplified heat transfer equation across the heat sink is given in eqn. (2-7).

$$Q = \frac{(T_a - T_{s1})}{R_c + R_h} \quad (2-7)$$

Where

Q : Heat removed from the system (watts)

h_c : Heat transfer coefficient (watt /m. $^{\circ}$ C)

Ts : Surface temperature of the chip connected to the heat sink($^{\circ}$ C)

Ta : Ambient temperature($^{\circ}$ C)

Rc : Conduction Resistance

Rh : Convection Resistance

In this equation, surface temperatures of the heat sink and chip assumed to be equal since they are attached to each other. If surface temperature and the ambient temperatures are constant, to maximize the heat removed from the system, the sum of the conduction resistance and convection resistance should be minimized. Considering eqn.(2-3) and (2-6) to minimize the resistance values, thermal conductivity value and

the surface area should be maximized. Therefore, while deciding material and geometry for the heat sink two most important design criteria are material selection and geometry of the heat sinks. These criteria are investigated in detail in the following chapters.

2.3.5.1. Material Selection

The thermal conductivity value is the most important criteria for material selection for a heat sink when high thermal conduction is necessary. In order for the heat sink to perform well, thermal conduction value should be as high as possible, because materials with high thermal conductivity can better transmit heat. Considering only the thermal conductivity value, it is sufficient to use materials with high heat transfer coefficient such as copper and aluminum as heat sink material, but there is a second requirement limiting the designers in the heat sink design which is the CTE of the material used. The CTE value determines how much the material will expand with temperature. As shown in Figure 2.21 the heat sinks are used by attaching to the high performance integrated electronic chips. Thus, the CTE value of the heat sink material should be compatible with the CTE values of the chip materials such as Al_2O_3 , BeO and AlN [1], so that both parts expand at the same rate when there is a temperature change. Otherwise, if there is a mismatch in the CTE values, both parts will expand at a different rate, resulting in thermal stresses on the joint interface, resulting in cracks and fractures on the chip. Since the CTE values of the IC (chip) elements are around $4\text{-}8 \times 10^{-6}/\text{K}^{-1}$, it is stated in the literature that the ideal CTE of the heat sink material should be also between $4\text{-}8 \times 10^{-6}/\text{K}^{-1}$ and thermal conductivity value should be high [3].

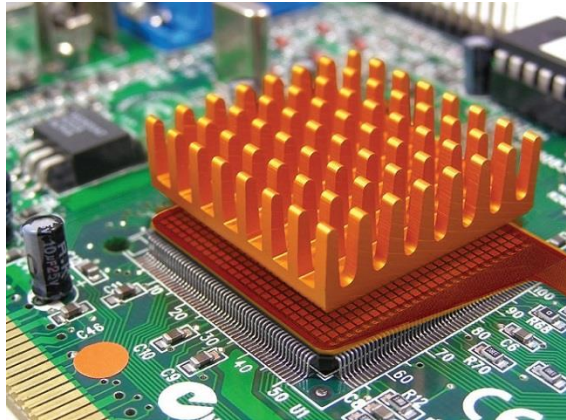


Figure 2.21. Heat sink used in a system

Table 2.1 illustrates the thermal conductivity and CTE values of the materials. When high thermal conductivity is the design requirement, the most commonly used material is Copper. Aluminum, on the other hand, is not as conductive as copper, but its low density makes it appropriate for the applications where the low weight is required such as laptop computers and aircraft electronics. However, both suffer from a high value of the CTE. There are metals like molybdenum, tungsten and alloy invar which have low CTE values, however, their conductivity values are also very poor. Diamond's conductivity value is very high and it has low CTE, but it is very expensive [6].

Table 2.1. Thermal properties of various materials at room temperature[19]

Type of Travel	Thermal Conductivity (W/m K)	CTE ($10^{-6}/^{\circ}\text{C}$)
Aluminum	24.10	23
Gold	22.83	14
Copper	398	17
Lead	30	39
Molybdenum	142	4.9
Tungsten	155	4.5
Invar	10	1.6
Kovar	17	5.1
Diamond	2000	0.9

Since pure elements do not meet the necessary thermal requirements, new composite materials are developed such as W-Cu, MO-Cu, SiC-Al. These composites combine high thermal conductivity with matched CTE values appropriate for many heat sink applications. Thermal conductivity and CTE values of these composites are given in in Table 2.2. W-15Cu has higher thermal conductivity value compared to Mo-18Cu and it is a common heat sink composition. Mo-18Cu, on the other hand, has a lower density and it may be used for the applications where weight is important.

Table 2.2. Properties of tungsten-copper and molybdenum-copper heat sink materials[13]

	Thermal Conductivity (W/m K)	CTE ($10^{-6}/^{\circ}\text{C}$)
W-15Cu	190	7.4
Mo-18Cu	140-160	7

Today, composite materials of tungsten–copper (W–Cu) are used in many applications since this material successfully combines the adorable thermal and electrical properties of Cu and low CTE values, high melting temperature and high wear resistance of W. The physical properties of each material at room temperature are shown in Table 2.3. WCu composites are primarily used for electrical contacts, particularly in high voltage, welding electrodes, EDM machines, and heat sinks [21].

Table 2.3. The physical properties of W and Cu at room temperature [20]

<i>Properties(Unit)</i>	<i>W</i>	<i>Cu</i>
Density (g/cm^3)	19.32	8.96
Expansion Coefficient($10^{-6}/^{\circ}\text{C}$)	4.5	16.6
Thermal Conductivity(W/m·K)	174	403
Specific Heat Capacity(J.kg/ $^{\circ}\text{C}$)	136	385
Elastic Modulus(GPa)	411	145
Poisson Density	0.28	0.34
Melting Point ($^{\circ}\text{C}$)	3387	1083
Vapor Pressure(P_a at T_{melt})	1.3×10^{-7}	5.05×10^{-2}
Tensile Strength(MPa)	550	120

Considering these superior properties copper tungsten composite selected as heat sink material for this project. To decide the elemental composition, thermal properties of the copper tungsten with respect to element compositions given in Table 2.4 had been investigated. This table shows that as copper ratio increases, the CTE value and thermal conductivity values of the composite increase. As mentioned in 2.3.5.1 thermal design requirements for heat sink are to have high thermal conductivity values and CTE values between $4-8 \times 10^{-6}/^{\circ}\text{C}$. According to Table 2.4, W85Cu15 and W80Cu20 composites have thermal properties that are closest to thermal requirements, therefore in this work, these elemental compositions are decided to be used for heat sink production.

Table 2.4. Thermal properties of the copper-tungsten composite [22]

Material	<i>W90I0Cu</i>	<i>W85Cu15</i>	<i>W80Cu20</i>	<i>W75Cu25</i>
Tungsten Content	90±1	85±1	80±1	75±1
Density at 20°C (g/cm ³)	17	16.3	15.6	14.9
Coefficient of Thermal Expansion (10 ⁻⁶ /°C)	6.5	7.0	8.3	9
Thermal Conductivity (W/m·K)	180-190	190-200	200-210	220-230

W and Cu do not dissolve on each other [20]. Moreover, the melting temperatures are widely differing from each other, and these materials do not alloy, therefore CuW parts are produced by powder metallurgy techniques [23]. There are different powder metallurgy techniques available but when the produced parts are complex in geometry the recommended technique is Metal Injection Molding (MIM).

With MIM it is possible to produce parts with complex geometries as easily as simple geometries, thus enabling design freedom. MIM can also fulfill the tolerance requirements so there is no need for secondary operations [17]. The details about the MIM process is given in section 2.5.

2.3.5.2. Geometry

As stated earlier heat sink surface area is one of the most important parameters that influences the heat sink performance. Heat sinks have usually pins or extensions to increase the amount of heat that they can transfer to the ambient air stream.

The most widely used pin fins are pin fin, straight fin and flared fin designs as shown in Figure 2.22 [25]. The most common heat sink type available in the market is pin fin type. In pin heat sink, there are pins extending from the base. The pins may be cylindrical, square or elliptical depending on the application. Straight fin is another common type of heat sink fin arrangement. In this type of heat sink, fins run the entire length of the heat sink. Flared heat sinks have fins that are not parallel to each other which creates more convection surface area and also decreases flow resistance.

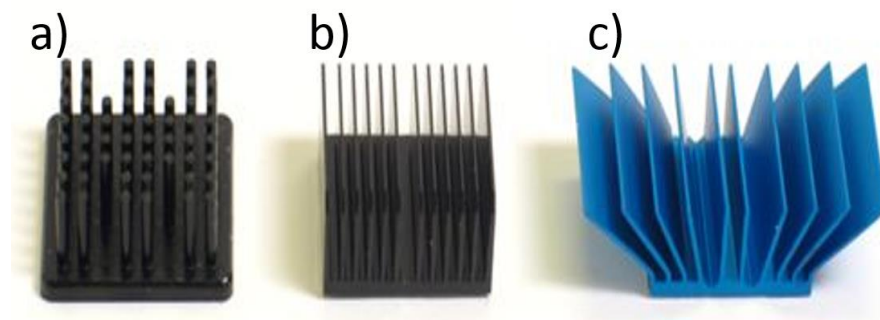


Figure 2.22. Pin (a), straight (b) and flared(c) fin designs

A pin heat usually offers better performance compared to the other type of heat sinks since the surface area is greater and it allows air to flow around the fins without interruption.

In Figure 2.23 thermal resistances of fin-type and thin-walled type of heat sinks which have similar dimensions are given. As can be seen from the graph, thermal resistance of the plate-fin heat sinks are 2-3 times greater than that of the round-pin heat sink. Therefore, in this work a rounded pin type heat sink is chosen as heat sink geometry type.

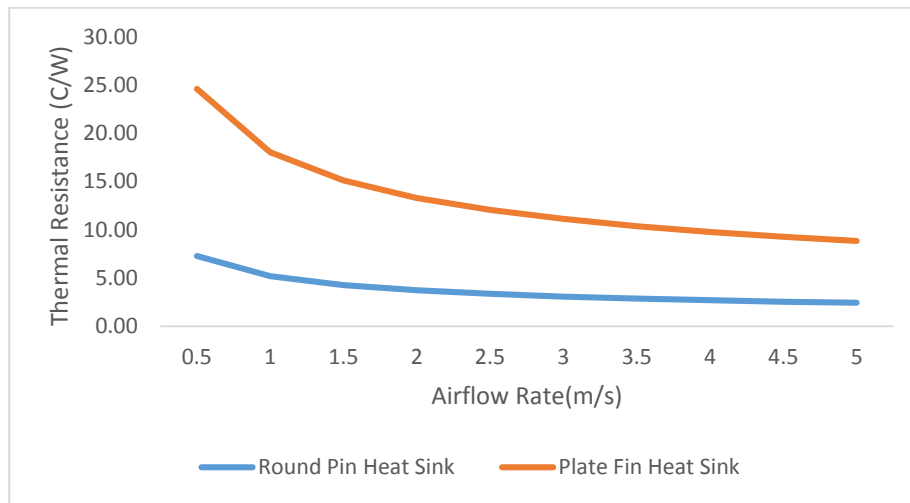


Figure 2.23. Thermal Resistances of fin-type and thin-walled type of heatsinks

2.4. Heat Sink Studies in Literature

There are many studies in the literature on the preparation of the structure of copper tungsten powder and analyzing the mechanical and thermal characteristics of the sintered parts. However, there are only a few published studies on the heat sink of copper tungsten parts produced by metal injection molding process. The studies in the literature about the Cu / WCu heat sinks which were produced with metal injection molding were summarized below.

J. Cheng et al. [26] studied producing small W-20 wt%Cu balls shown in Figure 2.24 by metal injection molding process by using commercial tungsten and copper powders as raw material. After injection defect-free parts were obtained and nearly all binders extracted by solvent and thermal debinding steps. With this MIM process, the parts which have relative density values of more than %95.58 could be achieved. The microstructure of the produced W-Cu balls was fine and homogeneous, and parts have good mechanical properties. This present work shows that for relatively easy geometry MIM process can provide excellent results.

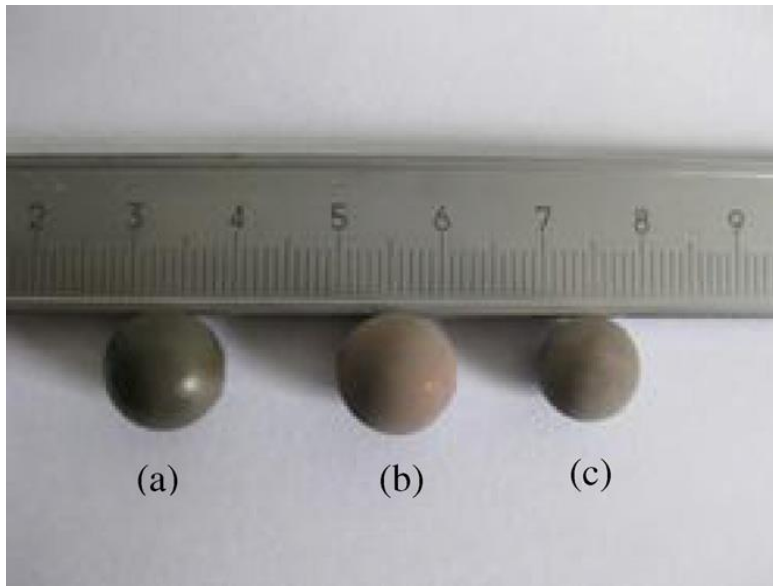


Figure 2.24 Images of the W-Cu balls [26]

M. Leers et al. [27] presented the current status of production of heat sinks with micro structured surfaces as shown in Figure 2.25 by MIM for thermal management applications in his study. This design has three parts bottom-middle and top. The cooling structure is contained in the top layer, the middle layer acts as a barrier and cooling water is supplied through the bottom layer. The goal is to achieve a sinter thickness of 1 mm. W80-Cu20 is used as heat sink material. Densities of more than %98 may be achieved by the sintering process.

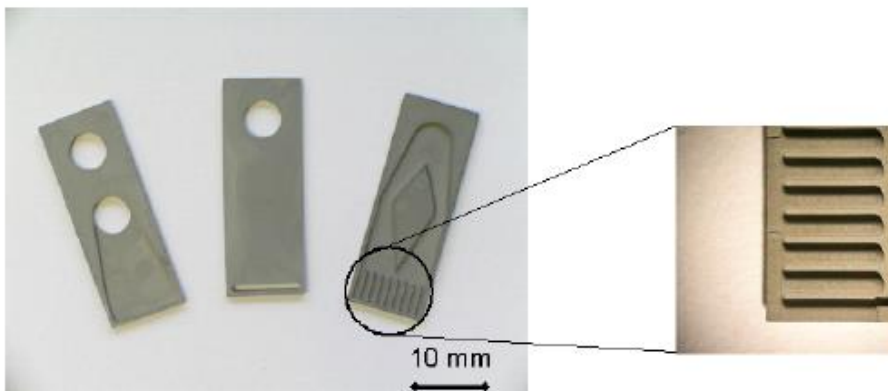


Figure 2.25 μ -MIM moulded heat sink parts

P.W.ho et al. [28] studied producing void free metal matrix composites to near net shape by two material MIM and liquid infiltrations. For this work a specially designed die which were intended to use for producing testing parts which contained features including linear gaps of varying separations, holes of various diameters, undercut platform and raised platform with features as shown in Figure 2.26. Study revealed the effect of the MIM parameters such as sintering temperature on the studied part.

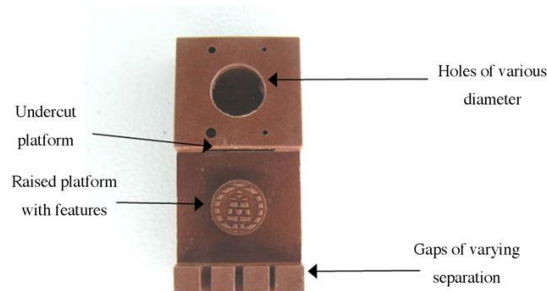


Figure 2.26 Test part used in the study

Johnson [29] mentioned a Cu heat sink shown in Figure 2.27 which was produced with MIM method. This design was approximately 20x20x2.5 mm in dimensions. The powder used was water-atomized and was mixed at solids loading of 52 vol% with a wax-polymer binder. Binder were removed during debinding and heating stage in sintering. Result was the parts whose relative density was 94% density and thermal conductivity was 296 W/ (m.K)



Figure 2.27 An example MIM Cu heat sink

Zauner et al. [30] also used copper powders to produce heat sinks for thermal management applications by MIM and investigated the thermal performance of the produced part. For this study, the heat sink shown in Figure 2.28 is produced by MIM process by using Cu powders. This part is a heat sink for automotive thermal

management applications where a power LED is mounted on a PCB on a flat surface. According to the results, four-fold increase in energy dissipation could be achieved as compared to a pressure aluminum die-cast solution which offers huge potential for similar applications.



Figure 2.28. LED heat sink for thermal management

Zlatka et al.[30] gave an example to Cu heat sink produced by MIM shown in Figure 2.29 In his study he emphasized the higher densities should be acquired to have high thermal conductivity values. Study also reveals that primary factors that control the thermal conductivity values are porosities and traces of metallic impurities. Therefore, the porosity and metallic impurities should be avoided during production.



Figure 2.29. PIM shaped copper heat sinks designed for cooling in electronics

Goudah et al. [30] prepared four different loading feedstocks from gas atomized copper powder with the wax binder system for his study. The injection molding was

carried out at a low pressure and solvent and thermal debinding were performed for binder removal. Sintering was carried out in argon atmosphere at 900 °C. According to the study, a feedstock containing 59% by volume copper produced and selected as optimum feedstock.

Johnson [13] summarized the thermal conductivity and CTE values of the copper-tungsten and copper-molybdenum heat sinks produced by MIM process as shown in Table 2.5. This table reveals that tungsten with 15-20 weight percent of copper (W-15Cu and W-20Cu) is a common heat sink composition. Molybdenum with 18% by weight copper (Mo-18Cu) also used for heat sink material but it has a lower thermal conductivity compared to W-Cu composites. However, since its density value is lower, it may be used in applications where weight is important. CTE values of both composites are lower than pure copper, they are suitable for use as heat sinks for chips in electronics.

Table 2.5. Thermal properties of the copper-tungsten and copper-molybdenum

	MIM W-15Cu	Infiltrated W- 15Cu Sheet	MIM Mo- 18Cu	Infiltrated Mo- 15Cu Sheet
Density (g/cm ³)	15.6-16.2	16.4	9.3-9.5	10
Thermal Conductivity (W/mK)	180-190	190	140-160	160
Coefficient of Thermal Expansion (10 ⁻⁶ /°C)	7.2	7.4	7.0	7.0

Zlatka et al. [33] studied molybdenum and tungsten copper alloys which are promising materials for HF microelectronic housing. In the study MIM operations were performed with three different feedstock. According to the study, the sintering behavior strongly depends on the copper content and tungsten particle size. The mechanical and physical properties of the produced parts meet the requirements and properties can be further optimized by varying copper content.

2.5. MIM Operations

As explained in section 2.3.5.1 composites W-85Cu and W-20Cu were selected as heat sink material for the study. Since copper and tungsten do not alloy and their melting temperatures are widely different, CuW parts are produced by powder metallurgy techniques [23]. There are different powder metallurgy techniques available but when the produced parts are complex in geometry the recommended technique is MIM. The features of metal injection process are listed below:

- Up to %99 theoretical density values.
- Excellent surface finish therefore no need for secondary operations.
- Great shape complexity

The researches show that global metal injection molding market size exponentially increasing (see Figure 2.30). Manufacturers in the world prefer metal injection molding because of minimum finishing operations which reduces the material wastage and enabling the production of unlimited components with enhanced properties

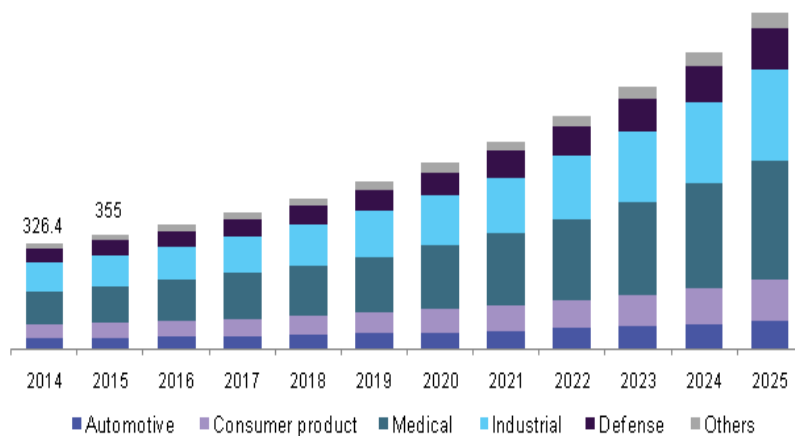


Figure 2.30. Global Metal Injection Molding Market [50]

Advantages of MIM operations compared to other manufacturing methods are given in Table 2.6 [31].

Table 2.6. Comparison of MIM with other manufacturing methods

	<i>Metal Injection Molding (MIM)</i>	<i>Press and Sintering (P/S)</i>	<i>Investment Casting</i>	<i>Machining</i>
Density (%)	95-100	85-95	95-99	100
Strength (%)	95-100	70-90	95-98	100
Surface Finish (μm)	0.4 to 0.8	<2	3	0.4 to 2
Wall thickness (μm)	0.1 to 10	≥ 2	≥ 5	≥ 2
Complexity	high	medium	medium	high
Suitable Production Volume	medium to high	medium to high	low to medium	low
Size Range	0.003g to 250g	0.1 to 10 kg	≥ 1 g	≥ 0.1 g

Process selection based on the quantity and complexity of the produced parts is also shown in Figure 2.31. According to this figure, compared to die casting with MIM it is possible to produce more complex parts. Similarly, with traditional powder metallurgy techniques it is not possible to produce complex designs. These complex designs are possible with EDM or CNC machining but for large volume since the production cost will be very high it will not be a proper choice. Finally, with MIM it is possible to provide more accurate details and better surface finish compared to investment casting. If the manufactured part is small, MIM method is more competitive compared to casting.

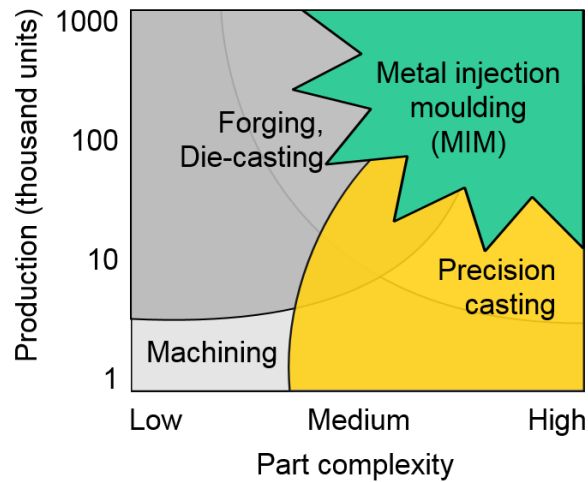


Figure 2.31 Comparison of MIM to the other process [33]

The MIM process consists of four basic steps as shown in Figure 2.32. First, a powdered mixture of polymer and metal called “feedstock” is prepared. Second, the feedstock is molded by feeding into an injection molding machine to form into any desired geometry, just as in plastic molding. Third, for removing the binder, the molded part is placed inside to the low temperature oven and the powder skeleton structure of the original shape and size is left. Finally, the debound parts are sintered in a high-temperature furnace and controlled atmosphere to achieve a net-shaped, full density metal part. Depending on the requirements, after MIM operations secondary operations such as machining, coining or surface treatment may be required [34].

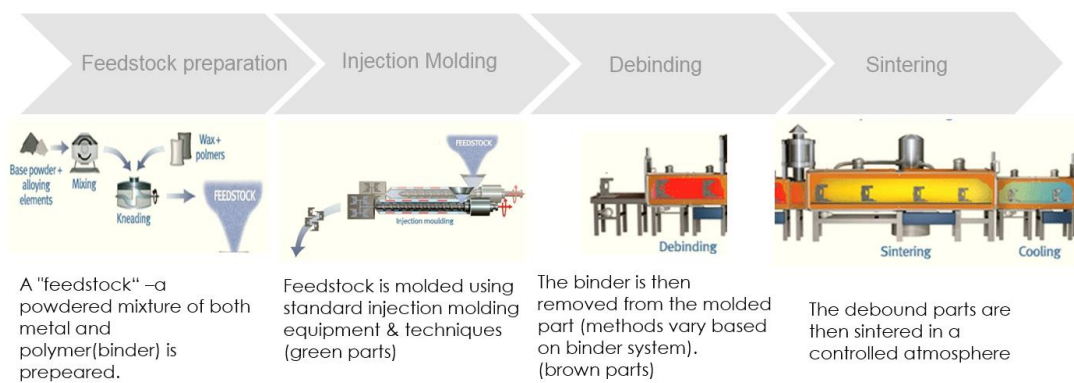


Figure 2.32. Metal Injection Molding Steps

2.5.1. Feedstock Preparation

Feedstock is a mixture of metal powders and binder systems. Binder systems enable metal powders to be moulded as plastic parts. The feedstock's attributes are determined by the type of metal powder, binder composition, particle size and shape, and powder binder ratio and mixing methods. To provide dimensional control in the finished products the feedstock should be carefully designed so that it will be stable with time, it will have sufficient uniformity to provide dimensional control and it will be easy to mould.

The feedstock preparation steps are shown in Figure 2.33. First, the binder is heated to its melting temperature, then the metal powder is added to the binder for a specified time period. During mixing special care is required to achieve uniform mixture. Then the mixture is cooled and removed from the mixer. The next step is extruding and cutting the mixture into pellets for easy feeding the feedstock into the moulding machine. While preparing the feedstock weighing and monitoring must be precise, otherwise, small change in any operation gives rise to variations in final properties after sintering [37].



Figure 2.33. Feedstock Preparation Steps

Optimum binder composition is critical for successfully manufacturing metal injected parts. To exact compositions and procedures of the binder formulas are still proprietary secrets, however, the main ingredients of the most binder systems are mixtures of organic compounds, natural waxes or synthetic polymers. Other substances may be added to modify the properties. Table 2.7 indicates the main binder systems for debinding systems [38].

Table 2.7. Main Binder systems used in MIM

Binder	Main Ingredients	Polymer Backbone	Additives
Thermoplastic Binders	Paraffin / Microcrystalline / Carnauba / Beeswax / Vegetable / Peanut oil / Acetanilide / Antipyrine / Naphthalene / PEG	PE, PP, PS, PA PE-VA, PE-A, PP-A, PMBA-E-VA	Stearic / Oleic acid and esters thereof, phthalic acid esters
Polyacetal Binder	Polyoxymethylene		Proprietary
Gelatine Binders	Water	Methyl cellulose / Agar	Glycerine / Boric acid

2.5.2. Injection

The second step of MIM process is Injection Molding which includes heating the feedstock to the elevated temperature such that they are melted, then forcing this melt into the chamber where it cools and attains the final compact shape. The aim is to achieve the desired shape with a homogeneous distribution of powder which is free of voids or other defects [37].



Figure 2.34. Injection Molding Machine (Courtesy Arburg)

This step operates much the same way as plastic injection molding. For injection operations, injection machines with similar tool designs are used. However, because of the metal ingredients, the feedstock materials are more abrasive than plastics, and they are injected at higher pressures. Therefore, for the parts that come into contact with the feedstock, materials which are wear-resistant used. So today, many manufacturers of injection molding machines supply machines specially equipped for MIM process [38].

Compared to the plastic injection molding process, it is more complex and difficult to monitor MIM process because in MIM the moulded parts are not in their final phase and therefore all final properties cannot be watched during moulding state. With injection molding only the shape of the parts is retained, other mechanical and thermal properties are developed during the following steps of the process [38].

2.5.3. Debinding

As stated in previous chapter, the feedstock is a mixture of binders and metal powders that makes the mixture moldable in an injection molding machine. In debinding step, binders should be removed from the mixture. Usually, binder has two ingredients. The first one is used for opening a network of pores through which the second binder may escape. Therefore, the first binder may be easily removed in low temperatures by water or solvent debinding. Second binder, however, should retain its shape until high temperatures where diffusion bonds between the metal powders are established so that molded shape is maintained. This binder melts and escapes through the channels at high temperatures through the network channels which the first binder opened up. Some additional components are added to binder formula so that binder can wet the powder surfaces and a bond between two binder components may be established. These additional components are removed during either primary or secondary debinding [29].

2.5.3.1. Primary Debinding

In primary debinding a solvent i.e. perchloroethylene, trichloroethylene, n-propyl bromide, methylene chloride and hexane are used to remove soluble ingredients of the binder. This process is performed at low temperatures therefore easy to apply. First injected parts are immersed in a solvent sufficiently long time until all the primary binder is dissolved. Then the parts are taken from the solvent and at a certain temperature, parts dried to solvent free condition for a specific time. The time required for successful debinding depend on the part shape and binder type. The method for determining the successful debinding time is monitoring the samples by weighing them in every 30 minute. When the weight loss stops it means the debinding process for the part is over. So this time and temperature are noted and used for the consequent debinding operations [29].

2.5.3.2. Secondary Debinding

The purpose of using secondary binders is holding the powder particles and retain the moulded shape after the primary binders are removed via solvent debinding. When the primary binders removed a network of inter-connected pore is generated without causing any defects in the shape. The secondary binders removed thermally at elevated temperatures. This is accomplished by heating the parts slowly to the temperature where the evaporation begins and keep the temperature until all the binders are removed. After secondary debinding parts are ready for sintering [29]. Figure 2.35 shows the sketch of debinding process [40].

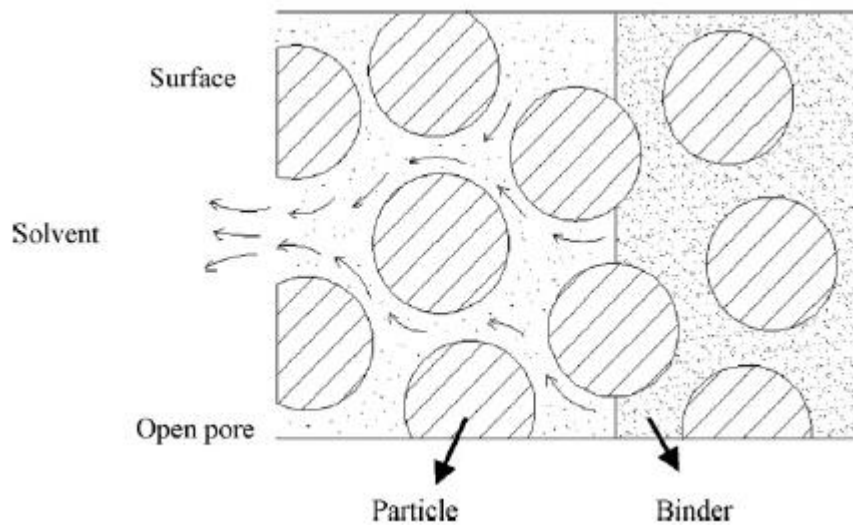


Figure 2.35. Sketch of the solvent debinding process

2.5.4. Sintering

Sintering is the last process of metal injection molding process and the purpose is to remove the remaining binder from the material and convert the powder into a strong metal part.

By sintering, it is possible to reduce the empty spaces to around 1% which enables the production of high-density metal parts with up to 95-99% theoretical sinter rate. After sintering, usually there is no need for secondary operations to improve part tolerance or surface finish. There are three types of sintering mechanisms:

- Solid Phase Sintering
- Liquid Phase Sintering
- Reactive Phase Sintering

The melting points of W and Cu largely differ from each other and the wetting angle of liquid Cu on W surfaces is very high. Therefore, the liquid phase sintering process is widely applied to sinter W-Cu composites [20].

2.5.4.1. Liquid Phase Sintering

In the liquid phase sintering one of the components melt and liquid forms. This liquid assists densification. Therefore, the sintering temperature should be set above the melting temperature of one of the components. For an effective liquid phase sintering liquid should wet the particles. In liquid sintering of W-Cu parts, molten Copper wet the Tungsten Particles.

Figure 2.36 shows the liquid phase sintering mechanism. At initial state powders were mixed and there exist pores between the particles. During heating, a melt forms and the newly formed liquid penetrates between the solid grains, dissolves the sinter bonds and induces grain rearrangement [40].

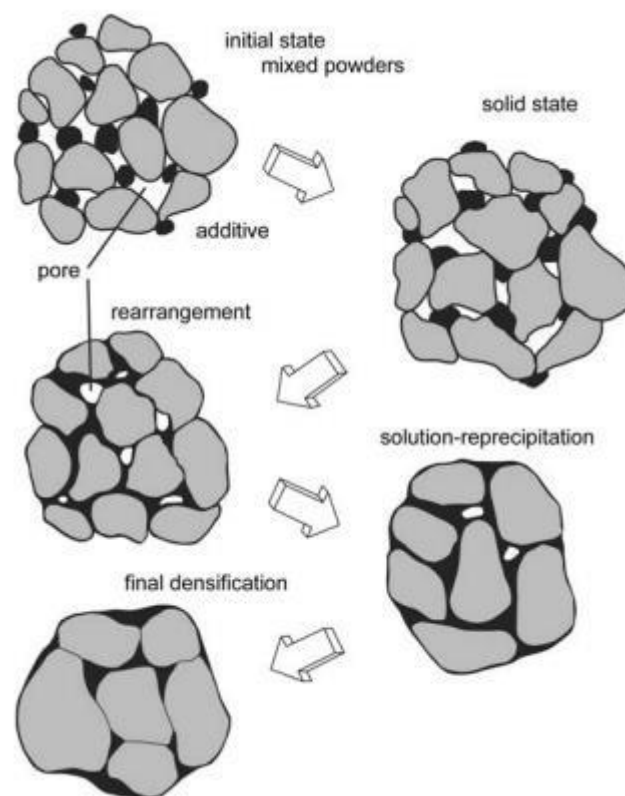


Figure 2.36. Liquid Phase Sintering Mechanism [40]

2.5.4.1. Sintering Atmosphere

The final properties of the parts produced by MIM process also depend on the atmosphere where sintering is performed. Sintering atmosphere prevents metal parts from oxidation by protecting them from the effect of air, because sintering should be never performed in air or oxygen-rich atmosphere. Oxide is normally present on all materials. The contact between metal particles and the subsequent bonding is prevented by this oxide layer. Therefore, this oxide layer should be reduced to allow the particles to come in contact. The typical sintering furnace atmosphere contains hydrogen. As a result of the reaction between the hydrogen and oxygen in the oxide layer, oxidation is performed [37].

CHAPTER 3

EXPERIMENTAL STUDY

3.1. Feedstock Purchase

As explained in section 2.3.5.1, composites W-20Cu and W-15Cu were selected as heat sink materials. For MIM operations the first requirement is to have well-prepared feedstock material. To provide dimensional control in the finished products this feedstock should be carefully designed so that it will be stable with time, it will have sufficient uniformity to provide dimensional control and it will be easy to mould. There are companies in the world which are specialized in preparing feedstocks for MIM process. The feedstocks were purchased from these companies in order to prevent problems that may arise due to the feedstock quality during MIM operations. According to project requirements and product availability, the feedstocks W-20Cu and W-15Cu were purchased from two separate producers. The technical information's about these feedstock's are given in Table 3.1

Table 3.1. Feedstock Properties

	W-20Cu Feedstock	W-15Cu Feedstock
Tungsten/Copper Ratio	80/20	85/15
Debinding Method	Water	Solvent
Debinding Weight Loss	%3.8	%2.4
Oversize Factor	1.355	1.2318
Sintered Density (g/cm ³)	14.95	17.6407

3.2. Part Design

Five different models were designed for this study by using Creo Design Program. Two of the designed models are heat sink geometries which are the main objective of this study. In order to understand the limitations of the process in terms of geometry,

two heat sink geometries were prepared. First heat sink geometry consists of 81 pins with a height of 36 mm on a 30x30 mm wide base area as shown in Figure 3.1. The second geometry has a simpler structure with 16 pins positioned on the base are of 14x14 mm width as shown in Figure 3.2.

Apart from two heat sink geometries, three more models were prepared for tensile strength, CTE and thermal conductivity measurements. The information about all models are discussed in the following sections.

3.2.1. Heat Sink 9x9

Heat sink geometry is prepared according to thermal and design requirements and for moldability reasons, some radius and mold angles are added to the design. Final heat sink geometry ready for injection molding and dimensions are given in Figure 3.1. Model has a square base are with dimension 30.03 mm. It consists of 81 pins with the bottom diameter of 3.48 mm and top diameter 2.22 mm. The height of the pins is 30 mm and draft angles are 1mm.

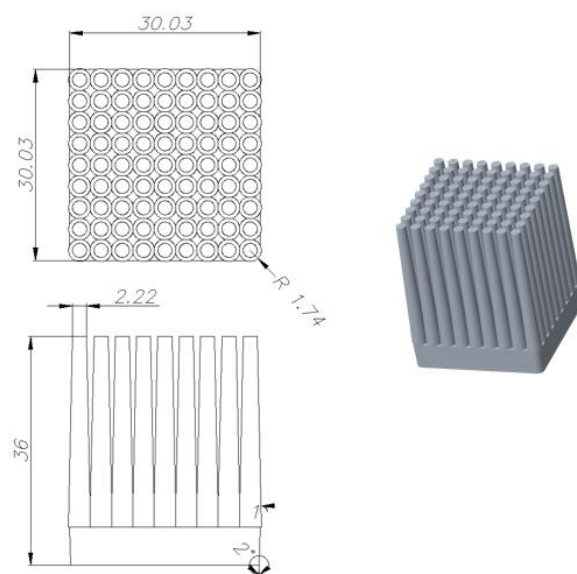


Figure 3.1. Heat Sink 9x9

3.2.2. Heat Sink 4x4

This model has a square base are with dimension 14.66mm. It consists of 16 pins with the bottom diameter of 2.86 mm and top diameter 2.00 mm. The height of the pins is 8.20 mm. The draft angle is 1mm.

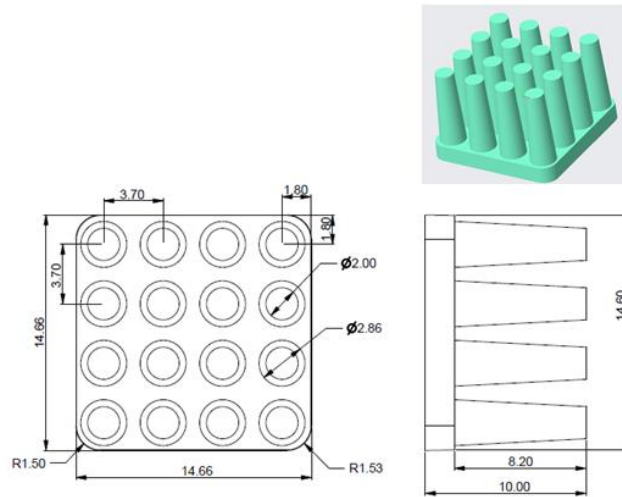


Figure 3.2. Heat Sink 4x4

3.2.3. Expansion Specimen

The geometry of the expansion sample is determined according to CTE value test requirements of the Ceramic Research Center in Anadolu University. The prepared model for the CTE test is given in Figure 3.3

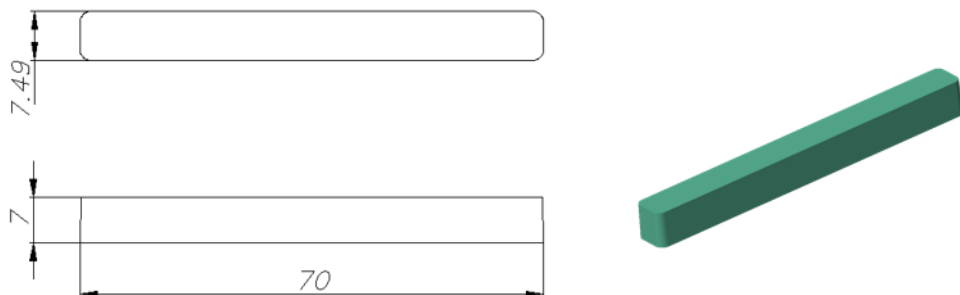


Figure 3.3. Thermal Expansion Specimen

3.2.4. Conduction Specimen

Conductivity measurements are also performed in the Ceramic Research Center in Anadolu University. Conductivity sample is prepared according to test requirements and shown in Figure 3.4

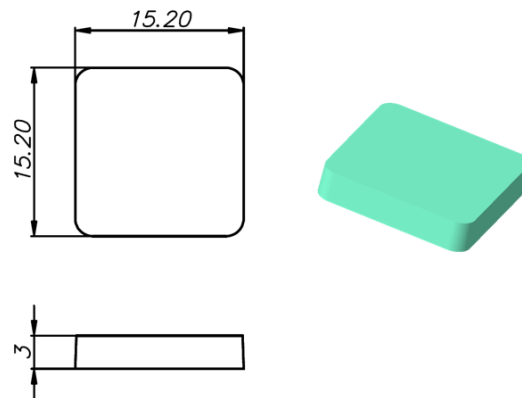


Figure 3.4. Conductivity Specimen

3.2.5. Tensile Specimen

Tensile Specimen sample for measuring tensile strength is prepared according to the ISO 2740 standard which defines tensile test specimen standards in powder metallurgy. The prepared model is shown in Figure 3.5. The specimen has smooth transitions and no sharp edges in the geometry to allow uniform flow which ensures homogenous mould filling. The mould parting line exists in the middle of the cavity.

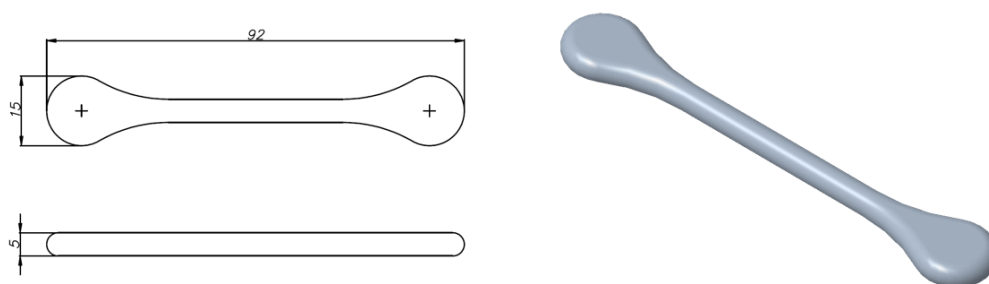


Figure 3.5. Tensile test specimen according to ISO 2740

3.3. Mold Design

Mold design is an important step for MIM operations. To have high quality parts in terms of mechanical and thermal properties a well-designed mold is necessary. A typical mold includes parts shown in Figure 3.6.

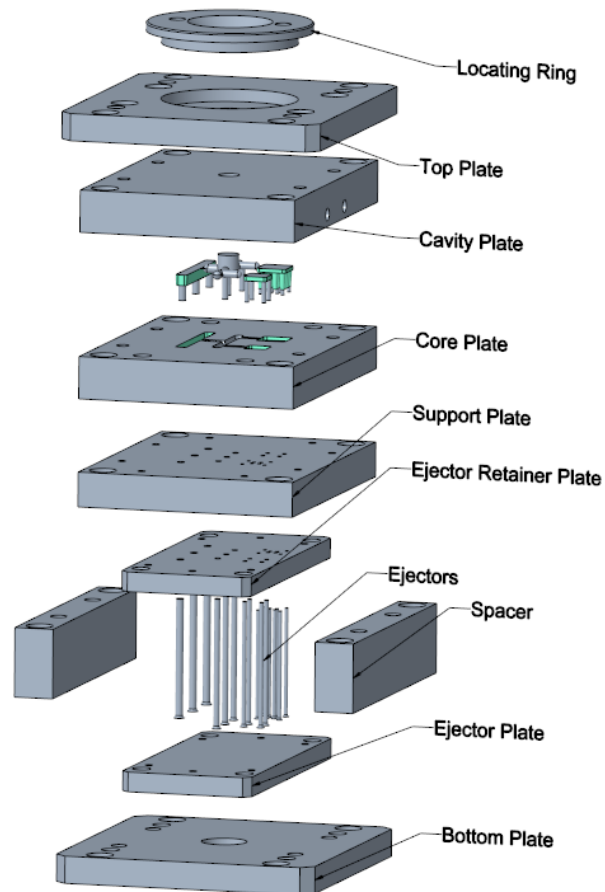


Figure 3.6. Typical Mold Parts

There are number of important design criteria that must be considered while designing a mold. For example, adequate cooling of the mold is very important since mold temperature parameter directly influences the molding surface quality and part ejection. Besides if the cooling is not adequate there may be warpage due to internal stress. Normally the material temperature rises to 200 °C, however, mold temperature

should not exceed 75 °C and that is assured by the help of cooling channels inside which water flows. The cooling channels in the mold design is shown in Figure 3.7.

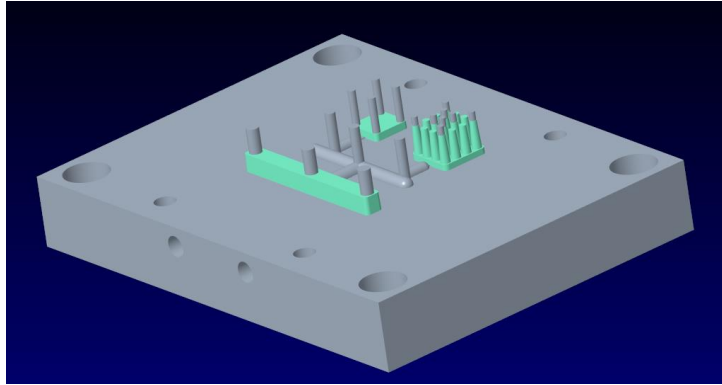


Figure 3.7. Cooling channels in the mold

In general venting of the mold is an important aspect of injection molding. If the mould seal is not designed properly, air won't be able to get out of the mold since it is filled with feedstock. This will result in voids and pore chains and the incomplete filling within the part [38]. This problem may be solved by allowing the air to get out of the mould at the place where it is filled last. Normally for this purpose very fine venting channels are used however since ejectors channels available in the design they act also as venting channels. The ejector pins are also shown in Figure 3.7

Thick sections should be used for the inflow of the feedstock instead of thin sections. Moreover, if the material flows openly into the mould it will cause jetting. Therefore, flow should be held back by some geometrical features such as a wall or wide pin. Draft angles should be added to the design so that ejection will be easier. Also, ejector pins should be used so that part will be easily removed from the mould. The number of ejectors to be used depends on the geometry of the part and rigidity of the feedstock used. By considering these points three molds are designed and produced which are shown in Figure 3.8. Technical drawings of the molds are shown in Figure 3.9

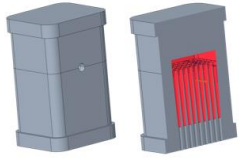
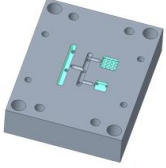
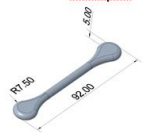
MOLD DESCRIPTION	PART DESCRIPTION		
<p>Mold for Heat Sink 9x9</p> 	<p>Heat Sink 9x9</p> 		
<p>Mold for Heat Sink 4x4, Conduction and Expansion Samples</p> 	<p>Heat Sink 4x4</p> 	<p>Expansion Sample</p> 	<p>Conduction Sample</p> 
<p>Mold for Tensile Sample</p> 	<p>Tensile Sample</p> 		

Figure 3.8. Designed Molds

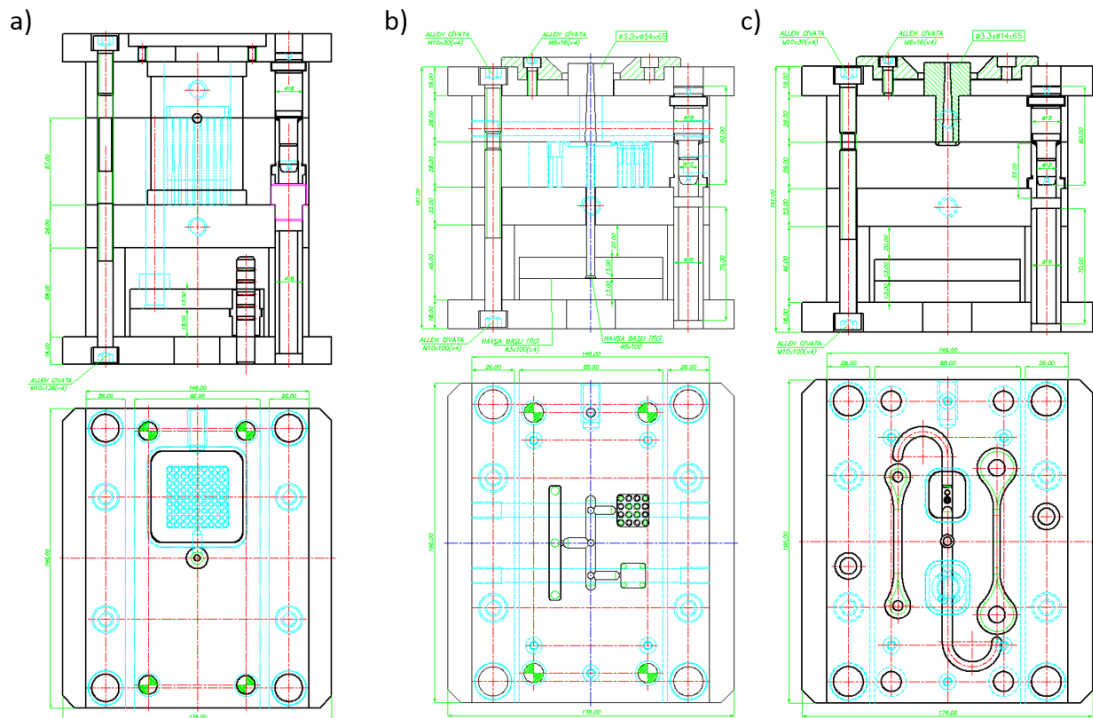


Figure 3.9. Technical Drawing of Molds a) for Heat Sink 9x9 b) for Heat Sink 4x4, Conduction and Expansion Samples c) for Tensile Samples

3.4. Mold Production

For production of the molds, DMG DMU 3 axis milling machine and Charmilles 2LC-ZNC die sinking electrical discharge machining were used as shown in Figure 3.10.

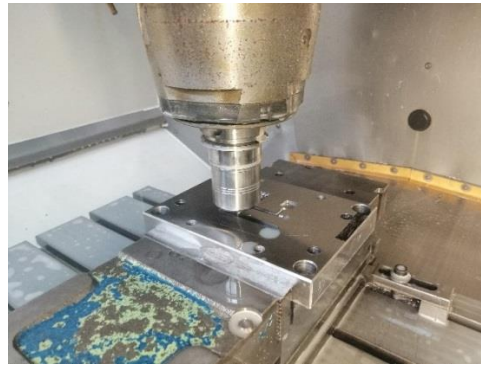


Figure 3.10. Production in milling machine

The computer aided manufacturing programs used for milling was prepared by using Power Mill High Speed CAM software. Three produced molds are shown in Figure 3.11, Figure 3.12 and Figure 3.13 respectively.



Figure 3.11. Mold for Heatsink 9x9

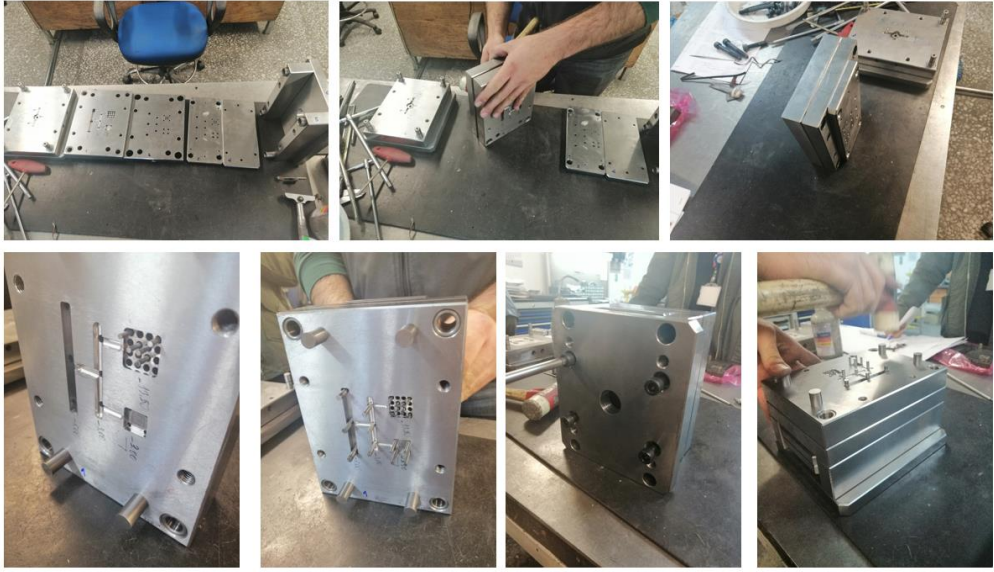


Figure 3.12. Mold for Heatsink 4x4 and Thermal Specimens



Figure 3.13. Mold for Test and Tensile Specimen

3.5. Injection

For injection operations, Arburg 221-175-50 injection machine shown in Figure 3.14 is used. Normally for metal injection operations some modifications necessary because the components which come in contact with the feedstock may wear due to abrasive property of feedstock. The injection procedure for MIM operations is given in the following section.



Figure 3.14. Arburg 221-175-350 Injection Molding Machine

3.5.1. Injection with W80Cu20 Feedstock

For the injection with W80Cu20 feedstock the injection parameters which are given in Table 3.2 were used. These parameters were suggested by the feedstock manufacturer.

Table 3.2. Injection Parameters for Feedstock 1

Parameters	Values			
	Zone 1	Zone 2	Zone 3	Zone 4
Cylindrical Temperature	185 °C	188 °C	192 °C	200 °C
Tool Temperature	60°C			
Injection Speed	30 cm ³ /s			
Injection Pressure	1000 bar			
Hold Pressure	900 bar			
Back Pressure	25 bar			

Before starting injection operations, in case different materials mix in the barrel, screw and check valve of the injection machine is carefully cleaned. The screw pulled and all remaining material was carefully removed before purging the feedstock through the heated barrel. Otherwise it is possible that small amount of material contamination may damage the feedstock which results failure in debinding step. The final configuration of in the mold in the injection machine is shown in Figure 3.15



Figure 3.15. Mold assembled to the Injection Molding Machine

The barrel temperatures are set to parameters given in Table 3.2. However, during measurements temperatures deviations around $\pm 5^\circ$ recorded. It is assumed such a deviation will have no significant impact on injection molding process. In order to achieve constant dosage and constant shot weight, a low back pressure is set. The screw turning speed was not set to a high value (between 6 and 10 m/min) since high-speed values may lead to thermal damage of the metal powder compound. Injection pressure is set to maximum pressure available and hold pressure is adjusted according to hold pressure and gradually decreased from there. Tool Temperature is another important factor that influences the molding surface quality and part ejection. So the mold is carefully heated and value is recorded as 65°C by taking into consideration all the details mentioned above the parts are molded and first samples so-called green parts are obtained. No sign of defects within the sample observed after the injection molding process. The produced parts are shown in Figure 3.16

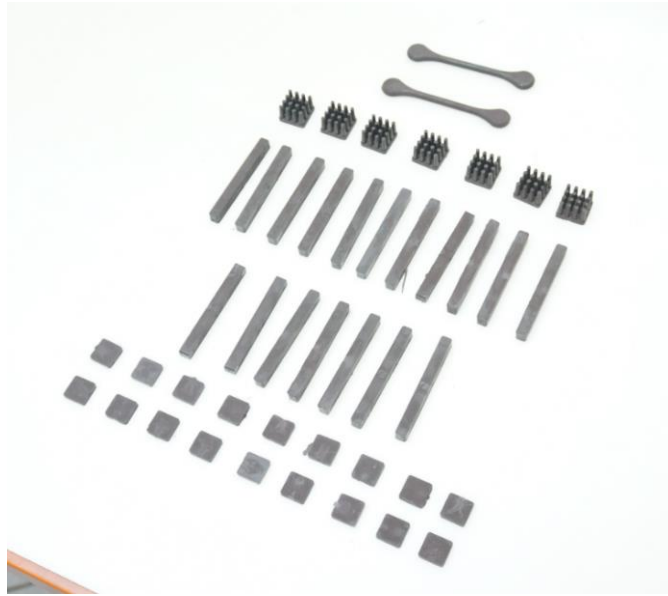


Figure 3.16. Parts Produced from W80Cu20 Feedstock

3.5.2. Injection with W85Cu15 Feedstock

Injection parameters used for W85Cu15 feedstock and injected samples are shown in Table 3.3 and Figure 3.17 respectively.

Table 3.3. Injection Parameters for W85Cu15 Feedstock

Parameters	Values			
	Zone 1	Zone 2	Zone 3	Zone 4
Cylindrical Temperature	165 °C	170 °C	175 °C	180 °C
Tool Temperature	50 °C			
Injection Speed	50 cm ³ /s			
Injection Pressure	1000 bar			
Hold Pressure	900 bar			
Back Pressure	10 bar			

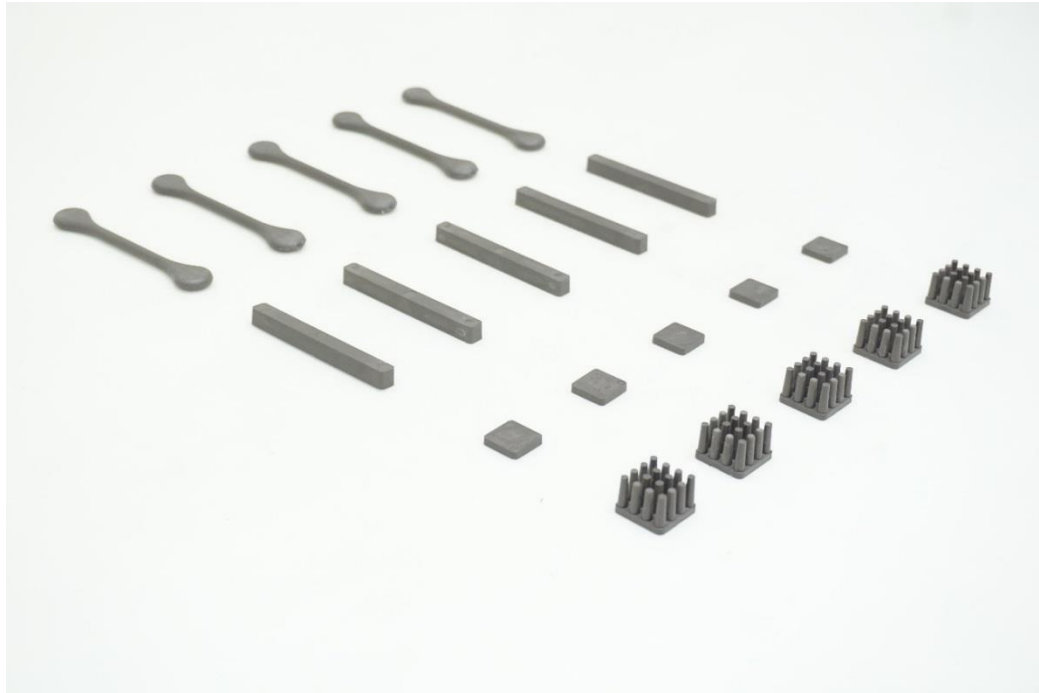


Figure 3.17. Parts Produced from W85Cu15 feedstock

3.6. Debinding

Debinding is performed before the sintering process to remove binder from feedstock. The time required for debinding process depends on the thickness of the parts and the debinding method applied. To method used for determining the optimum time for debinding is to immerse samples in a solvent and weight and catalog then remove one part every 1 hour, dry it and check the weight loss. When the weight loss stops it means debinding process is over. For water debinding and solvent debinding the experimental procedure followed is described below.

3.6.1. Water Debinding with W80Cu20 Feedstock

For water debinding to determine the optimum time for debinding process for each part 10 samples were selected and they were immersed in water at 60°C. Then for every 3 hours, one of the part is taken from the water, dried and measured. The debinding operation setup is shown in Figure 3.18 and the recorded weight measurements are shown in Figure 3.19



Figure 3.18. Water Debinding Operations

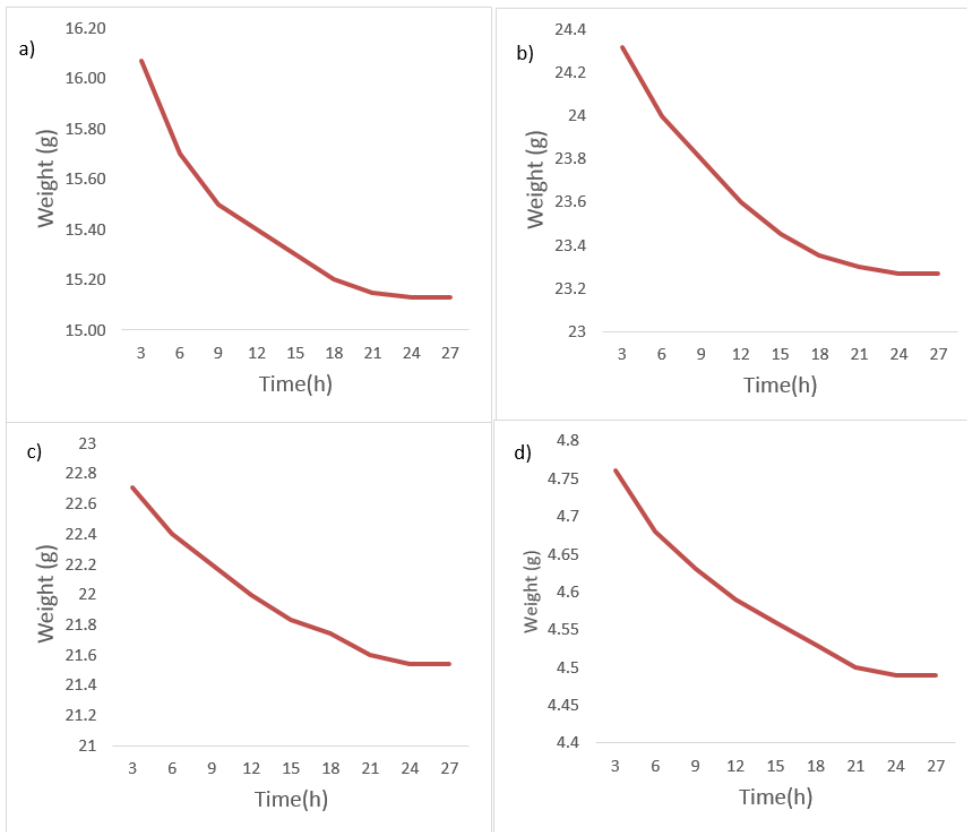


Figure 3.19. Weight Loss During Solvent Debinding of a)Heat Sink 4x4 b)Tensile sample
c)Expansion Sample d)Conduction Sample

According to these results weight loss stops after 21 hours, so optimum water debinding time for the parts are chosen as 21 hours. Rest of the parts were debinded according the parameters given in Table 3.4.

Table 3.4. Water Debinding Parameters

Parameters	Values
Debinding Temperature /Time	60°C / 21 hours
Drying Temperature /Time	100°C / 2 hours

3.6.2. Solvent Debinding with W85Cu15 Feedstock

Solvent debinding of the W85Cu15 samples was carried out by means of Trichloroethylene as solvent at 60°C. For determining the optimum time for debinding process for each part 10 samples were selected and they were immersed in solvent. Then for every 3 hours one of the part is taken from the water, dried and measured. The debinding operation setup is shown in Figure 3.20 and the recorded weight measurements are shown in Figure 3.21



Figure 3.20. Solvent Debinding Operations

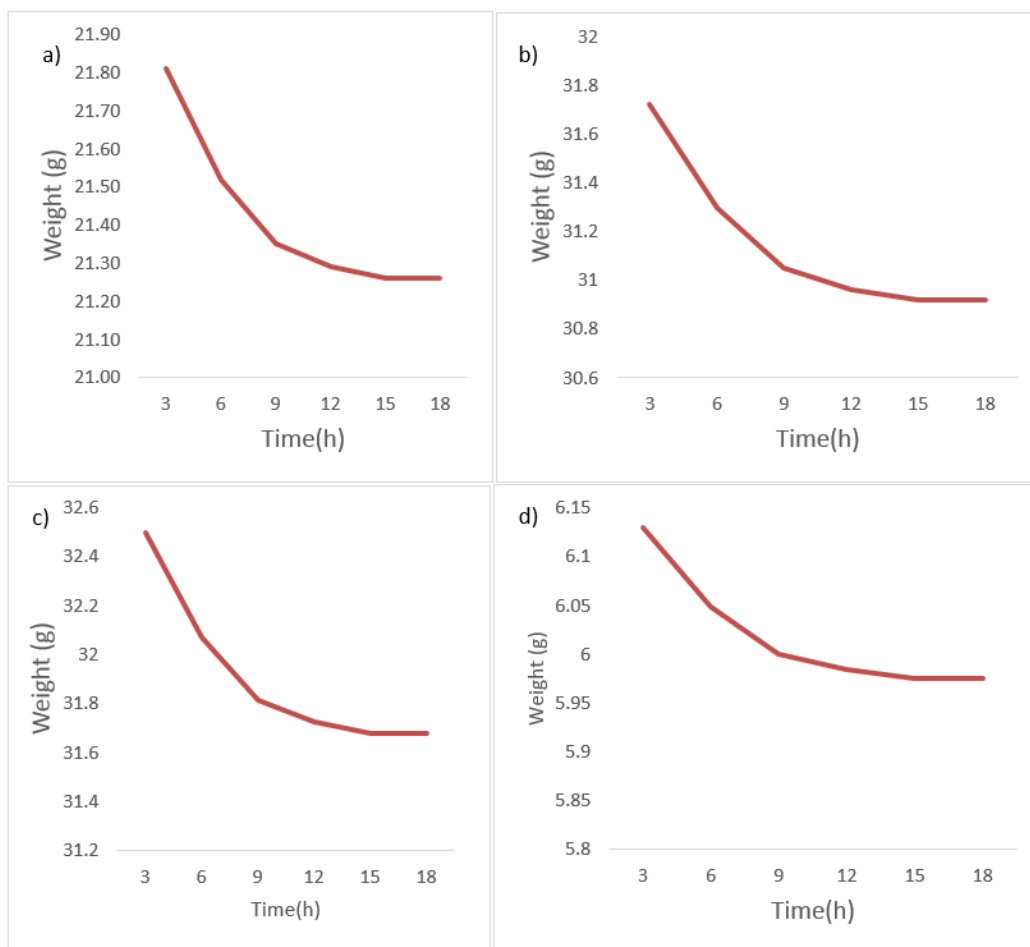


Figure 3.21. Weight Loss During Solvent Debinding of a)Heat Sink 4x4 b)Tensile sample c)Expansion Sample d)Conduction Sample

According to these results weight loss stops after 15 hours, so optimum water debinding time for the parts are chosen as 15 hours. Rest of the parts were debinded according the parameters given in Table 3.5

Table 3.5. Solvent Debinding Parameters

Parameters	Values
Debinding Temperature /Time	60°C / 15 hours
Drying Temperature /Time	100°C / 2 hours

3.7. Sintering

The last step of MIM operations is sintering. For sintering operations, laboratory type CM Furnaces (Rapid Type Assembly, 1512 H2 GS FL) shown in Figure 3.22 was used. CM furnaces are reliable and widely used lab furnaces available in the market. The sintering atmosphere is hydrogen for preventing oxidation. This furnace has two hydrogen inlets.



Figure 3.22. Sintering Furnace, CM 1512 H2 GS FL

After debinding step, since the binder is eliminated mostly from the parts, parts have approximately 40% empty space by volume. After sintering this empty space reduce up to 1% therefore, there is a great amount of expected shrinkage in the parts. The expected shrinkage ratios according to materials used are shown in Table 3.6 and the appearance of the parts in the furnace is shown in Figure 3.23.

Table 3.6. *Theoretical Shrinkage Ratios*

Feedstock	Oversize Factor	Theoretical Shrinkage Ratio
W80Cu20	1,355	%26,2
W85Cu15	1,2318	%18,8



Figure 3.23. Parts in Sintering Furnace

3.7.1. Sintering Parameters

As stated in section 2.4.4, the melting points of W and Cu are largely different than each other, therefore liquid phase sintering is the appropriate sintering type for this composite. In liquid phase sintering, it should be arranged that the sintering temperature should be above the melting temperature of one of the components. Since the melting temperature of Copper is 1083°C , the sintering temperature should be higher than this temperature. However, an increase in the sintering temperature results in a decrease in the viscosity of the copper melt and increases the interactivity of copper and refractory metal. Moreover, the boiling point of copper is low so at higher temperatures, there is a risk of copper evaporation and contamination of the sinter furnace [43]. So the samples were sintered between 1200°C and 1350°C [32]. All the sintering operations are performed in a %99.92 pure hydrogen atmosphere to avoid oxidation.

Time for sintering and sintering temperatures are two of the most important sintering parameters which directly influence the final properties (i.e. thermal and mechanical) of the produced MIM parts. Therefore, a different set of parameters were used to investigate the effect of these parameters on sample properties. During the experiments, samples are firstly heated at a rate of 3°C up to 500°C . The samples were kept in this temperature for 1 hour for thermal debinding. Then samples were heated to 1020°C for 30 min so that solid phase sintering may be performed. Then to see the effect of time and temperature

samples were divided into three groups. In the first case, the temperature of the furnace was heated to 1350 °C and samples were sintered at that temperature for 3 hours, the second group was sintered in the same temperature for 1 hour. The third group was sintered at a lower temperature, 1200 °C, for 3 hours. Finally, all the sintered samples were cooled with a rate of 15 °C /min h using water as the cooling system. The sintering curve for all three groups is shown in Figure 3.24.

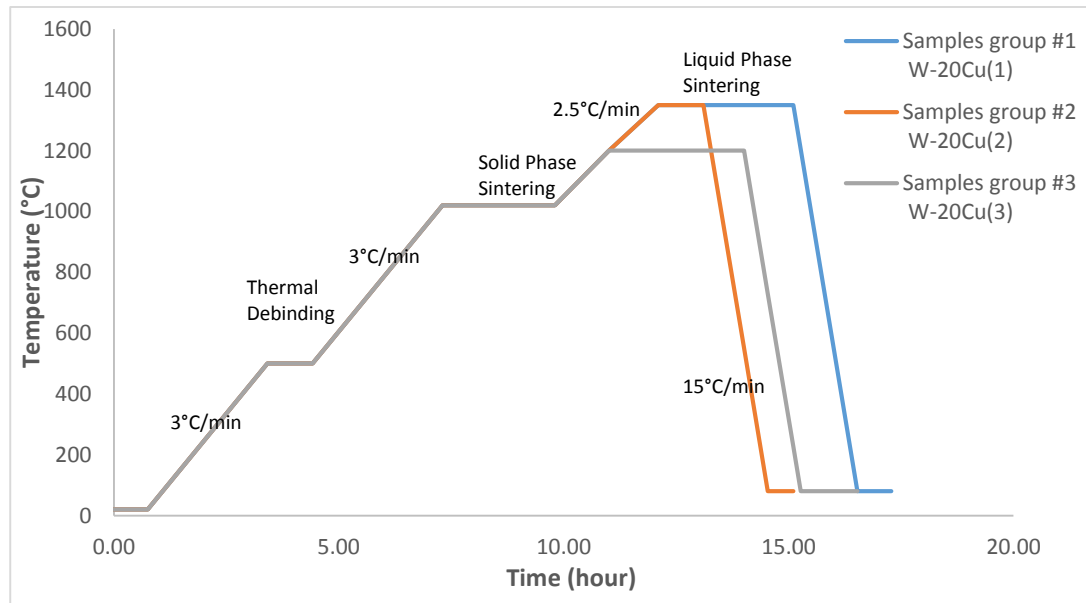


Figure 3.24. Sintering Curve

CHAPTER 4

RESULTS AND DISCUSSION

4.1. Injection Operations

4.1.1. Injection of Heat Sink 9x9

Injection practices are started with the Heat Sink 9x9 parts. However, the attempts resulted in failure for both feedstock. The main problem was the incomplete filling of the fins. The most fins of the produced heat sinks were either missing or only had the half-length of the ideal height as shown in Figure 4.1.



Figure 4.1. Injected heat sink 9x9 with defects.

This defect shows that molten feedstock could not reach everywhere inside the cavity. The reason for this failure could be that the gate gets solidified before the cavity is completely filled. Therefore, the gate size was increased and mould temperature was increased. However, these precautions didn't fix the problem. So coating of the mould was another

option to help the filling since coating decreases the sliding friction in the inner walls of the mold. However, the coating also didn't help since the model has very deep holes where coating couldn't reach adequately. The injection parameters had been changed, the back pressure and injection speeds were increased until the limits of the injection machine however it was not possible to produce defect-free parts. Therefore it was decided to change the design of the heat sink by shortening the pin lengths by 10 mm as shown in Figure 4.2 (b)

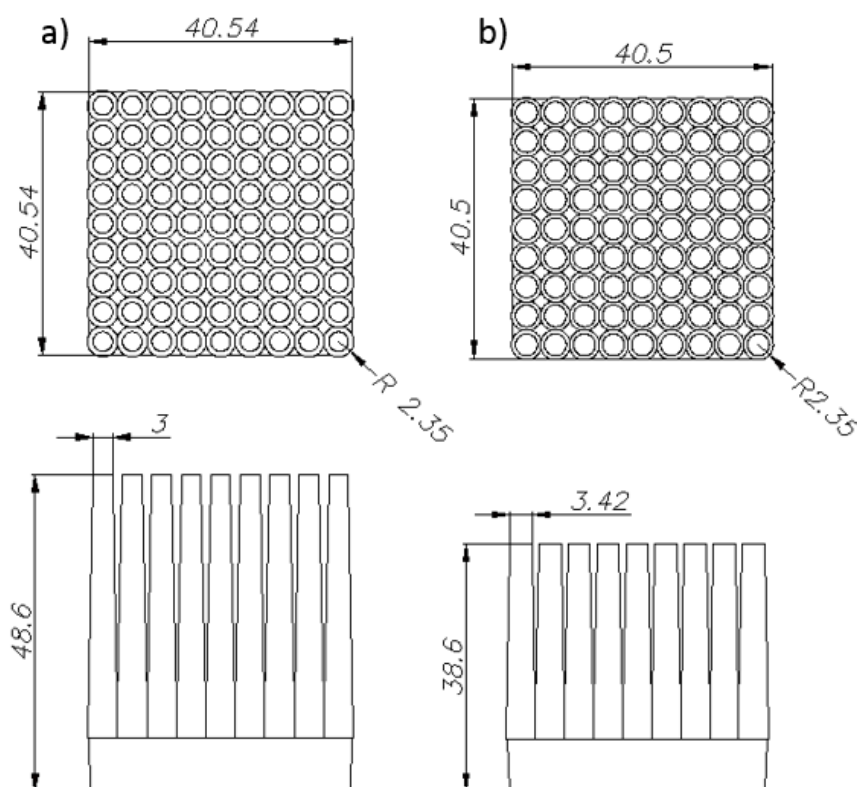


Figure 4.2. Heat Sink 9x9 design a) original, b) short Pin version.

Necessary modifications were performed on the mold for producing the short pin version of the heat sink. However, expected fins without defect still couldn't be produced as shown in Figure 4.3. The same procedure is followed as before, injection parameters were changed, the coating option was tried, mould temperature was increased however it was not possible to produce defect-free parts. Finally, after a considerable amount of time and

effort has been spent for injecting these parts successfully, it is decided that with the present equipment's it is not possible to produce parts with this level of complexity.



Figure 4.3. Injected short finned version of heat sink 9x9 with defects.

4.1.2. Injection of other parts

During injection operations of other parts, the problems mentioned in the previous chapter haven't been encountered. For injection the parameters mentioned in chapter 3.5 were used. The injection operations are first performed with W80Cu20 feedstock than W85Cu15 feedstock. All injected parts had regular shapes without any defects. Fins of the heat sink 4x4 were complete and no brake or crack were observed. The only problem was the flash which were the buildup of excess material around the tensile sample as shown in Figure 4.4. This is possible when the pressure inside the mold is greater than the force keeping the mold together. Decreasing the injection pressure helped prevention of flash forming.



Figure 4.4. Excess material around the molded part

The injected samples from W80Cu20 feedstocks and W85Cu15 feedstocks are shown in Figure 4.5 and Figure 4.6 respectively.

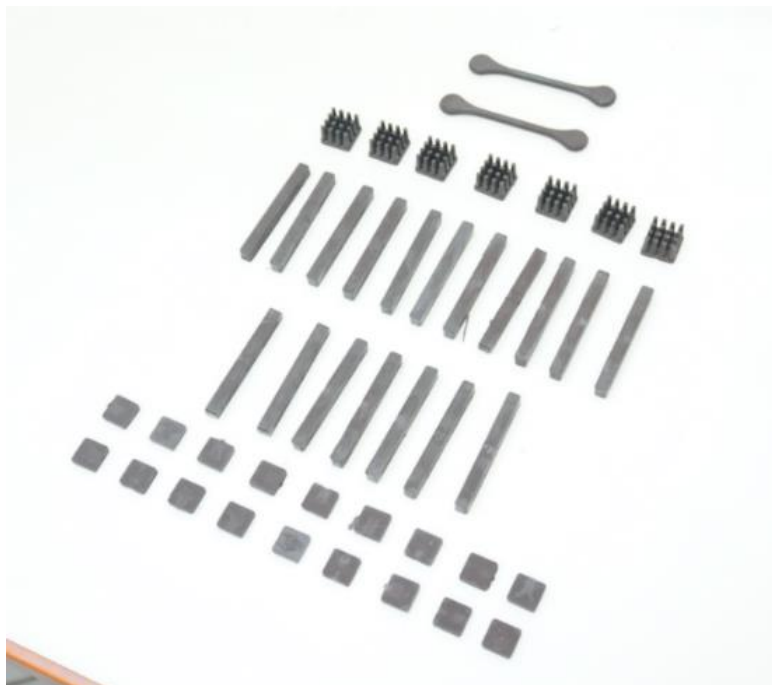


Figure 4.5. Injected samples from W80Cu20 feedstock

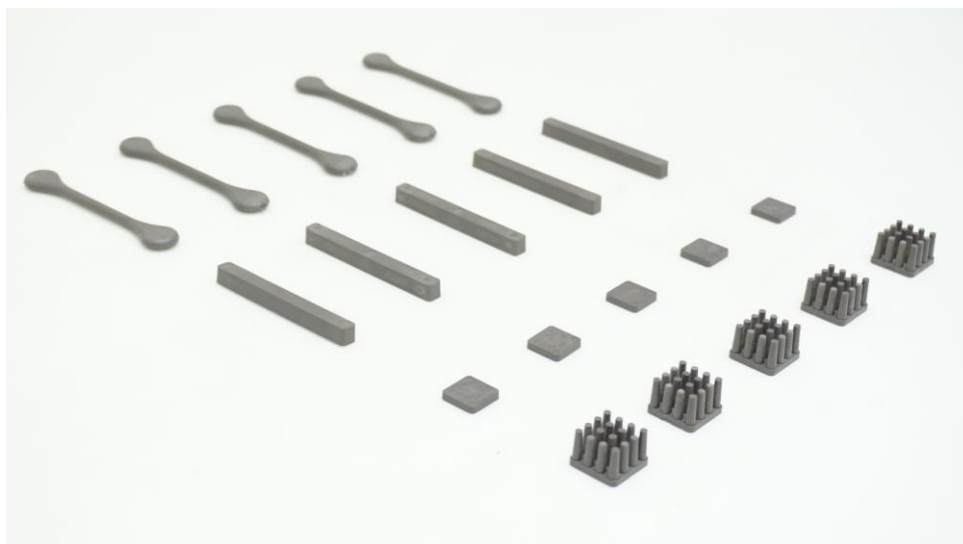


Figure 4.6. Injected samples from W85Cu15 feedstock

4.2. Debinding Operations

4.2.1. Water Debinding of W80Cu20 Feedstock

According to experiments performed in section 3.6.1 the optimum debinding parameters for Poylmim Feedstock is shown in Table 3.4. Using these parameters debinding is performed by immersing all parts in a tank full of water and binders are removed. For poylmim feedstock since the binders are removed during debinding a more than %3.8 weight loss is expected. Table 4.1 gives the weight of the samples before and after debinding operations. According to these results debinding operation is successful. Samples before and after debinding operation is shown in Figure 4.7.

Table 4.1. Weight of the samples before and after water debinding process

Part Description	Weight Before Debinding(g)	Weight After Debinding(g)	Weight Loss	Target Weight Loss	Pass/Fail
Heat Sink	16,378	15,2	7,19%	>%3.8	Pass
Tensile Specimen	4,71	4,43	5,94%	>%3.8	Pass
Expansion Specimen	24,215	22,24	8,16%	>%3.8	Pass
Conduction Specimen	22,72	21,83	7,19%	>%3.8	Pass

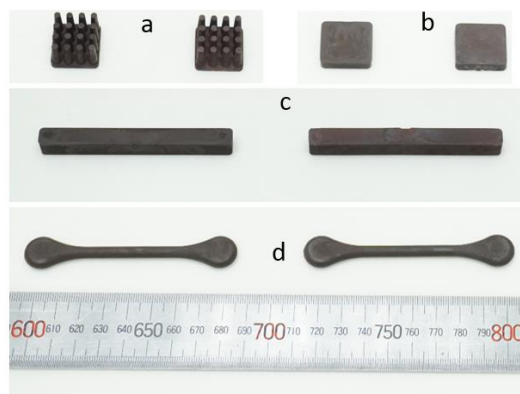


Figure 4.7. W80Cu20 samples before and after debinding a)Heat Sink b)Conduction Specimen c)Expansion Specimen d)Tensile Specimen

Figure 4.8 shows the heat sink part and microstructure before and after water debinding. Soluble ingredients in the feedstocks were mostly extracted after debinding process as shown in the figure.

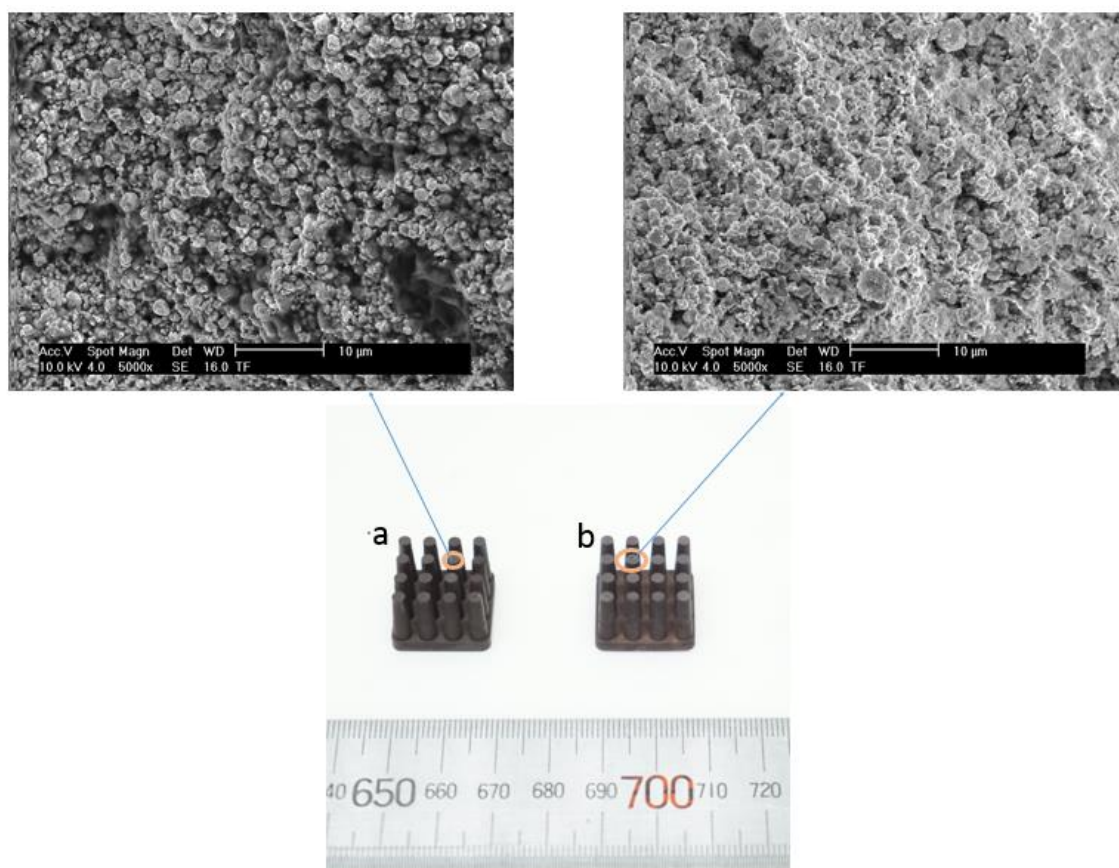


Figure 4.8. SEM microstructure of injected samples before and after debinding

4.2.2. Solvent Debinding of W85Cu15 Feedstock

According to experiments performed in section 4.2.2 the optimum debinding parameters for W85Cu15 Feedstock is shown in Table 3.5. Using these parameters debinding is performed by immersing all parts in a tank full of Trichloroethylene as solvent at 60°C and binders are removed. For W85Cu15 feedstock since the binders are removed during debinding a more than %2.43 weight loss is expected. Table 4.2 gives the weight of the samples before and after debinding operations. According to these results debinding

operation is successful. Samples before and after debinding operation is shown in Figure 4.9

Table 4.2. Weight of the samples before and after water debinding Process

Part Description	Weight Before Debinding(g)	Weight After Debinding(g)	Weight Loss	Target Weight Loss	Pass/Fail
Heat Sink	21.77	21.24	2.43%	>%2.43	Pass
Tensile Specimen	31,72	30,92	2,46%	>%2.43	Pass
Expansion Specimen	32,5	31,7	2,46%	>%2.43	Pass
Conduction Specimen	6,25	6,09	2,56%	>%2.43	Pass

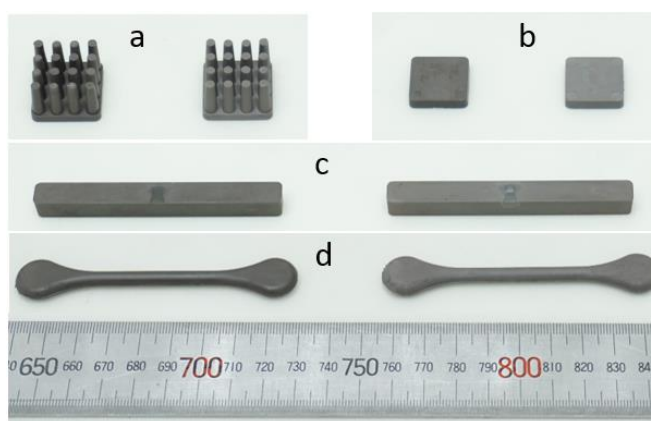


Figure 4.9. W85Cu15 samples before and after debinding a)Heat Sink b)Conduction Specimen c)Expansion Specimen d)Tensile Specimen

4.3. Sintering

4.3.1. Sintered W80Cu20 parts

As stated in section 3.7.1 three different sets of parameters are used to investigate the effect of sintering parameters on the mechanical and thermal properties of the samples. The first group of samples were sintered at 1350 °C for 3 hours, whereas the second group sintered at the same temperature for 1 hour. The last group was sintered at 1200 °C for 3 hours. The sintering parameters used for each group of specimen for W80Cu20 feedstock is summarized in Table 4.3.

Table 4.3. Sintering Parameters used for sintering W80Cu20 parts

	Samples group #1 (WCu ₁)	Samples group #2 (WCu ₁)	Samples group #3 (WCu ₃)
Material	W80Cu20	W80Cu20	W80Cu20
Sintering Temperature[°C]	1350	1350	1200
Sintering Time[h]	3	1	3

The sintered samples for the measurements are shown in Figure 4.10. Thermal, mechanical and microscopic measurements performed on these samples and results are explained in following sections.

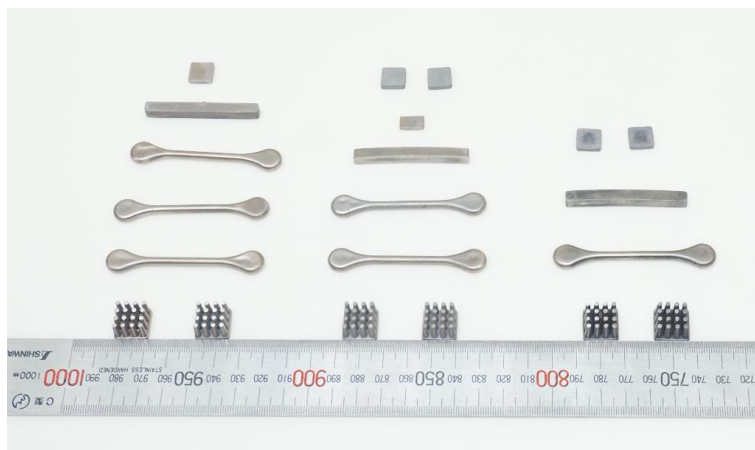


Figure 4.10. Three groups of W-Cu20 parts sintered

4.3.2. Sintered W85Cu15 parts

Different sets of parameters were also used for sintering W85Cu15 parts. However, the sintering operations for this material have failed. Densification hasn't been completed and shrinkage results were far from expected ratios. Changing the sintering parameters did not change the situation and in all the cases the sintered parts were easily broken with hand. The broken sintered parts are shown in Figure 4.11. The reason for this failure investigated in the following chapters.



Figure 4.11. The easily broken sintered w-15Cu parts.

4.4. Shrinkage Ratios

The shrinkage ratio of the samples important to determine if the sintering operation is performed successfully. For a successful sintering operation, the measured shrinkage ratio should be as close as to the theoretical shrinkage ratios announced by the feedstock manufacturer which is given in Table 4.4. The actual shrinkage determined by dimension reduction. The percentage of the dimension reduction is calculated according to (4-1).

$$\text{Shrinkage} = \frac{L_0}{L_f} \quad (4-1)$$

Where

L_0 Dimension before sintering

L_f Dimension after sintering

The dimensions of all the samples before and after sintering were measured and shrinkage ratios were calculated. a dial gauge micrometer of 1 μm sensitivity was used to measure the dimensions of the specimens.

Table 4.4. Shrinkage Ratios of the Feedstocks

	W80Cu20	W85Cu15
Tungsten/Copper Ratio	80/20	85/15
Shrinkage Ratio	1.355	1.2318

4.4.1. Shrinkage Ratio of W-20Cu parts

4.4.1.1. Heat Sink

The sample heat sink part before and after sintering is shown in Figure 4.12. Measurements result and the calculated shrinkage ratio is given in Table 4.5.



Figure 4.12. Heat Sink Part before and after sintering

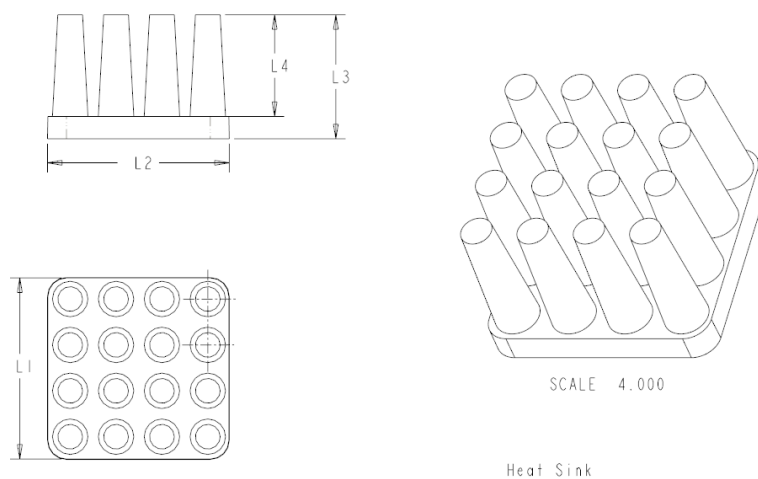


Figure 4.13. Heat Sink Dimensions Notations

Table 4.5. Heat Sink Dimensions before and after sintering

	Samples group #1 (WCu ₁)	Samples group #2 (WCu ₂)	Samples group #3 (WCu ₃)
Dimensions Before Sintering (L ₁ x L ₂ x L ₃)	19,70 x 13,50 x 11,07	19,70 x 13,50 x 11,07	19,70 x 13,50 x 11,07
Dimensions After Sintering (L ₁ x L ₂ x L ₃)	14,50 x 14,49 x 9,86	14,90 x 14,79 x 10,04	15,15 x 15,10 x 10,28
Shrinkage Ratio	1,36	1,33	1,31

4.4.1.2. Tensile Specimen

The sample heat sink part before and after sintering is shown in Figure 4.14. Measurements result and the calculated shrinkage ratio is given in Table 4.6.



Figure 4.14. Tensile Specimen before and after sintering

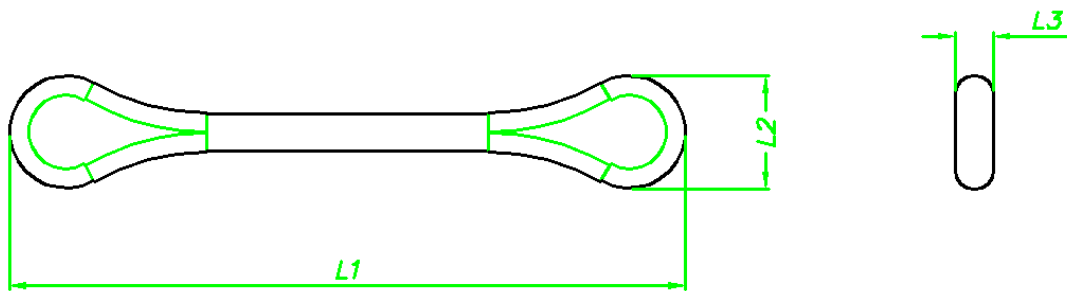


Figure 4.15. Tensile Specimen Notations

Table 4.6. Tensile Specimen Dimensions before and after sintering

	Samples group #1 (WCu ₁)	Samples group #2 (WCu ₂)	Samples group #3 (WCu ₃)
Dimensions Before Sintering (L ₁ x L ₂ x L ₃)	93,30 x 15,55 x 5,35	93,30 x 15,55 x 5,35	93,30 x 15,55 x 5,35
Dimensions After Sintering (L ₁ x L ₂ x L ₃)	68,50 x 11,40 x 3,92	69,67 x 11,80 x 4,01	70,03 x 11,70 x 4,06
Shrinkage Ratio	1,36	1,33	1,33

4.4.1.3. Conductivity Specimen

The conduction specimen part before and after sintering is shown in Figure 4.16. Measurements result and the calculated shrinkage ratio is given in Table 4.7.



Figure 4.16. Conduction specimen before and after sintering

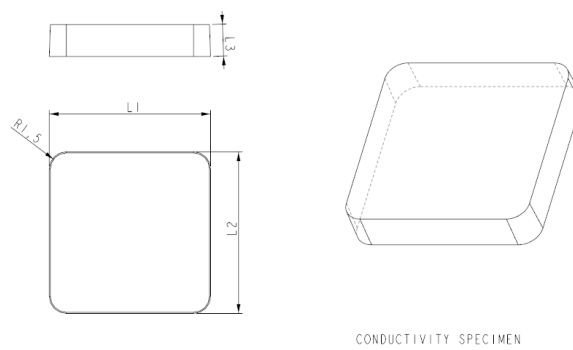


Figure 4.17. Heat Sink Dimensions Notations

Table 4.7. Conduction Specimen Dimensions before and after sintering

	Samples group #1 (WCu ₁)	Samples group #2 (WCu ₂)	Samples group #3 (WCu ₃)
Dimensions Before Sintering (L ₁ x L ₂ x L ₃)	15,15 x 15,15 x 3,07	15,15 x 15,15 x 3,07	15,15 x 15,15 x 3,07
Dimensions After Sintering (L ₁ x L ₂ x L ₃)	11,23 x 11,23 x 2,26	11,39 x 11,39 x 2,31	11,57 x 11,57 x 2,35
Shrinkage Ratio	1,35	1,33	1,31

4.4.1.4. Expansion Specimen

The sample expansion specimen part before and after sintering is shown in Figure 4.18. Measurements result and the calculated shrinkage ratio is given in Table 4.8.



Figure 4.18. Expansion Specimen before and after sintering

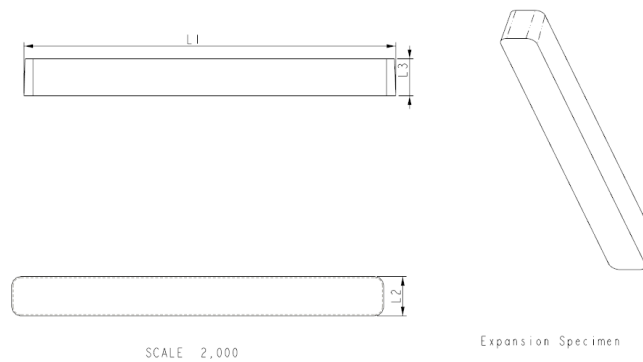


Figure 4.19. Expansion Specimen Dimensions Notations

Table 4.8. Expansion Specimen Dimensions before and after sintering

	Samples group #1 (WCu ₁)	Samples group #2 (WCu ₂)	Samples group #3 (WCu ₃)
Dimensions Before Sintering (L ₁ x L ₂ x L ₃)	70,60 x 7,45 x 7,08	70,60 x 7,45 x 7,08	70,60 x 7,45 x 7,08
Dimensions After Sintering (L ₁ x L ₂ x L ₃)	52,28 x 5,53 x 5,26	53,09 x 5,64 x 5,33	53,92 x 5,69 x 5,42
Shrinkage Ratio	1,35	1,33	1,31

4.4.2. Shrinkage Ratio of W-15Cu parts

4.4.2.1. Heat Sink

The sample heat sink part before and after sintering is shown in Figure 4.20 Measurements result and the calculated shrinkage ratio is given in Table 4.9.



Figure 4.20. Heat Sink Part before and after sintering

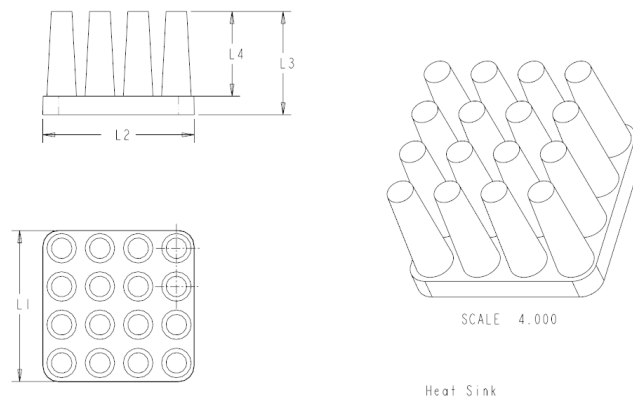


Figure 4.21. Heat Sink Dimensions Notations

Table 4.9. Heat Sink Dimensions before and after sintering

Dimensions	L ₁ (mm)	L ₂ (mm)	L ₃ (mm)
Before Sintering	19,50	19,50	13,30
After Sintering	18,90	18,90	12,92
Shrinkage Ratio	1,03	1,03	1,03

4.4.2.2. Tensile Specimen

The sample heat sink part before and after sintering is shown in Figure 4.22. Measurements result and the calculated shrinkage ratio is given in Table 4.10.



Figure 4.22. Tensile Specimen before and after sintering

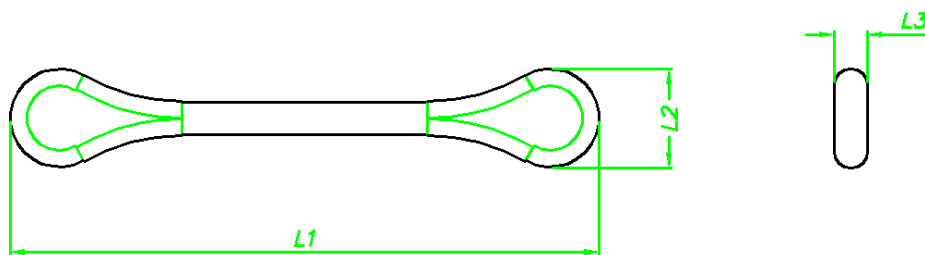


Figure 4.23. Tensile Specimen Notations

Table 4.10. Tensile Specimen Dimensions before and after sintering

Dimensions	L ₁ (mm)	L ₂ (mm)	L ₃ (mm)
Before Sintering	92,40	15,35	5,25
After Sintering	89,50	14,72	5,20
Shrinkage Ratio	1,03	1,04	1,01

4.4.2.3. Conductivity Specimen

The conduction specimen part before and after sintering is shown in Figure 4.24. Measurements result and the calculated shrinkage ratio is given in Table 4.11.



Figure 4.24. Conduction specimen before and after sintering

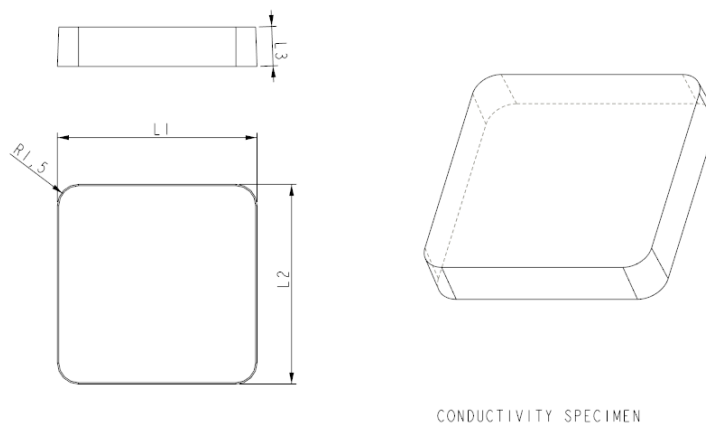


Figure 4.25. Heat Sink Dimensions Notations

Table 4.11. Conduction Specimen Dimensions before and after sintering

Dimensions	L ₁ (mm)	L ₂ (mm)	L ₃ (mm)
Before Sintering	14,97	14,97	2,98
After Sintering	14,45	14,45	2,84
Shrinkage Ratio	1,04	1,04	1,05

4.4.2.4. Expansion Specimen

The sample expansion specimen part before and after sintering is shown in Figure 4.26. Measurements result and the calculated shrinkage ratio is given in Table 4.12.



Figure 4.26. Expansion Specimen before and after sintering

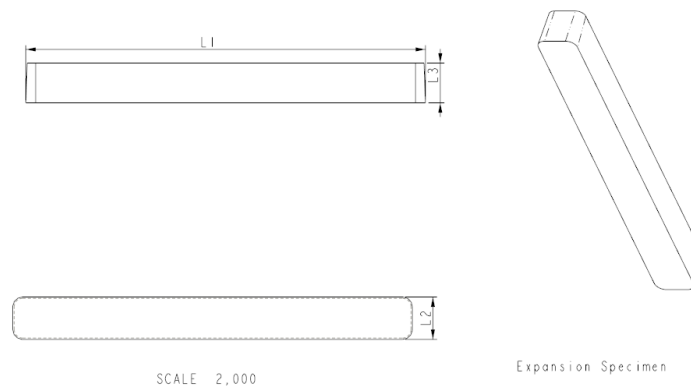


Figure 4.27. Expansion Specimen Dimensions Notations

Table 4.12. Expansion Specimen Dimensions before and after sintering

Dimensions	L ₁ (mm)	L ₂ (mm)	L ₃ (mm)
Before Sintering	69,55	7,35	6,93
After Sintering	67,10	7,05	6,66
Shrinkage Ratio	1,04	1,04	1,04

4.4.3. Discussion of the shrinkage ratios

The shrinkage ratio of the samples important to determine if the sintering operation is performed successfully. For a successful sintering operation, the measured shrinkage ratio should be as close as to the theoretical ratios announced by the feedstock manufacturer.

Table 4.13 gives the average shrinkage ratios for W80Cu20 feedstock obtained by the measurement explained in 4.4.1. According to these results shrinkage ratio of the W–Cu parts depends greatly on sintering temperature and time. As sintering time and sintering temperature increase shrinkage ratio of the W-Cu samples also increases. The average shrinkage ratio of the WCu₁ samples which are sintered at 1200 °C for 3 hours was found to be about 1.31 which is lower ratio than expected. However, when the same samples sintered at 1350°C for one hour the shrinkage ratio increases to %1.33 which is almost the theoretical shrinkage ratio. When the sintering time increased from 1 hour to 3 hours at 1350°C further increase in shrinkage ratio recorded and almost the theoretical shrinkage ratio is obtained. These results show that for W80Cu20 feedstock, 1350°C sintering temperature and 3 hours sintering time gives the best shrinkage quality.

Table 4.13. Theoretical and measured average shrinkage values for W-20Cu Parts

	Theoretical Value	Samples group #1 (WCu ₁)	Samples group #2 (WCu ₂)	Samples group #3 (WCu ₃)
Shrinkage Ratio	1.35	1.34	1.33	1.31

Table 4.14 gives the average shrinkage ratios as for W85Cu15 feedstock obtained by the measurement explained in section 4.4. The measured value is 1.03 which is far from the theoretical ratio announced as 1.28 by the manufacturer. These results shows that the sintering operations failed and there are extreme problems with the parts.

Table 4.14. Theoretical and measured average shrinkage values for W-15Cu Parts

	Theoretical Value	Average Measured Value
Shrinkage Ratio	1.28	1.03

4.5. Density Measurements

The density value of the sintered material is important since the physical and mechanical properties of the sintered W–Cu samples depend greatly on sintering densification. If the density values are lower than expected it means, there is porosity available on the sintered W–Cu parts and grain size grows is not enough. Therefore, density measurement was performed to check if sintering performed successfully.

The density of the specimens was measured according to the formula given (4-2), which is based on Archimedes' principle [44].

$$\rho = \frac{m_{air}}{m_{air} - m_{water}} \cdot \rho_0 \quad (4-2)$$

Where

(m_{air}): the weight of the object in air

(m_{water}): the weight of the object in the water

(ρ_0): density of water at the given temperature

The density measurements of the samples were performed by using Precisa Laboratory Prime XB-320 High precision laboratory balance. For the measurements, first the samples were weighed in air (m_{air}) and then in water (m_{water}) as shown Figure 4.28. The density was then calculated from the two weightings according to the formula given in (4-2).

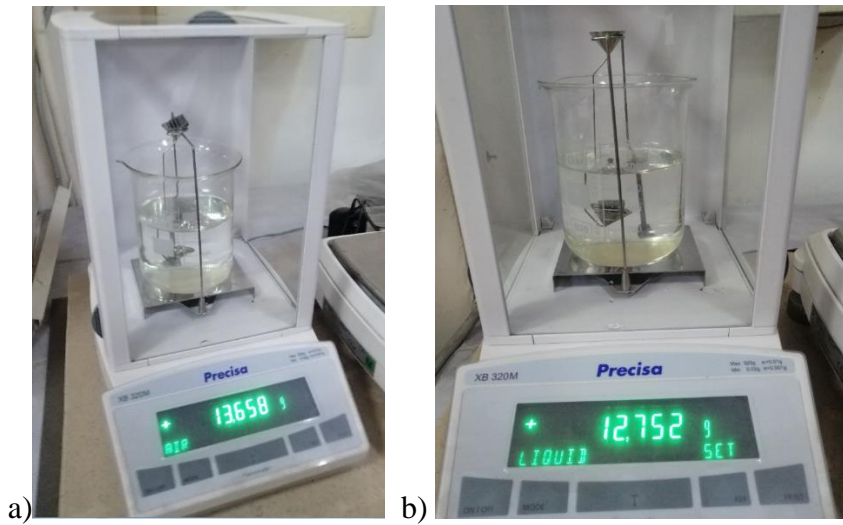


Figure 4.28. Weighing of samples a)in air, b)in water

4.5.1. Density of W-20Cu parts

The measured density values of the samples and relative densities according to the theoretical value of 15.6 g/cm³ given in Table 4.15.

Table 4.15. Measured Density Values for W-20Cu

	Samples group #1 (WCu ₁)	Samples group #2 (WCu ₂)	Samples group #3 (WCu ₃)
Material	W80Cu20	W80Cu20	W80Cu20
Sintering Temperature (°C)	1350	1350	1200
Sintering Time (hours)	3	1	3
Density (gr/cm ³)	15.295	15.048	14.113
Relative Density (%)	98.04	96.46	90.47

According to these results sintering densification of the W–Cu parts depends greatly on sintering temperature and time. As sintering time and sintering temperature increase, sintered density of the W-Cu samples also increases. The relative densities of samples which are sintered at 1200 °C for 3 hours were found to be about %90.47. However, when the same samples sintered at 1350°C for one hour the relative density

increase to %96.46. This increase can be related to the melt fluidity. At higher temperatures melt fluidity of the copper will be high therefore the homogeneous distribution of solid W particles in liquid copper will be possible which results in density increase. When the sintering time increased from 1 hour to 3 hours at 1350°C further increase in relative density is recorded. This may be due to that 1 hour is not enough for or liquid-phase sintering and homogeneous redistribution of solid W particles in the presence of Cu liquid.

As shown in Table 4.15 it was possible to have samples which has %98 relative density values when the sintering temperature is set to 1350 °C and parts are sintered for 3 hours. So these parameters are determined to be optimum parameters for this application. Parts sintered with these parameters are expected to have the best microstructure, shrinkage and compressive strength values.

4.5.2. Density of W-15Cu parts

The measured density values of the samples and relative densities according to the theoretical value of 16.4 g/cm³ is given in Table 4.16. According to this result %79 relative density value obtained which is an unacceptable ratio for MIM operations where at least %90 relative densities should be acquired. This is an expected value since these parts shrinkage ratio is only %3 as explained in section 4.4.3

Table 4.16. Measured Density Values for W-15Cu

W-15Cu Feedstock	
Material	W85Cu15
Sintering Temperature (°C)	1350
Sintering Time (hours)	3
Density (gr/cm ³)	12.95
Relative Density (%)	79.04

4.6. Microstructure Analysis

For the analysis of the microstructures, three samples from three group of W80Cu20 parts which were sintered using different sintering parameters (see Table 4.15) and one sample from W-15Cu parts were used. Specimens used for measurements were obtained from these samples by abrasive cutting. Then specimens were mounted in bakelite with cross-sections on top and they were ground flat with successfully finer grades of SiC papers, and they were polished with an Aluminum paste. FEI XL30 S FEG ultra high-resolution scanning electron microscope was used to the morphology of the specimens' microstructure.

4.6.1. SEM Analysis

Figure 4.29 shows the typical SEM image of a W-Cu composite. The light gray and dark grey areas show the copper-rich zone and W-skeleton respectively, whereas black holes show impurities such as corrosion i.e. As described in section 2.5.4.1 during liquid phase sintering copper powders melts and fill the gaps among tungsten particles. If the gaps among tungsten particles cannot be effectively filled by copper particles, blind holes may be formed. However, if there is a good dispersion granted between copper and tungsten particles, thermal properties of the sintered parrts will enhance [45]. If not, undesirable empty zones may appear between tungsten particles which decreases the thermal efficiency.

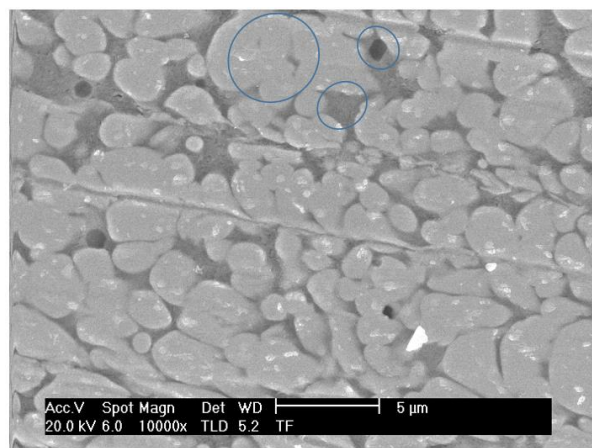


Figure 4.29. Copper-Tungsten Microstructure

4.6.1.1. SEM Analysis of W-20 parts

A comparison between the microstructures of three specimens can be done by studying the microstructure in the images shown in Figure 4.30 . Figure 4.30 (c) shows the SEM image of the specimen which is sintered at 1200 °C for 3 hours. When compared this image to the other images of specimens which is sintered at 1350°C, it is clearly seen that copper-rich areas shown in dark grey is less among all the specimens and slight connectivity between the Cu regions can be seen. This indicates that melt fluidity of copper at sintering temperature 1200 °C is not enough for Copper to fill gaps among Tungsten particles. Moreover as shown in Figure 4.31 (a) there exist huge pore structures in these samples which indicates that sintering hasn't been completely succeeded. When sintering temperature is increased from 1200 °C to 1350 °C, the amount of copper-rich zones increases as shown in Figure 4.30 (b) which also leads the formation of contacts between the copper areas which enhances the thermal properties of the specimen. However, in this image, there exists still some pore structures may be observed as shown in Figure 4.30 (b) which degrades the thermal conductivity. When sintering time is increased from 1 hour to 3 at 1350°C further improvement in the microstructure can be seen as shown in Figure 4.30 (c). No porosity can be identified in the SEM image of these images and a more homogeneous distribution of W and copper particles exist. W and Cu phases distribute homogeneously in the structure and every W particle is capsulated by copper networks. This reveals that 1 hour of sintering time is not enough for or liquid-phase sintering and homogeneous redistribution of solid W particles in the presence of Cu liquid.

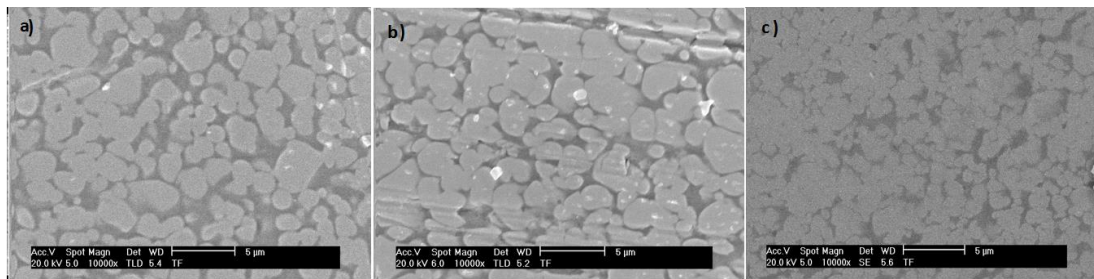


Figure 4.30. Electron-Sem Images of samples a) sintered at 1350 °C for 3 hours, (b) sintered at 1350 °C for 1 hour, c) sintered at 1200 °C

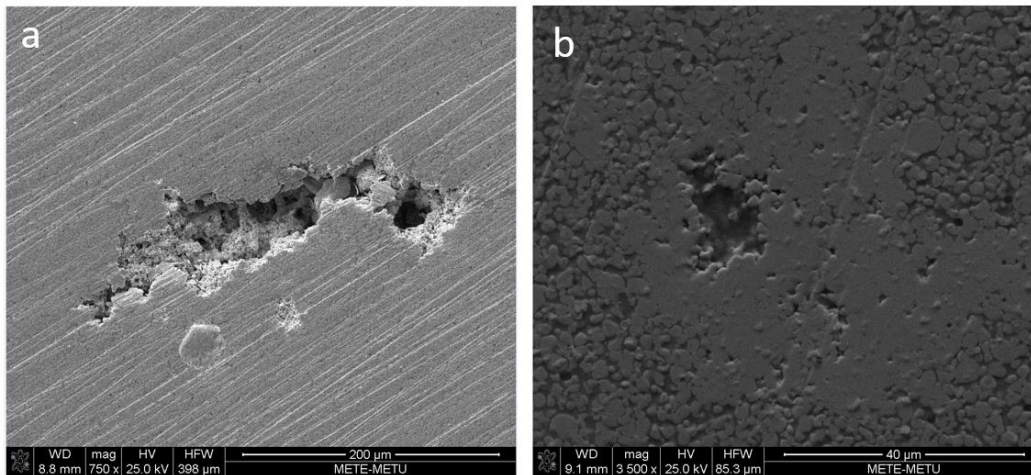


Figure 4.31. Porosities found in samples a) sintered at 1350 °C for 1 hour, b) sintered at 1200 °C

4.6.1.2. SEM Analysis of W-15 parts

Figure 4.32 (a) and (b) shows the 5000x SEM image of W-20Cu and W-15Cu samples. Images indicate that compared to W-20Cu image copper rich areas shown in dark grey is less and there is almost no connectivity between the Cu regions. Full wetting of the tungsten grains can be achieved during the absence of the Cu matrix. This points to failure in the liquid phase sintering since the copper powders couldn't fill the gaps among tungsten particles. The reason for this behavior will be investigated in EDX analysis.

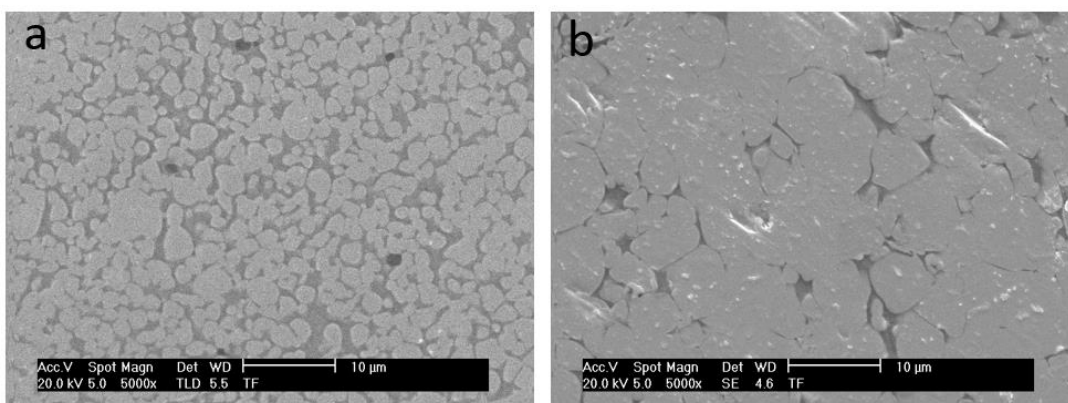


Figure 4.32. 5000x SEM image of a) W-20Cu samples b) W-15Cu samples

4.6.2. EDX Analysis

EDX analysis is performed to provide elemental identification and quantitative compositional information. To characterize the elemental composition volume of each sample analyzed and results are summarized below.

4.6.2.1. EDX Analysis of W-20Cu parts

A comparison between elemental composition volumes of three W-20Cu specimen can be done by studying the EDX images and elemental analysis of W-20Cu samples shown in Figure 4.33. Elemental composition of each sample W_{Cu1} which are sintered at 1350 °C for 3 hours, W_{Cu2} which are sintered at 1350 °C for 1 hour and W_{Cu3} which are sintered at 1200 °C for 1 hour shown in a,b,c parts of the figure respectively. According to these results Cu composition is highest with %21.02 among all the samples prepared. This is an expected result since SEM images already showed that in this sample all W particles encapsulated by copper networks and there are more copper-rich zones available in the microstructure. When sintering time decreases to 1 hour, copper availability on the surface decreases to %19.75 as may be seen in Figure 4.33(b). The copper percentage decreases further to %18.94 when sintering temperature decreases to 1200 °C. These results match with the findings in SEM analysis that melt fluidity is very important factor in liquid phase sintering. At higher temperatures melt fluidity of the copper will be high therefore a homogeneous distribution of solid W particles in liquid copper will be possible which results in more copper availability on the surface.

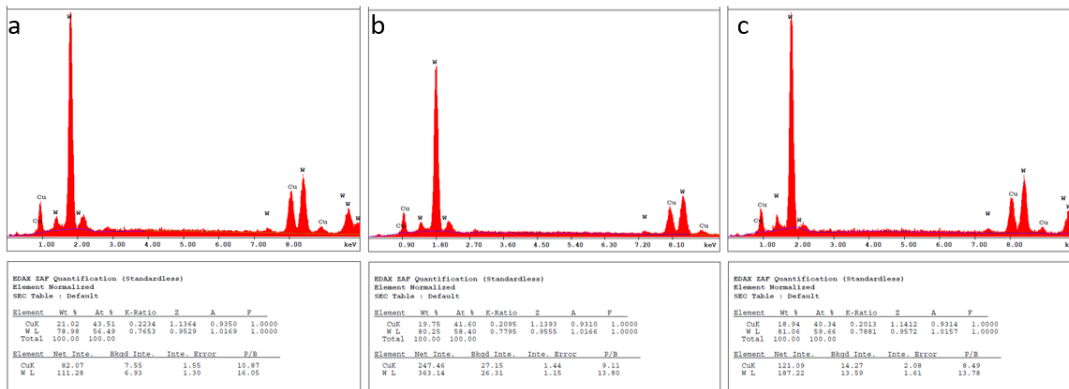


Figure 4.33. EDX Images of samples a)W-20Cu(1)(b) W-20Cu(2)c) W-20Cu(3)

The distribution of copper and tungsten elements from one side to another side for all samples were analyzed by Line-scan which are shown in Figure 4.34, Figure 4.35, and Figure 4.36 respectively. Figure 4.34 shows the line-scan of the sample belonging the group 1 samples which were sintered with optimum sintering parameters. Figure 4.35 and Figure 4.36 show the line scan results of the samples which were sintered in lower EDX temperatures and shorter time. As seen from the sample Figure 4.34 according to line analysis there is smooth transition between the phases which shows that copper atoms could successfully diffuse in tungsten particles when the samples were sintered with optimum parameters. However as sintering time and temperature decreases, the transition zone between the phases gets sharper as seen in Figure 4.36. This indicates that copper atoms could not effectively diffuse in tungsten particles during sintering for these samples so that bonding between W and Cu is extremely poor. Therefore, these samples are expected to show brittle behavior under the load which also conforms with experimental results explained in section 4.9

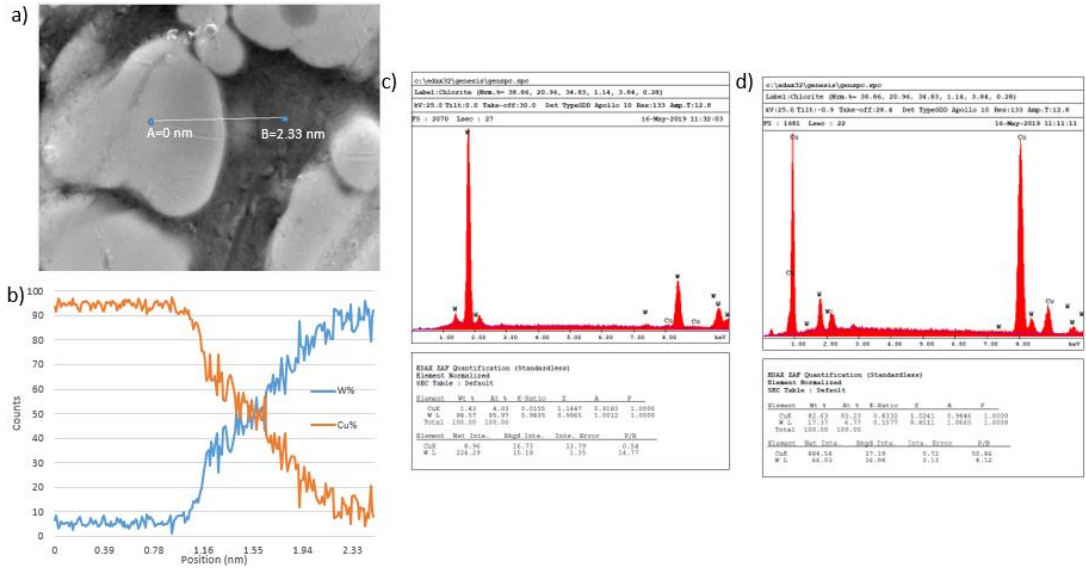


Figure 4.34. Line analysis of samples group #1(WCu1) a) Microstructure image b) Copper and tungsten distribution along the specified line c)Elemental composition in point A d) Elemental composition in point B

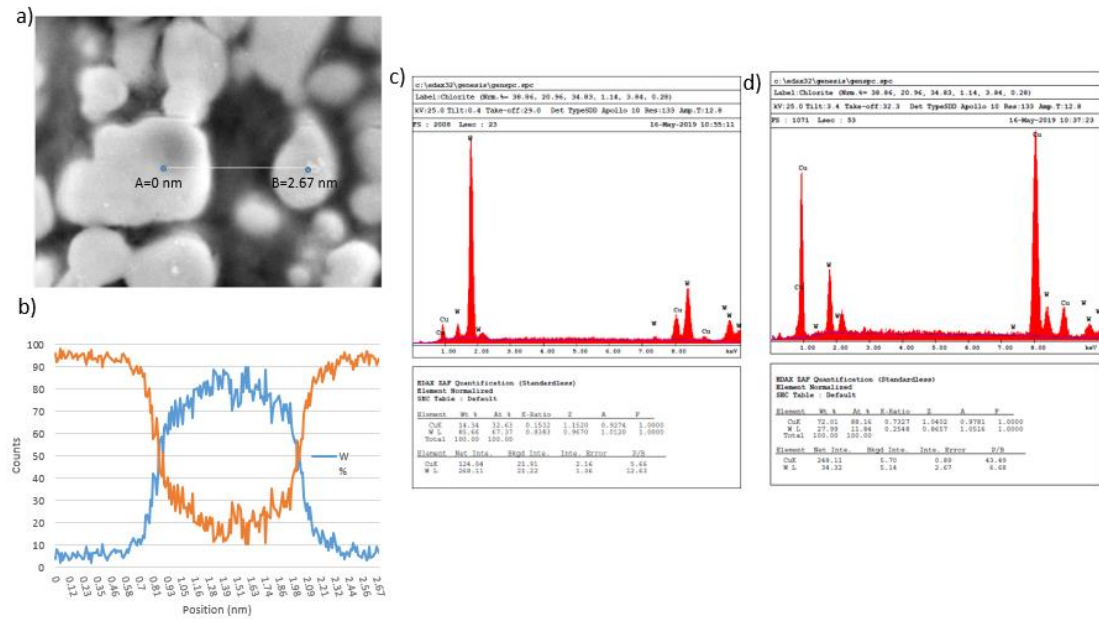


Figure 4.35. Line analysis of samples group #2(WCu2) a) Microstructure image b) Copper and tungsten distribution along the specified line c)Elemental composition in point A d) Elemental composition in point B

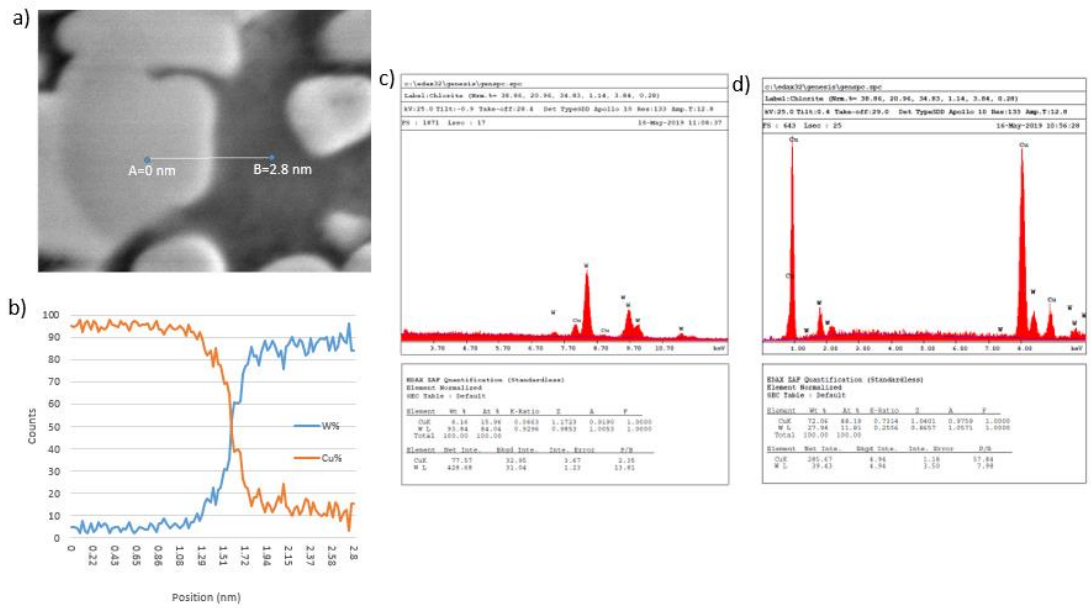


Figure 4.36. Line analysis of samples group #2(WCu2) a) Microstructure image b) Copper and tungsten distribution along the specified line c)Elemental composition in point A d) Elemental composition in point B

4.6.2.2. EDX Analysis of W-15Cu parts

Figure 4.37 shows the elemental composition volume of sample W85Cu15. The elemental analysis shows that copper percentage in the composite is only %6.43 whereas the expected value is around %15. This ratio indicates that there is a problem with feedstock properties since the measured tungsten ratio is 10% lower than specified value in the technical data sheet. As explained before, for MIM operations the first requirement is to have well-prepared feedstock material. To provide dimensional control in the finished products this feedstock should be carefully designed so that it will be stable with time, it will have sufficient uniformity to provide dimensional control and it will be easy to mould. Therefore, the reason for failing during sintering of W85Cu15 parts may be due to feedstock which is not properly prepared. Further investigations about the reason for failure will be conducted as future studies.

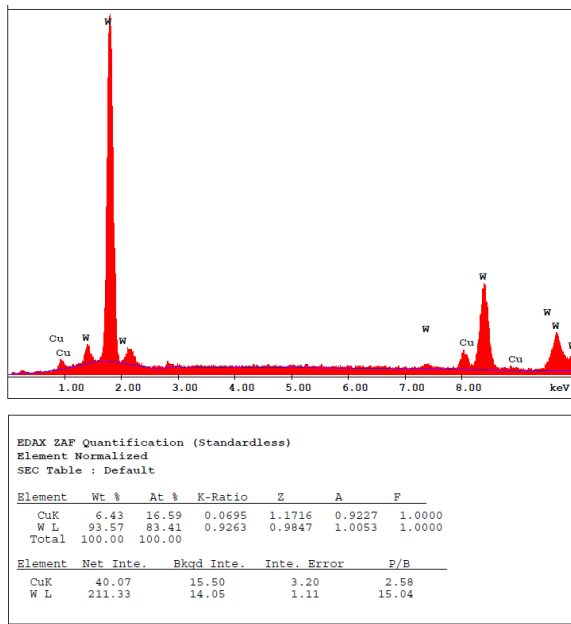


Figure 4.37. EDX Images of W-15Cu sample

4.7. Thermal Properties

To measure the thermal properties (i.e. thermal conductivity and thermal expansion coefficient) of the produced heat sink, the specimens whose information are given in section 3.2 were used. The geometry of the test specimens was determined according to thermal test requirements and they were produced by injection using the same mold as the heat sink. The samples produced for the thermal measurements are shown in Figure 4.38



Figure 4.38. The samples for measurements a) thermal conductivity and b) thermal coefficient of expansion

Three groups of samples from W80Cu20 materials were prepared to analyze the effect of sintering parameters on thermal properties. First group of samples were sintered at 1350 °C for 3 hours, whereas the second group sintered at same temperature for 1 hours. The last group was sintered at 1200 °C for 3 hours. Thermal properties of all these sintered samples were measured and results were compared with theoretical values given in Table 4.17. The measuring procedure and the results of the measurements were explained in the following sections.

Table 4.17. Thermal properties of W80Cu20 [46]

Material	W80Cu20
Tungsten Content	80±1
Density (g/cm ³)	15.5
Coefficient of Thermal Expansion (10 ⁻⁶ /°C)	8.3
Thermal Conductivity (W/m·K)	200-210

4.7.1. Thermal Conductivity

Thermal conductivity (λ) of the specimens was calculated using the estimated specific heat capacity (C_p), the measured thermal diffusivity (α), and the measured density (ρ) of the specimens, according to the formula given in (4-3) [47].

$$\lambda = \alpha \cdot \rho \cdot C_p \quad (4-3)$$

For thermal diffusivity measurements, the laser micro flash method connectivity measurement device (LFA 457, Netzsch, Germany) was used. The samples first cut to 10x10 mm in order for placement samples to the device and the measurements performed for the temperatures between 50°C and 300 °C. The C_p values were measured using differential scanning calorimeter (STA 449F3A; Netzsch, Germany). The density values were obtained from Table 4.15. The calculated thermal conductivity values by using these parameters are given in Figure 4.39.

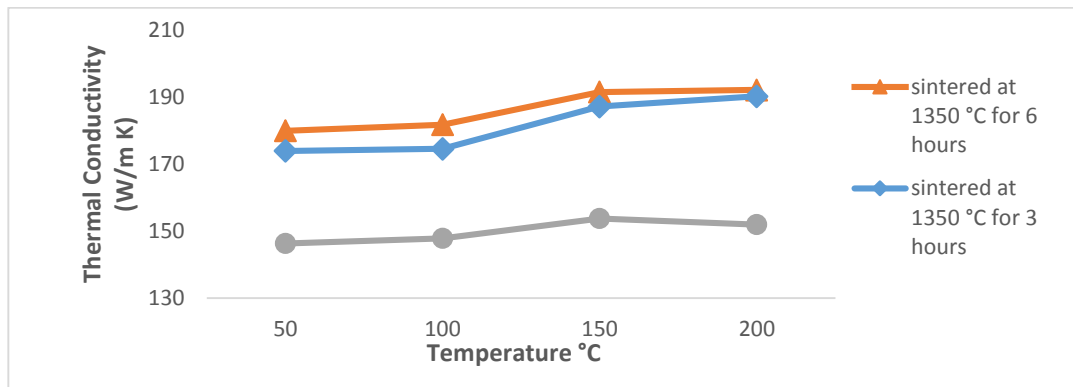


Figure 4.39. Thermal conductivities of Copper-Tungsten Composites

As stated in the literature, the high thermal conductivity depends on Cu, which provides more free electrons in the composites than W [48]. Conduction preferentially occurs through Cu phase which has three times higher than the thermal conductivity of W phase [1]. So as the copper ratio increase the thermal conductivity value also increases. However, Figure 4.39 also reveals that even for the same material sintering parameters directly influences the thermal conductivity values. Group #1 samples, which were sintered at 1350 °C for 3 hours and which have highest relative density values also have the highest thermal conductivity values whereas the samples sintered at 1200 °C which have lowest density values have the poorest conductivity values.

This means that high thermal connectivity values are directly related with the microstructure and densification results. High-density values show that there exists strong interfacial bonding between copper and tungsten powders which results in better thermal conductivity. Also, this result show that a continuity in CU-network through the sample is also a significant factor for high thermal conductivity.

4.7.2. Coefficient of Thermal Expansion Measurements

For CTE measurements, Netzsch 402 PC Dilatometry device was used. For measurements, the samples first cut to 25x5x5 mm dimensions. Then, they are put in a laboratory incubator until all the samples are completely dried. (Until the weight difference between two weighings is under %0.1) Then samples are conditioned in room temperature. Afterward, they are heated until 700 °C with a rate of 10 °C

/minute. The dimensional change is recorded in every 50 degrees. According to these measurements, the measured thermal expansion of coefficient values are given in Table 4.18

Table 4.18. Coefficient of thermal expansion values of the samples

	<i>Sample Groups</i>		
	(WCu ₁)	(WCu ₂)	(WCu ₃)
Sintering Temperature (°C)	1350	1350	1200
Sintering Time (hours)	3	1	3
CTE (10 ⁻⁶ /°C)	8.16	9.02	9.03

Results show that CTE value of samples sintered at 1350 °C for 3 hours is closest to the theoretical value of 8.3, which is given in Table 4.17, whereas CTE values of other samples are greater than this value. This result also verifies that the samples with the best microstructure and highest density values have the optimum CTE values whereas pores and voids in the other samples are the main factors which increase the CTE of W-Cu composite.

4.8. Thermal Performance Assessment of the Heat Sink

Efficacy of a standard pin fin heat sink is functions of the geometry, *i.e.* spacing, shape, length of the pins *etc.*, and the thermal conductivity of the heat sink material. In the current work, geometric details of the heat sink produced were determined based on a standard commercial product, which is suited for natural convection cooling based applications. Conductivity of the material, on the other hand, is closely related with the parameters utilized during the manufacturing (sintering) process. Although conductivity of samples with basic shapes were determined by measurement tests conducted by a certified test center, conductivity of the material may differ within a complex-shaped sample due to undesired non-homogeneities throughout the sample or internal cracks. Therefore, an *in situ* performance experiment is carried out to secure the proper functioning of the heat sink produced by MIM process. Following the

experiment, a computational fluid dynamics (CFD) analysis is performed to determine the range of the thermal conductivity of the heat sink.

4.8.1. Experimentation

In order to evaluate and report the cooling performance of the heat sink, an experimental setup is constructed. A photograph of the experimental setup is given in Figure 4.40

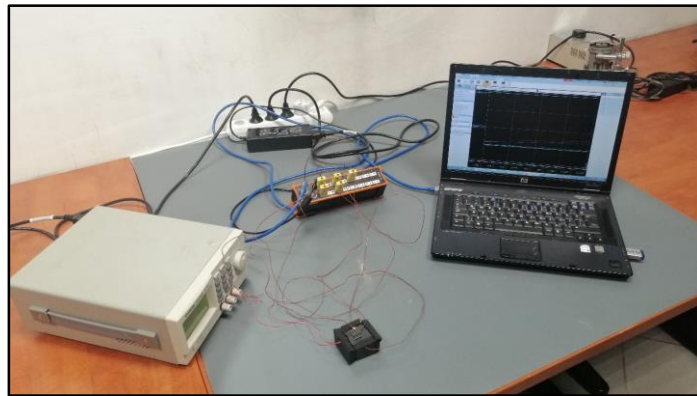


Figure 4.40. Experimental setup

Individual components utilized during the experiment are shown in Figure 4.41.

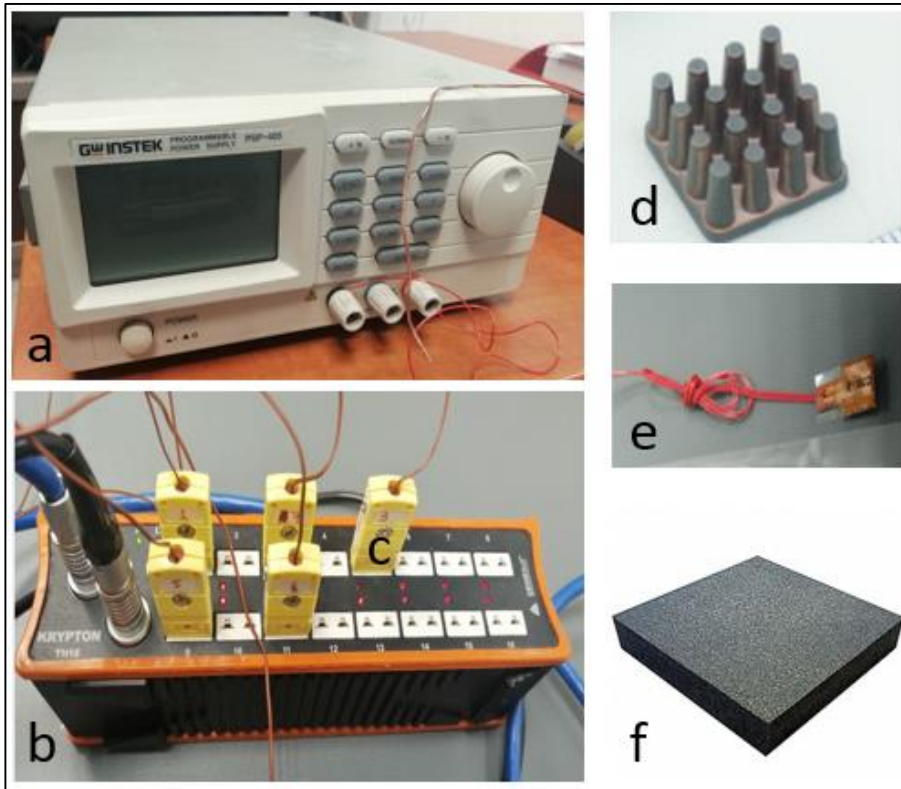


Figure 4.41. Components utilized during the experiment

Details of the components are listed as follows:

- a) DC Power Supply (GW Instek PSP-405)
- b) Temperature Data Logger (Krypton TH16)
- c) K-type thermocouples (Omega):
 - Fin-tip temperature
 - Base temperature
 - Insulator-1
 - Insulator-2
 - Ambient temperature
- d) Heat Sink
- e) Film Heater (Minco HK5572R26.5L12F)
- f) Insulating material (Poron)

Firstly, a film heater is attached to the heat sink using its self-adhesive tape (please see Figure 4.42).

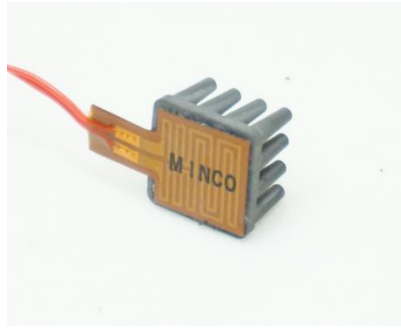


Figure 4.42. Heater attached to the heat sink

DC power supply is used to generate the heating within the film heater. To convey the heat in the direction of the heat sink, film heater is covered by insulating material, which is seen in Figure 4.43 .

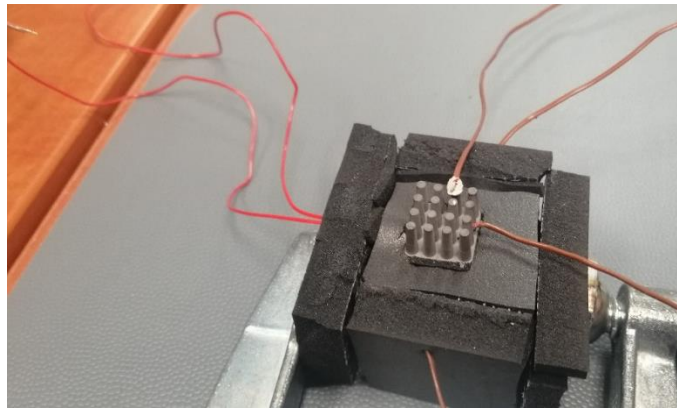


Figure 4.43. Close up view of the heat sink and insulating material together with thermocouples

Minco Heater attached to the heat sink is connected to the GW instek PSP-405 Power Supply. To measure the temperatures in the different locations K-type thermocouples are used. Two of them attached to the base and fin tip of the heat sink to measure temperature for the heat sink. Two thermocouples are used for measuring the insulator temperatures while the last one used for recording the ambient temperature.

Positions of the thermocouples are also seen in Figure 4.43. One of the thermocouples is fixed to a tip of a fin using a two-component thermally conductive epoxy adhesive. Another thermocouple is attached to the base plane of the pin fins. While one

thermocouple is assigned to measure the ambient temperature, other two are used to determine the average temperature of the surface of the insulating material.

During the experiment, heat dissipated in the heater was 5 W. Data is collected during 400 minutes' test duration. Heat loss from the vertical surfaces of the insulator is calculated based on the heat transfer coefficient, \bar{h} , estimated at the side and bottom walls, as follows:

$$\dot{q}_{loss} = hA(T_s - T_\infty) \quad (4-4)$$

where A is the surface area, T_s is the average surface temperature and T_∞ is the ambient temperature. Calculation of heat transfer coefficient relies on the estimation of Nusselt number (Nu_L):

$$h = \frac{Nu_L}{L} \quad (4-5)$$

where k and L are thermal conductivity of the air and characteristic length of the surface where heat transfer takes place. Natural convection correlations for heated vertical plate [49] and for horizontal plates with heated surface put upward and downward [50] are given in Eq. (4-6), (4-7) and (4-8) respectively:

Nu_L for vertical plates:

$$Nu_L = \left\{ 0.825 + \frac{0.387Ra_L^{1/6}}{[1 + (0.492/Pr)^{9/16}]^{8/27}} \right\}^2 \quad (4-6)$$

Nu_L for horizontal plates with heated surface put upward:

$$Nu_L = 0.54Ra_L^{1/4} \quad (4-7)$$

Nu_L for horizontal plates with heated surface put downward:

$$Nu_L = 0.27Ra_L^{1/4} \quad (4-8)$$

where Pr is Prandtl number and Ra_L is Rayleigh number expressed as $Ra_L = \frac{g\beta(T_s - T_\infty)L^3}{\nu\alpha}$, where β , ν , and α are expansion coefficient, kinematic viscosity, and thermal diffusivity of the air calculated at the film temperature $(\frac{T_s + T_\infty}{2})$, respectively. During the experiment, the ambient temperature was 24.8°C and average surface temperature was 28.3°C . Accordingly, heat transfer coefficients for vertical walls, upper wall and lower wall are found as 3.97 , 2.37 and $4.74 \text{ W m}^{-1} \text{ K}^{-1}$, respectively. When these coefficients are used in Eq. (4-4), total heat loss rate is calculated as 0.7 W . The temperature measurements over the experiment is shown in Figure 4.44

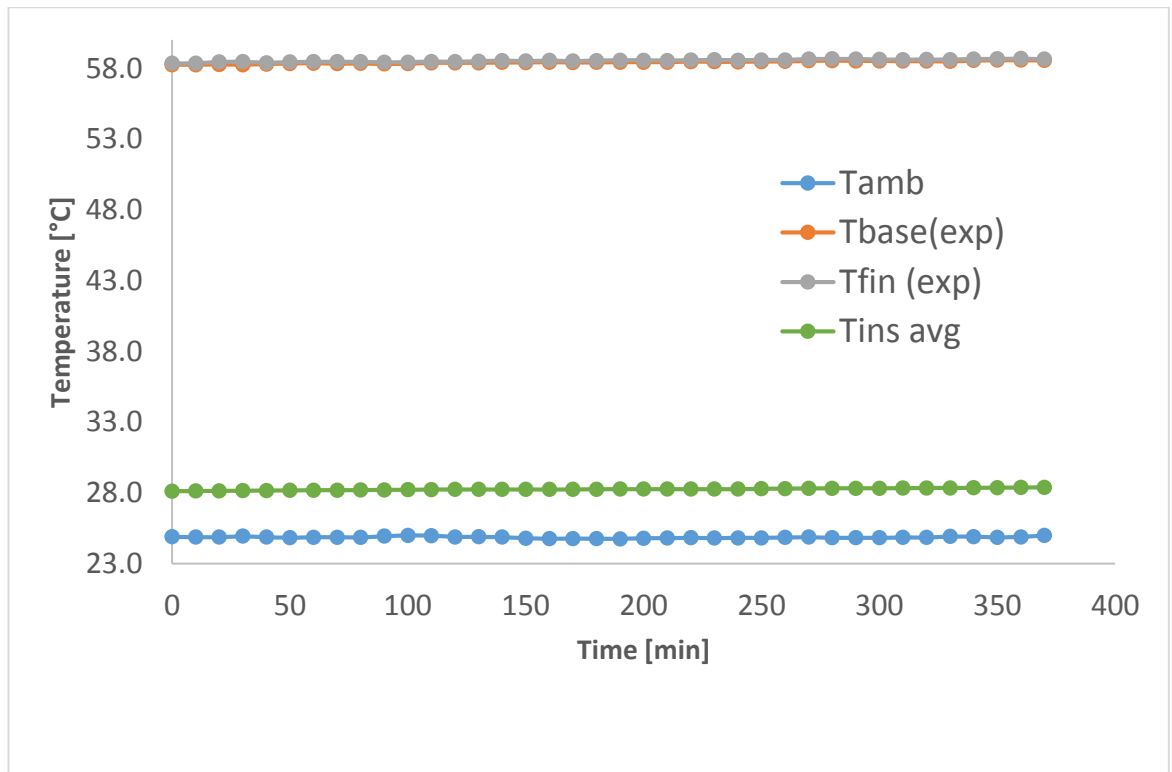


Figure 4.44. Heat Transfer Experimental Set-up

4.8.2. Simulation

Heat transfer analysis is performed using FloEFD, which is a widely used, finite volume based CFD software. 3-D representation of computational setup is shown in Figure 4.45

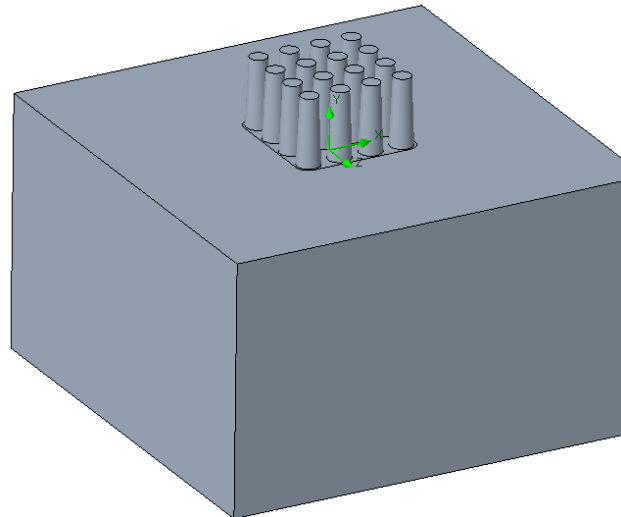


Figure 4.45. *Computational Set-up*

The box beneath the heat sink represents the insulating material. It should be noted that perfect insulation is assumed during CFD analysis. Therefore, heat input, which is applied onto the bottom surface of the heat sink, is the net heat transfer rate supplied to the heat sink during the experiment. It is basically equal to the difference between the heat dissipated by the film heater and the heat loss from the walls of the insulating material. Since the system is symmetrical in both x and y directions, as shown in Figure 4.46a, only a quarter of the system is simulated with the symmetry boundary conditions at the central planes. Meshing of the computational domain is demonstrated in Figure 4.46b. Number of fluid and solid cells were 3,623,800 and 294,657, respectively. Mesh independence of the results was also checked.

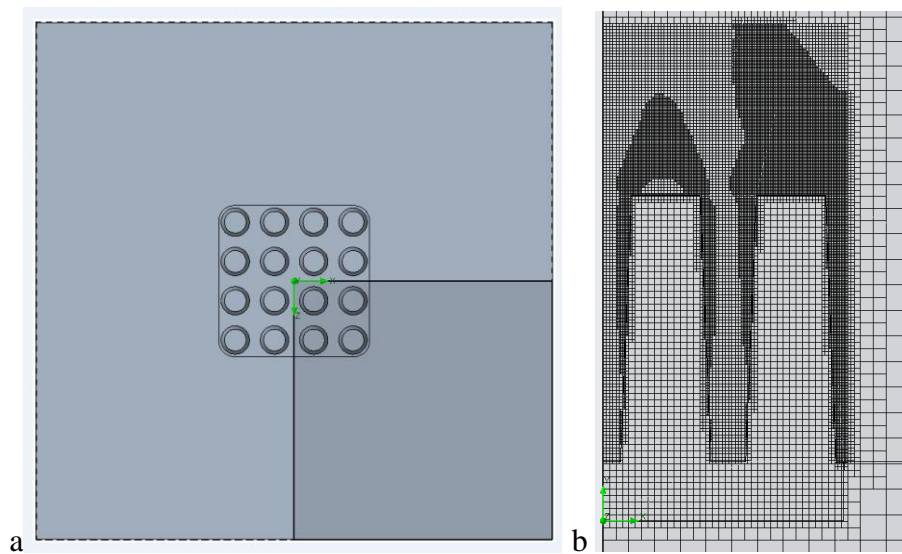


Figure 4.46. (a) Top view of the computational domain. (b) Front view of the computational domain

In addition to the convective heat transfer, radiative heat transfer is also considered in the simulations. Surroundings were assumed in thermal equilibrium with the ambient air. Emissivity of the heat sink assumed to be unity. Ambient temperature was the same with the one in the experiment.

Objective of the CFD simulation is simply to determine an effective thermal conductivity for the heat sink produced by sintering process. For this purpose, different thermal conductivity values were assigned to the heat sink material during simulations and a thermal conductivity range, which yields reasonable matching with the experimental results, was sought.

When the CFD analysis performed by taking thermal conductivity value for the heat sink is as 180 (watt /m.°C) which is the actual value measured by laser micro flash method explained in 4.7.1 c the temperature distribution over given Figure 4.47 is acquired. According to this distribution, the heat sink base temperature is found as 58.65 °C whereas fin tip temperature is 58.55 °C.

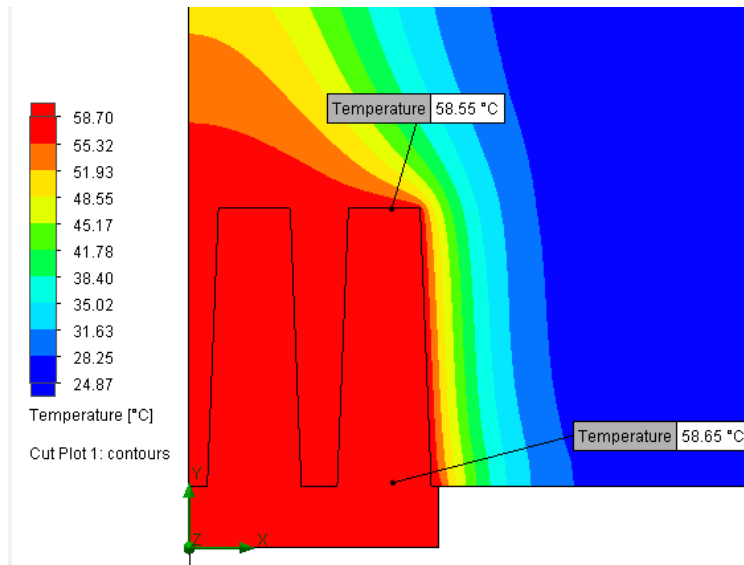


Figure 4.47. Temperature Distribution over the heat sink

The measured temperature values are shown in Figure 4.48 together with the analysis result for comparison when thermal conductivity value for the heat sink is taken 180 (watt /m.°C). Both results show almost perfect match. The fluctuations existing in temperature measurements in the experiments may be due to ± 0.1 °C measurement accuracy of the thermocouples and miss attachment of the thermocouples.

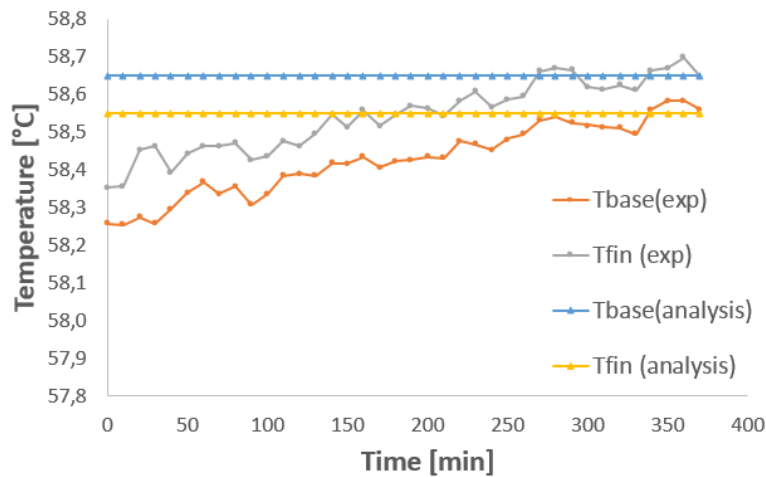


Figure 4.48. Temperature Measurements

Table 4.19 shows the base and tip temperatures of the heat sink according to analysis results when k values are selected between the ranges [10-400 watt /m. °C].

Figure 4.48 reveals that according to experiment results the difference between the T_{base} and T_{fin} temperatures are around 0.1 degree. When this value is compared to the DT values shown in Table 4.19, the closest conductivity value for the heat sink used in the experiment turns out to be 200 watt /m.°C. This result also confirms that conductivity of the heat sink match perfectly with the measured conductivity values of the specimen by certified test center and the heat sink part produced and used in the experiment is free of undesired non-homogeneities and internal cracks.

Table 4.19. Temperature ranges for different thermal conductivity values

Case	Conductivity(watt /m.°C)	T_{base}	T_{Tip}	dT
Experiment	To be determined	58.42	58.52	0.1
Simulation	10	60.32	58.21	2.11
Simulation	50	58.92	58.50	0.42
Simulation	100	58.75	58.53	0.22
Simulation	200	58.65	58.55	0.10
Simulation	300	58.62	58.55	0.07

4.9. Tensile Strength Measurements

For tensile strength measurements, the specimens were prepared according to ISO 2740 standard which defines tensile test specimens in powder metallurgy as explained in section 3.2.5. The prepared specimen for the test is shown in Figure 4.49



Figure 4.49. Tensile Strength Specimen

Three groups of tensile specimens were prepared to analyze the effect of sintering parameters on mechanical properties. First group of samples was sintered at 1350 °C

for 3 hours, whereas second group sintered at same temperature for 1 hours. The last group was sintered at 1200 °C for 6 hours. Mechanical properties of all these sintered samples were measured and results were compared with theoretical values given in Table 4.20.

Table 4.20. Mechanical properties of W80Cu20 [51]

Material	W80Cu20
Tungsten Content	80±1
Density (g/cm ³)	15.5
Tensile Strength (MPa)	600
Axial Strain at Break (%)	200-210

For the experiments Instron 5582 universal testing machine is used. The specimens were placed to testing machine and extended until the fracture. The elongation of the gauge section is recorded against the applied force. The records are used to measure tensile strength values. The experimental set-up and fractured samples in the experiments are shown in Figure 4.50 a and b respectively.



Figure 4.50. Experimental Tensile Test Setup and fractured samples

The measured tensile stress and axial strain values at break is given in Table 4.21. According to these results compressive strength of the W–Cu parts depends greatly on density which is related with sintering temperature and time. As sintering time and sintering temperature increases, sintered density of the W-Cu samples also increases so does tensile stress value. The samples which were sintered at 1350 C for 3 hours have the closest tensile strength values to the theoretical values given in Table 4.20.

This is an expected result since these samples have the greatest relative density values and correspondingly W particles are homogeneously distributed in the Cu matrix, the interface bonding between W and Cu is particularly strong. On the other hand, samples which are sintered at 1200 °C have poor tensile strength values which indicates that the bonding between W and Cu is extremely poor. As explained in section 4.6.1, in the samples that are sintered at 1200 °C, the copper could not effectively fill the gaps among tungsten particles, so blind holes were formed. Stress especially concentrates on these blind holes and porosities leading to crack nucleation and growth which results in poor compressive stress values [53]. The experimental results also show that all specimens exhibit very low elongation that verifies brittle behavior.

Table 4.21. Measured Mechanical Values

	Samples group #1	Samples group #2	Samples group #3
	(WCu ₁)	(WCu ₂)	(WCu ₃)
Sintering Temperature (°C)	1350	1350	1200
Sintering Time (hours)	3	1	3
Measured Density	180-190	185-195	190-200
Measured Tensile Stress (MPa)	568.28	550.228	226.724
Axial Strain at Break (%)	0.45	96.46	0.05

CHAPTER 5

CONCLUSIONS

In this thesis work properties of the complex-shaped Cu-W heat sink parts produced by the metal injection molding process for high-performance electronic devices were investigated. Two composite materials W80Cu20(%80W-%20Cu) and W85Cu15(%85W-%15Cu) were purchased from foreign suppliers in order to investigate the effects on thermal and mechanical properties when the ratio of substances in the composite change. To study the geometrical limitations associated with the MIM operations two different heat sink geometry were designed which have different level of complexity. Other than heat sink some test samples geometries were also designed for thermal and mechanical tests according to test requirements. Different set of parameters are used during production to investigate the effect of production parameters on produced parts. Geometrical and density measurements of the produced samples were performed in in situ, whereas thermal properties i.e. thermal conductivity and CTE values of the parts were measured in Eskisehir Ceramic Industry. Microstructure analysis and tensile strength measurements were accomplished by using METU facilities. Finally, an in situ performance experiment is carried out to secure the proper functioning of the produced heat sink which was also confirmed with a computational fluid dynamics (CFD) analysis. The summary of all the major findings and the conclusions obtained from this thesis is listed below:

- The level of complexity of the parts to be produced depends on the capabilities of the equipments even with MIM process. In the beginning of the study, injection operations with heat sink which have high level of complexity has failed. Although different injection parameters were used and some modifications were performed on the mold it was not possible to produce defect free parts. Therefore, a slight difference in the design of the heat sink design was performed by shortening the pins however it was still not possible to inject the parts. The injection molding machine producer company was informed and the reason for the failure investigated. According to the company report, capabilities of the existing injection

machine is not adequate to inject parts with that high level of complexity. Although MIM makes possible producing products with high complexity of geometrical shapes there are limits available associated with the equipment's. Therefore, replacing the old injection machine with new one which has superior properties was suggested by the company. Therefore, this part was skipped and operations were continued with the heat sink which has a low level of complexity.

- During injection of other parts buildup of excess material was encountered. Decreasing the injection pressure helped the prevention of flash forming. Other than this problem all parts were successfully injected. All parts had regular shapes without any defects
- During debinding for W80Cu20 Feedstock weight loss stopped after 21 hours, where as in solvent debinding for W85Cu15 feedstock was stopped after 15 hours. So for debinding operations these time durations are set for minimum debinding time.
- Three different set of parameters used to investigate the effect of sintering parameters on mechanical and thermal properties of the samples. First group of samples was sintered at 1350 °C for 3 hours, whereas second group was sintered at same temperature for 1 hours. The last group was sintered at 1200 °C for 3 hours. According to test results on mechanical and thermal properties of the samples, sintering at 1350 °C for 3 hours gives the best mechanical and thermal properties for W80Cu20 feedstock. For W85Cu15 feedstock all sintering operations resulted in failure.
- The shrinkage ratio of the samples important to determine if the sintering operation is performed successfully. For a successful sintering operation, the measured shrinkage ratio should be as close as to the theoretical shrinkage ratios announced by the feedstock manufacturer. According to shrinkage results shrinkage ratio of the W–Cu parts depends greatly on sintering temperature and time. As sintering time and sintering temperature increases shrinkage ratio of the W-Cu samples also increases. This increase is related to the melt fluidity. At higher temperatures melt

fluidity of the copper will be high therefore homogeneous distribution of solid W particles in liquid copper will be possible which results in density increase. When the sintering time increases further increase in relative density is recorded. This indicates that there should be enough time for homogeneous redistribution of solid W particles in the presence of Cu liquid during sintering.

- During liquid phase sintering copper powders melts and fill the gaps among tungsten particles. If copper cannot effectively fill the gaps among tungsten particles, blind holes are formed. However, if there is a good dispersion granted between copper and tungsten particles, the final specimen would exhibit excellent thermal conductivity properties
- Melt fluidity is very important factor in liquid phase sintering. At higher temperatures melt fluidity of the copper will be high therefore homogeneous distribution of solid W particles in liquid copper will be possible which results in more copper availability on the surface.
- Sintering process with W85Cu15 feedstock resulted in failure. The modifications in the sintering parameters didn't help and parts could not reach the required densification results. Mechanical properties of the produces parts were so improper that it was possible to break the parts with hand. The reason for the failure investigated and according to elemental analysis shows that copper percentage in the composite is only %6.43 whereas the expected value is around %15. This result indicated miss preparations of feedstock which may be the reason for the failure.
- High thermal connectivity values are directly related to the microstructure and densification results. High-density values show that there exists strong interfacial bonding between copper and tungsten powders which results in better thermal conductivity. Also, this result shows that continuity in CU-network through the sample is also a significant factor for high thermal conductivity
- Blind holes and porosities are a suitable site for crack nucleation and growth, where the stress may concentrate which leads poor compressive stress values

- Heat sink produced with W80Cu20 feedstock using optimum sintering parameters meet all thermal and mechanical requirements according to test results. The performance of the produced part was also verified by the in situ experiment which also verified by the CFD analysis. Therefore, an alternative solution for producing complex-shaped heat sinks for dealing with thermal management issues in the high-performance electronic devices had been found. As this product may be readily used in future devices as it stands, by doing necessary modifications on the geometry it may be easily meet the requirements on similar devices.

In conclusion, with this work, Complex-Shaped CuW heat sinks with necessary thermal properties were produced by using MIM process to deal with thermal management issues in future high performance electronic devices.

CHAPTER 6

SUGGESTED FUTURE WORK

The research shows that global metal injection molding market size exponentially increasing. Manufacturers in the world prefer metal injection molding because of minimum finishing operations which reduces the material wastage and enabling the production of components with complex geometries and enhanced properties. However, in our country, this process hasn't got the necessary considerations that it deserves. According to our market analysis in there is only one company in Turkey who is dealing with MIM process and their products are restricted with ferrous metal such as steel. The reason for this underrating is that process is still heavily dependent on foreign sources. For example, the feedstock is one of the main element and most important constituent of the MIM process. Preparing a proper feedstock is very critical for successful production and the exact components and procedures are still proprietary secrets. Feedstock should be purchased from the foreign suppliers since there is no local producer. Depending on the foreign sources brings a lot of risks which include long delivery times, the defective constituents (as in our case), lack of purchasing the product because of an embargo or discontinue of production etc. So developing the domestic feedstock is one of the most important milestones in order MIM process to become widespread. There are some efforts especially in universities on developing the feedstocks but there hasn't been any research that turned on the product yet. The lack of financial support is the main reason for that the research's hasn't reached the desired levels yet.

By considering all these factors, as future studies the domestic feedstock which may be used directly in MIM operations to deal with thermal management issues is aimed. In this way, it will not only remove the risk related with depending on foreign sources but also it will possible to modify the feedstock properties in order to have desired thermal and mechanical properties.

As further studies, the producing own-feedstock is planned in order to nationalize the MIM process and to be able to modify the thermal and mechanical properties depending on each future project requirements.

REFERENCES

- [1] Young Do Kim, Nang Lyeom Oh, Sung-Tag Oh, In-Hyung Moon, “Thermal conductivity of W–Cu composites at various temperatures”, *Materials Letters* 51 (2001) 420–424
- [2] Michael Leers, E.Liermann, P. Imgrund, L. Kramer, J. Volkert, “Expansion matched heat sinks made by μ -metal injection molding”. *Proc. of SPIE Vol. 7583 75830H-2*
- [3] Th. Schubert, B. Trindade, T. Weißgärber, B. Kieback “Interfacial design of Cu-based composites prepared by powder metallurgy for heat sink applications”. Th. Schubert et al. / *Materials Science and Engineering A* 475 (2008) 39–44
- [4] M. Ahangarkani, S. Borgi, H. Abbaszadeh, A.A. Rahmani, K. Zangeneh-. “The effect of additive and sintering mechanism on the microstructural characteristics of W-40 composites” *Int. Journal of Refractory Metals and Hard Materials* 32 (2012) 39–44
- [5] Isabel Montealegre-Meléndez , Cristina Arévalo 1, Eva M. Perez-Soriano , Erich Neubauer, Cristina Rubio-Escudero, Michael Kitzmantel “Analysis of the Influence of Starting Materials and Processing Conditions on the Properties of W/Cu Alloys”. *Materials* (2017), 10, 142
- [6] ATS Advanced Thermal Solutions, “Heat Sink Manufacturing Technologies” viewed 09.02.2019, www.qats.com
- [7] Lian-Tuu Yeh “Thermal Performance Evaluation of Various Heat Sinks for Air Cooling”. 13th IITHERM Conference. 2009
- [8] G. E. Moore, Reprinted from *Electronics*, 38 (8), 1965, pp. 114 ff. *IEEE solid-state circuits society newsletter*, 20(3), pp.33-35, 2006
- [9] *Electronics manufacturing initiative technology roadmap*. iNEMI; 2004
- [10] Sunil Hireholi, K.S. Shashishekar, George. S. Milton “Experimental and Theoretical Study of Heat Transfer by Natural Convection of a Heat Sink” e-ISSN: 2278-7461, p-ISSN: 2319-6491 Volume 2, Issue 2 (January 2013) PP: 01-09

- [11] Wikipedia, "Heat sink" viewed 24.12.2019, www.en.wikipedia.org/Heat_sink
- [12] John L. Johnson, Randall M. German "Heat sink Design and Properties: Opportunities for Molders" AM Tellect Publication,(6/11/2002)
- [13] John L. Johnson. "Metal Injection Molding Of Heat Sinks", Design, Heat Sinks, Materials, Compounds, Adhesives, Substrates, Number 4, Volume 10, (01.10.2004)
- [14] ABL Heatsinks, "Heat Sink Design and Selection" viewed 10.02.2019, www.abl-heatsinks.co.uk/heatsink-selection-material.htm
- [15] Gabrian, "6 Heat Sink Types" viewed 10.02.2019, www.gabrian.com/6-heat-sink-types
- [16] MyHeatSinks, "Manufacturing Methods" viewed 10.02.2019, www.myheatsinks.com
- [17] Qpedia "Heat Sink Manufacturing Using Metal Injection Molding" Qpedia thermal Magazine, April 2013
- [18] Wakefield-wette, "Heat Sink Design Facts & Guidelines for thermal analysis" Technical Brief, www.wakefield-wette.com
- [19] D.D.L. Chung "Materials for thermal conduction". D.D.L. Chung / Applied Thermal Engineering 21 (2001) 1593-1605
- [20] L.L. Donga, M. Ahangarkanib, W.G. Chenc, Y.S. Zhanga "Recent progress in development of tungsten-copper composites: Fabrication, modification and applications" International Journal of Refractory Metals & Hard Materials 75 (2018) 30–42
- [21] A. Ibrahim a, M. Abdallah, S.F. Mostafa, A. Abousree Hegazy, "An experimental investigation on the W–Cu composites" Materials and Design 30 (2009) 1398–1403
- [22] WHs Sondermetalle, "Tungsten Copper Composite Data Sheet", viewed 05.03.2019, www.whs-sondermtalle.de/images/pdf/Wcu_Tungsten-Copper_web.pdf
- [23] Wang C, Lin YC.. "Feasibility study of electrical discharge machining forW/Cu composite." J Refract Met Hard Mater ((2009);27:872–82.

- [24] F.T.N. Vüllers, R. Spolenak, From solid solutions to fully phase separated interpenetrating networks in sputter deposited “immiscible” W–Cu thin films, *Acta Mater.* 99 (2015) 213–227.
- [25] Qpedia, “Heat Sink Selection Methodology in Electronics Cooling”, Qpedia thermal Magazine, December 2010
- [26] Cheng Jigui , Wan Lei, Cai Yanbo, Zhu Jinchuan, Song Peng, Dong Jie. “Fabrication of W–20wt.%Cu alloys by powder injection molding” *Journal of Materials Processing Technology* 210 (2010) 137–142
- [27] Michael Leers, E. Liermann, P. Imgrund, L. Kramer, J. Volkert “Expansion matched heat sinks made by μ -metal injection molding” *Proc. SPIE* 7583, High-Power Diode Laser Technology and Applications VIII, 75830H (17 February 2010); doi: 10.1117/12.842064
- [28] P.W. Ho, Q.F. Li, J.Y.H. Fuh “Evaluation of W–Cu metal matrix composite produced by powder injection molding and liquid infiltration” *P.W. Ho et al. / Materials Science and Engineering* 485 (2008) 657–663
- [29] J . L. JOHNSON, “Metal injection molding (MIM) of thermal management materials in microelectronics” *Handbook of metal injection molding* (2012) 460–461
- [30] R. Zauner, R. Nagel, E. Neubauer, K. Portschy, P.A Davies, M.A.Kearns, “Development of Copper MIM Powders for Thermal Management Applications”
- [31] Zlatkov B, Griesmayer E, Loibl H, Aleksić O, Danninger H, Gierl C, Lukić L “Recent advances in PIM technology I. *Science of Sintering*” (2008) 40 (1):79-88
- [32] M. Knuwer, H. Meinhardf, K.-H. Wichmanrf “Injection Moulded Tungsten and Molybdenum Copper Alloys for Microelectronic Housings” 15" *International Plansee Seminar*, Eds. G. Kneringer, P. Rodhammer and H. Wildner, Plansee Holding AG, Reutte (2001), Vol. 1
- [33] FineMIM, “How does MIM compare to other process?” viewed 04.06.2019 www.finemim.com/how-does-mim-compare-to-other-processes.html
- [34] Satyajit (Satya) Banerjee, “Metal Injection Molding (MIM) Process and Production” DSH Technologies, LLC

- [35] G, Goudah ,F. Ahmad, O.Mamat MOhd. Afian Omar “Preparation and Characterization of Copper Feedstock for Metal Injection Molding” *International Applied Sciences* (2010) 10 (24):3295-3300,
- [36] Loh, N.H, S.b. Tor and K. A. Khor “Production of metal matrix composite part by powder injection molding” *J. Mater. Process Technology* (2001) 108:398-407
- [37] G . S. UPADHYAYA, “Powder Metallurgy Technology” Published by Cambridge International Science Publishing(2002), ISBN 1 898326 40 1
- [38] EPMA “Introduction to Metal Injection Moulding Technology” 4th Edition www.epma.com/mim
- [39] German, R.M.,. Theory of thermal debinding. *International Journal of Powder Metallurgy* (1987) 23 (4), 237–245.
- [40] Randall M. German, Pavan Suri, Seong Jin Park “Review: liquid phase sintering” *J Materç. Sci* (2009) 44:1–39
- [41] Fischer Heatsinks Catalogue 15/16 f.cool.e.08-2014 www.fischerelektronik.de
- [42] Sebastian Engström “ Metal Injection Molding, A review of the MIM process and its optimization” Degree Thesis *Plasttechnik* 2017
- [43] M. Knuwer, H. Meinhardf, K.-H. Wichmanrf “Injection Moulded Tungsten and Molybdenum Copper Alloys for Microelectronic Housings” 15th International Plansee Seminar, Eds. G. Kneringer, P. Rodhammer and H. Wildner, Plansee Holding AG, Reutte (2001), Vol. 1
- [44] S.S. Ryu, Y.D. Kim, I.H. Moon, *J. Alloys Compd.* 335 (2002) 233–240.
- [45] Isabel Montealegre-Meléndez , Cristina Arévalo, Eva M. Perez-Soriano, Erich Neubauer, Cristina Rubio-Escudero and Michael Kitzmantel, “Analysis of the Influence of Starting Materials and Processing Conditions on the Properties of W/Cu Alloys” *Materials* 2017, 10, 142
- [46] ATTL Advanced Materials Co “Tungsten Copper Composite properties” viewed 02.01.2019, www.attl.cn
- [47] Blumm, J. Das Laserflash Verfahren-aktuelle Entwicklungen und Tendenzen. In *Proceedings of the Tagungsband zum Symposium Tendenzen in der Materialentwicklung und die Bedeutung von Wärmetransporteigenschaften*, Stuttgart, Germany, 22–23 March 2007; pp. 1–2.

- [48] Jianqiang Li , Nan Deng , Peng Wu , Zhangjian Zhou “Elaborating the Cu-networkstructured of the WeCu composites by sintering intermittently electroplated core-shell powders” *Journal of Alloys and Compounds* 770 (2019) 405e410
- [49] Churchill, S.W. and Chu, H.H.S., “*Int. J. Heat Mass Tran.*,” (1975), 18
- [50] McAdams, W.H., *Heat Transmission*, 3rd ed., McGrawHill, New York, 1954, Chap. 7
- [51] Whs sondermetalle “Data Sheet Tungsten-Copper (W-Cu)”,viewed 02.03.2019 , www.whssondermetalle.de
- [52] Grand View Research 2016 “Metal Injection Molding (MIM) Market Estimates, Trend Analysis” viewed 01.04.2019, www.grandviewresearch.com
- [53] Ibrahim A, Abdullah M, Mostafa SF, Hegazy AA. An experimental investigation onthe W–Cu. *J Compos Mater Des* 2009;30:1398–403.
- [54] Wikipedia, “Cooling Methods” viewed 18.02.2019, www.en.wikipedia.org/Cooling_methods